# Part II
# Coronagraph Optical Design

Charley Noecker

# Section 3.
# Coronagraph Architecture Overview

Charley Noecker

Optical Design Approach
Optical System Description

# Design Approach and Optical Options

- Goals of coronagraph design process
  - Establishing performance requirements
  - Identifying the main engineering uncertainties & implementation challenges
  - Creating a baseline design for analysis
    - Preliminary existence proof / benchmark

- Two design classes studied — "classical" and "shaped pupil"
  - Each can be implemented within current baseline optical design
  - Both have a single entrance aperture, focal plane mask, subsequent camera
  - Same basic engineering challenges of wavefront stability and control
  - Differences only in the masks and pupils

# The Challenge – High brightness contrast at small angles

- Total Earth-like planet flux / star flux ~ $10^{-10}$
  - But, star flux lands in a different pixel than planet flux
- Planet-star separation angle:
  - As small as 40-80 mas, depending on depth of search
  - Up to ~1000 mas (FOV goal)
- Ordinary telescope diffracts star into planet pixel, down ~3000x at 5 Airy radii

⇒ Need >$10^6$ additional star attenuation at planet pixel

⇒ Need an "extra-ordinary" telescope (a.k.a. coronagraph)

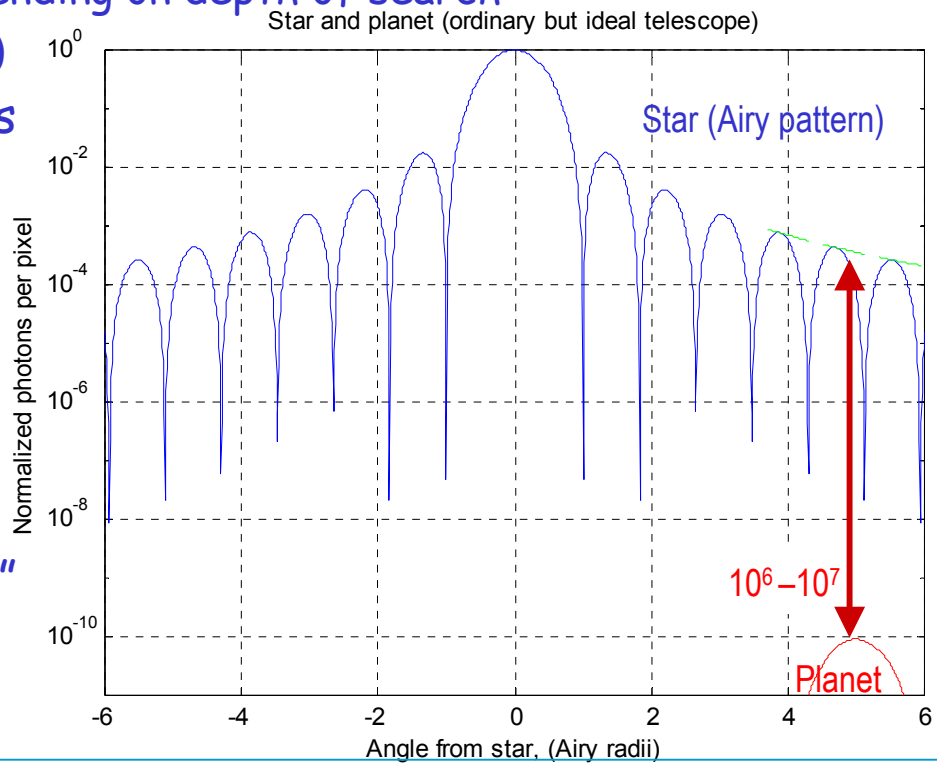

# The biggest issue is stray light

- Exo-zodiacal light in planet pixel is comparable to planet light (32 mag per 10 mas pixel for exo-zodi cloud equal to our own)
  - Ratio depends on planet flux and pixel size
  - Not an important source of background light for an imaging system
  - Coronagraph approach is robust to higher zodi levels and zodi clumps
- Stray starlight reaches the planet pixel by two routes:
  - Diffraction from aperture rim
  - Scatter from wavefront defects
  - Ghost images
- Stray sunlight via conventional stray light routes
- These challenge the planet detection in two ways
  - Added photon counting (statistical) noise
  - Instrumental variation (systematic noise)
- Requirements are based on these challenges

# Nature of noise sources

- Statistical photon error sources
  - Local and smooth exo-zodi, detector dark current, stray sunlight
  - Averages down as SQRT(integration time)
  - Could pick out faint planet against relatively large background (Q<<1)
- Systematic photon noise sources
  - Residual diffracted light (after pupil/focal plane masks and Lyot stop)
  - Residual scattered light (after DM and primary mirror actuators)
    - Time-variable, due to vibrations and thermal effects
    - Will not average down
  - To limit the contribution of time-variable backgrounds, we require planet to be at least as bright as background (Q ≥ ~1)
    - This choice of Q is based on subjective engineering judgement
    - As more is known about the instrument variations, we will be able to refine this upper-level requirement

# Strategies for background noise reduction

- What characteristics do we look for in a planet?
  - Localized in a pixel
    - Diffracted and scattered starlight will be speckly
    - Conventional stray sunlight will be more uniform
  - Fixed in the star field, not rotating with the telescope
  - Constant over days
  - Thermal and chemical spectral features
- Important additional discriminating strategies are
  - Rotating the telescope around the line of sight
  - Repeated measurements (where appropriate)
  - Spectra (where appropriate)
- Diffracted and scattered starlight are hard to discriminate from a planet quickly, e.g., in a single exposure
- They must be kept constant enough to apply these slower strategies

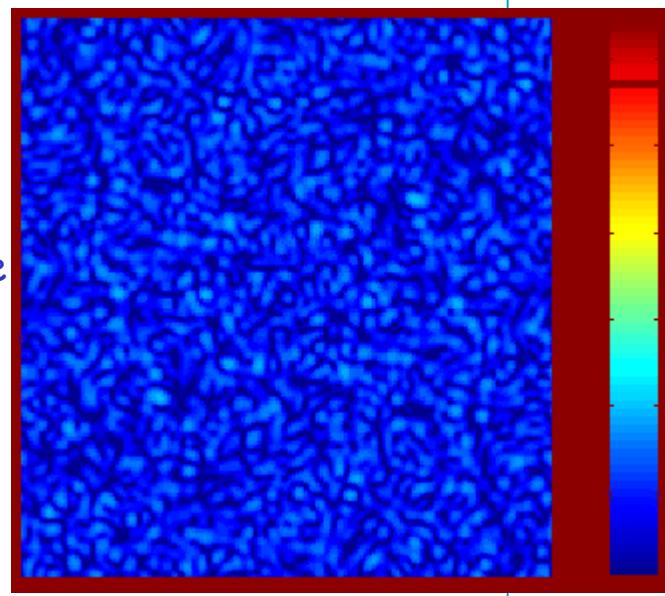

# We can ease the technical challenge by restricting range of azimuth

- It may be too hard to suppress starlight equally at all orientations
- Emphasize some orientations around LOS at the expense of others
  - Elongated aperture (e.g. our 10x4 ellipse)
  - Shaped pupils (e.g. square, Spergel types)
- Figure shows an example
  - "X-zone" is a region which is dark enough to permit planet searching
  - Its limits are
    - Inner working distance (IWD) and outer working distance (OWD)
    - Range of azimuth $\phi$ a.k.a. opening angle
  - These characteristics are open choices in design trades

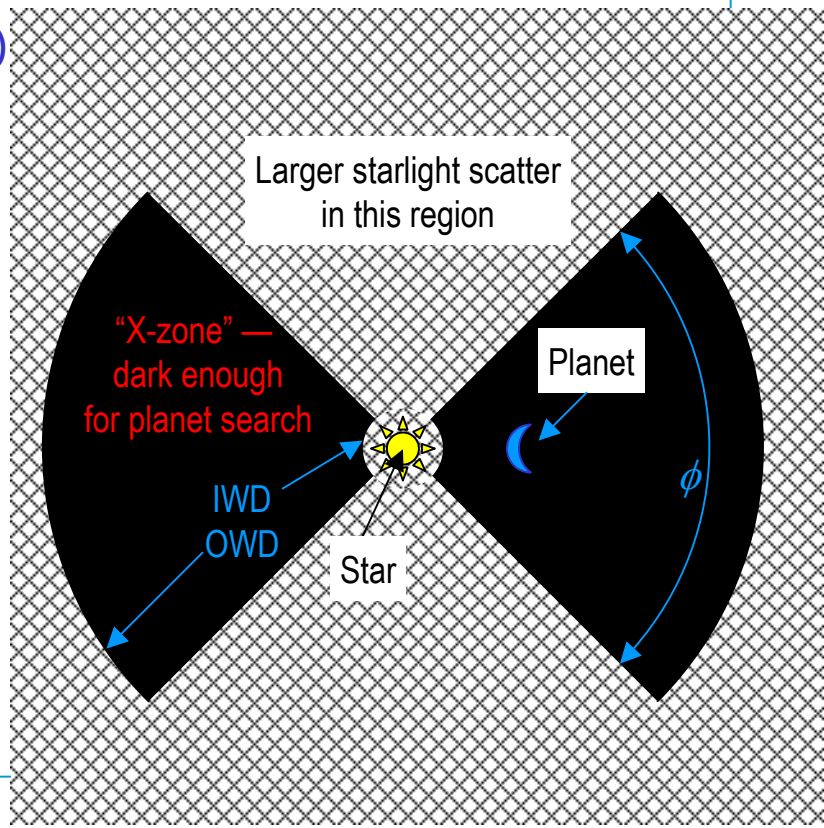

# Two Main Types Considered

- Shaped pupil coronagraph
  - Novel pupil shapes (Spergel)
    - Optimally suppress diffraction in "X-zone" of image plane
    - Send diffraction to other regions of image plane
  - No Lyot stop needed
  - Only binary masks required
    - Guaranteed manufacturability
    - Wavelength independent

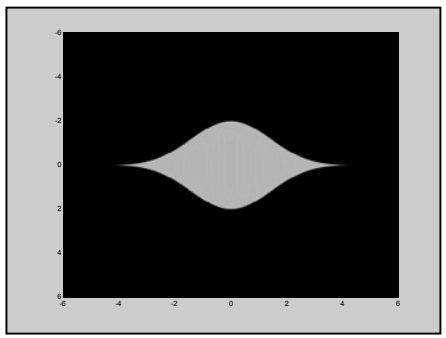

- Classical coronagraph
  - Gaussian or other band-limited field stop blocks the star
  - Lyot stop suppresses diffraction from pupil rim
  - Planet search over wider range of azimuth (rotation around LOS) per exposure

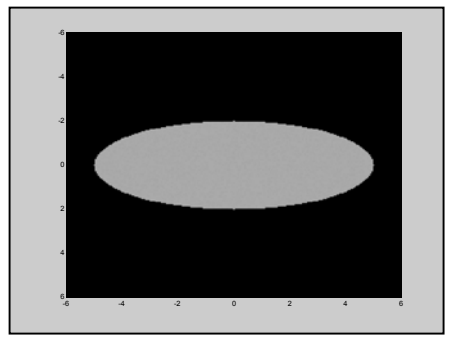

# Classical coronagraph approach

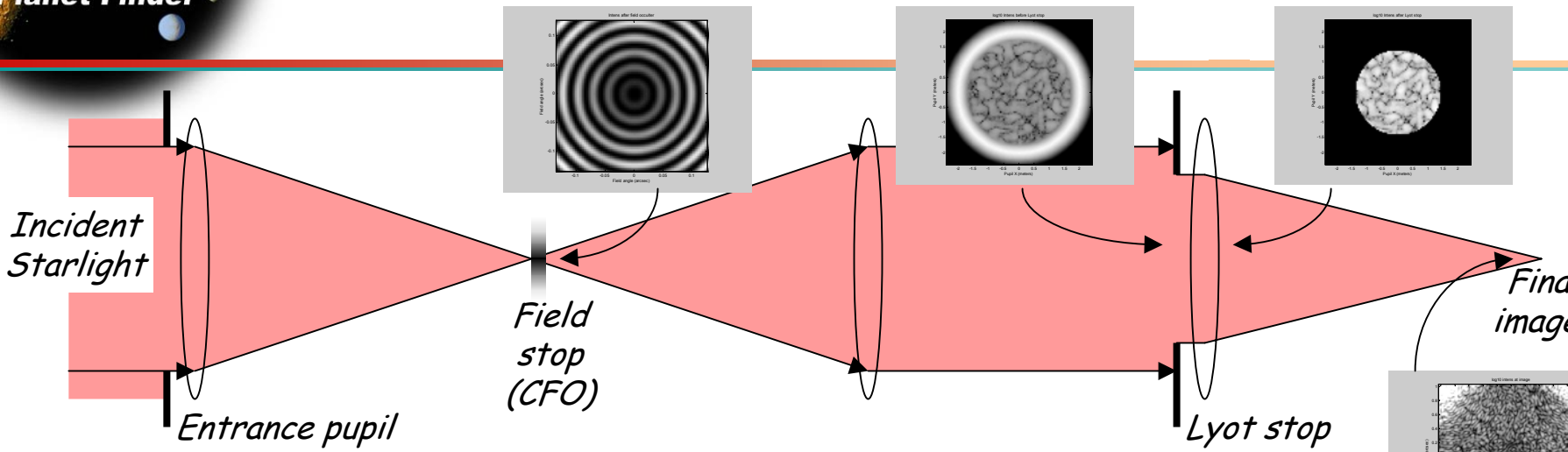


- Coronagraphic field occulter (CFO)
  - Graded-attenuation spot (e.g. gaussian — also see Kuchner & Traub)
  - Blocks central 3-5 Airy radii of star image
- Lyot stop
  - Mask at re-imaged pupil
  - Blocks starlight that escaped the CFO
  - Works by scraping the beam at the image of the rim
- These two together suppress ordinary aperture diffraction
- Scatter from wavefront error still contributes (can dominate)

# Shaped pupil approach

- Departure from circular symmetry in entrance pupil suppresses diffraction in regions of the point spread function (PSF)
- CFO+Lyot replaced by a different CFO
- Square pupil has reduced diffraction along diagonals
  - This figure does not show the substantial benefits of apodizing (graded attenuation of the pupil edges) [see PAR report from Boeing-SVS team] [backup charts]
- Spergel & Kasdin's novel shapes extend this idea to an optimum
  - Eliminates graded-attenuation masks
  - Mask shape alone is enough to suppress diffraction to required level
  - Allows some amplitude correction
  - This figure shows the near-ideal 2-segment design performance, using only an entrance pupil mask

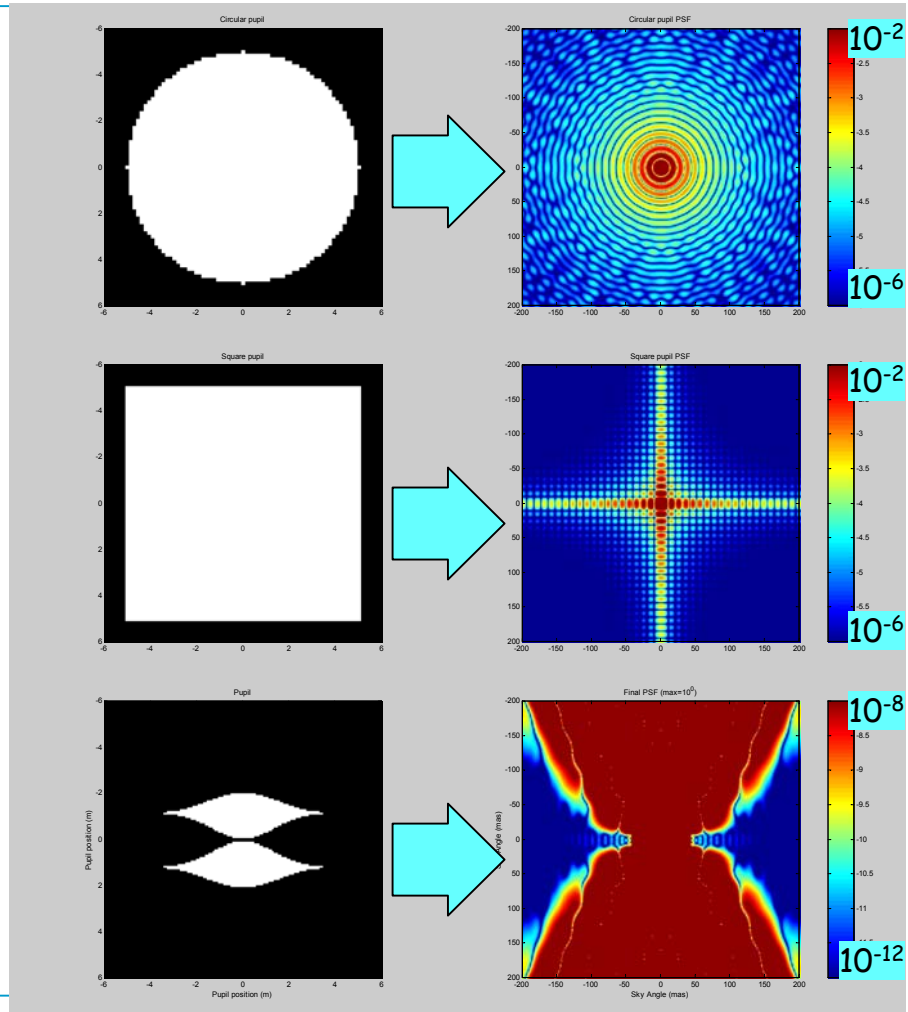

# Wavefront requirements

- After diffraction is sufficiently suppressed,
  **Wavefront Error (WFE) is the main concern**
- Assume deformable mirror (DM) leaves a residual WFE in the pupil with white spectrum (PSD independent of spatial frequency)
- Then

$$\sigma < \frac{N}{8}\sqrt{\alpha C}$$

  where
  - $\sigma$ is the allowed RMS WFE within the spatial frequencies controllable by DM
  - N is the number of actuators across the DM width
  - $\alpha$ is the throughput factor due to pupil stops
  - C is the ratio (integrated planet flux) / (integrated star flux)
- With N=256, 3 actuators/cycle, $\alpha$=0.5, and C=1E-10, $\lambda$=500 nm, we get

  $\sigma$ ~= 75 pm

  root-PSD ~ 0.8 pm·m

# Functional layout accommodates both Classical and Shaped Pupil

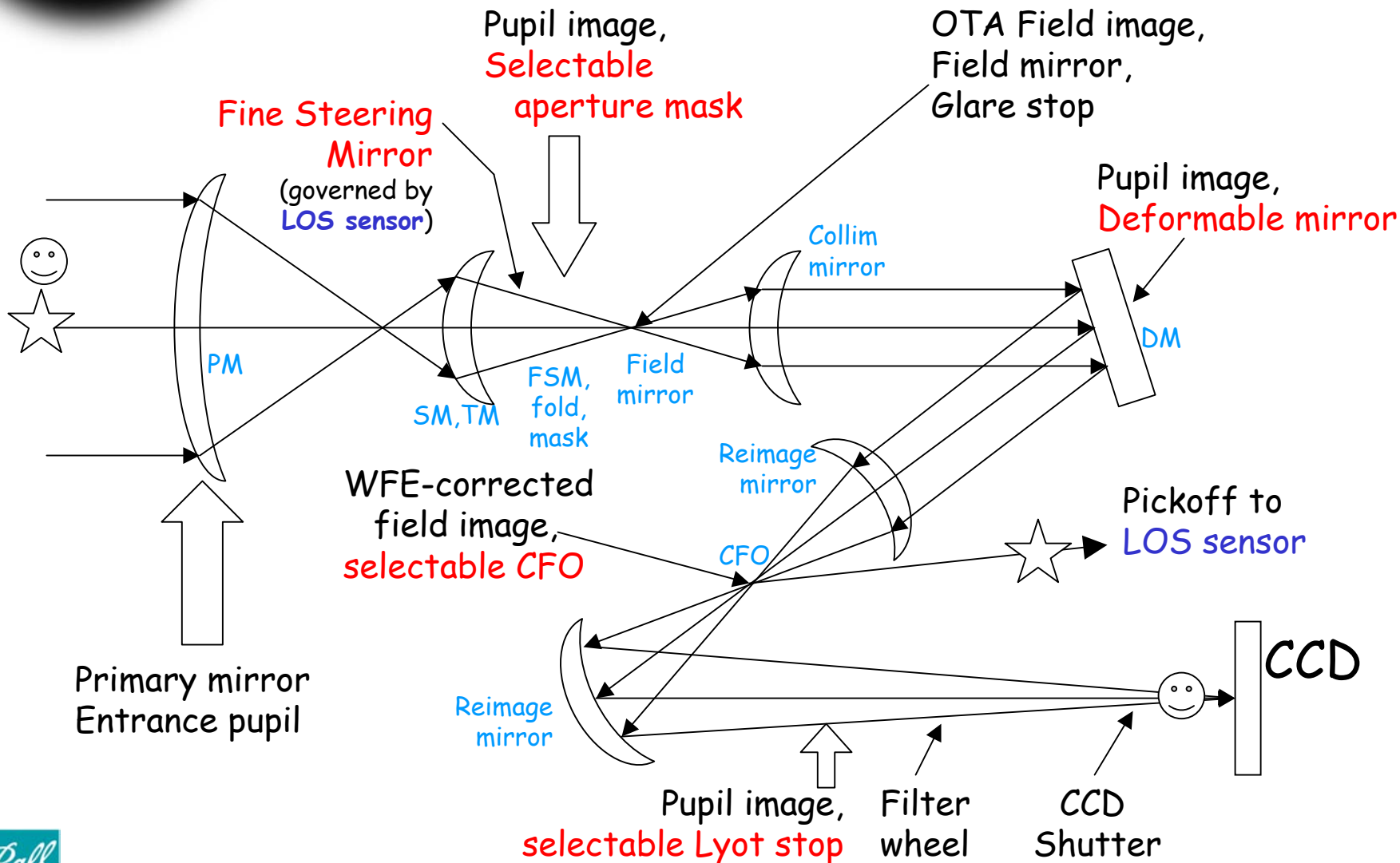

# Features of Optical System

## Primary

- 10x4 meter ellipse
  - max collecting area & longest dimension within launch shroud
  - an off-axis segment surface of a parent optic of 11m diam, f/1.5
- Unobscured monolith (one sheet)
  - Needed for stray light control
- ULE/Zerodur or fused silica
  - Meniscus, 4 cm thick
  - Lightweighted to 20-25 kg/m$^2$
- Graphite-cyanate backing structure
  - Adds ~10 kg/m$^2$
- Total mass ~940 kg

- Airy radius $r_A$=12.6 mas @ $\lambda$ = 500 nm
- Deformable mirror
  - 256x100 actuators across 2.5:1 pupil
  - Assume 3 actuators/cycle (sub-Nyquist)
  - OWD = 85 $r_A$ ~ 1.1 arcsec
- Classical typical parameters:
  - CFO mask radius ~3-5 $r_A$ = 38-60 mas
    - IWD ~ 40-60 mas (depends on assumptions)
  - Lyot stop radius ~few%-70%
- Shaped pupil typical parameters:
  - Optimum function is prolate spheroidal wavefunction
  - Kaiser is an excellent approximation
  - Typical Kaiser parameter is 13
    - Gives IWD ~ 4-5 $\lambda$/D = 40-50 mas at $\lambda$=500 nm
    - Trade IWD vs. residual PSF shoulders

# Back-end optics

- This is a view of the back side of the primary mirror
- Design uses the practical minimum number of optics before the CFO

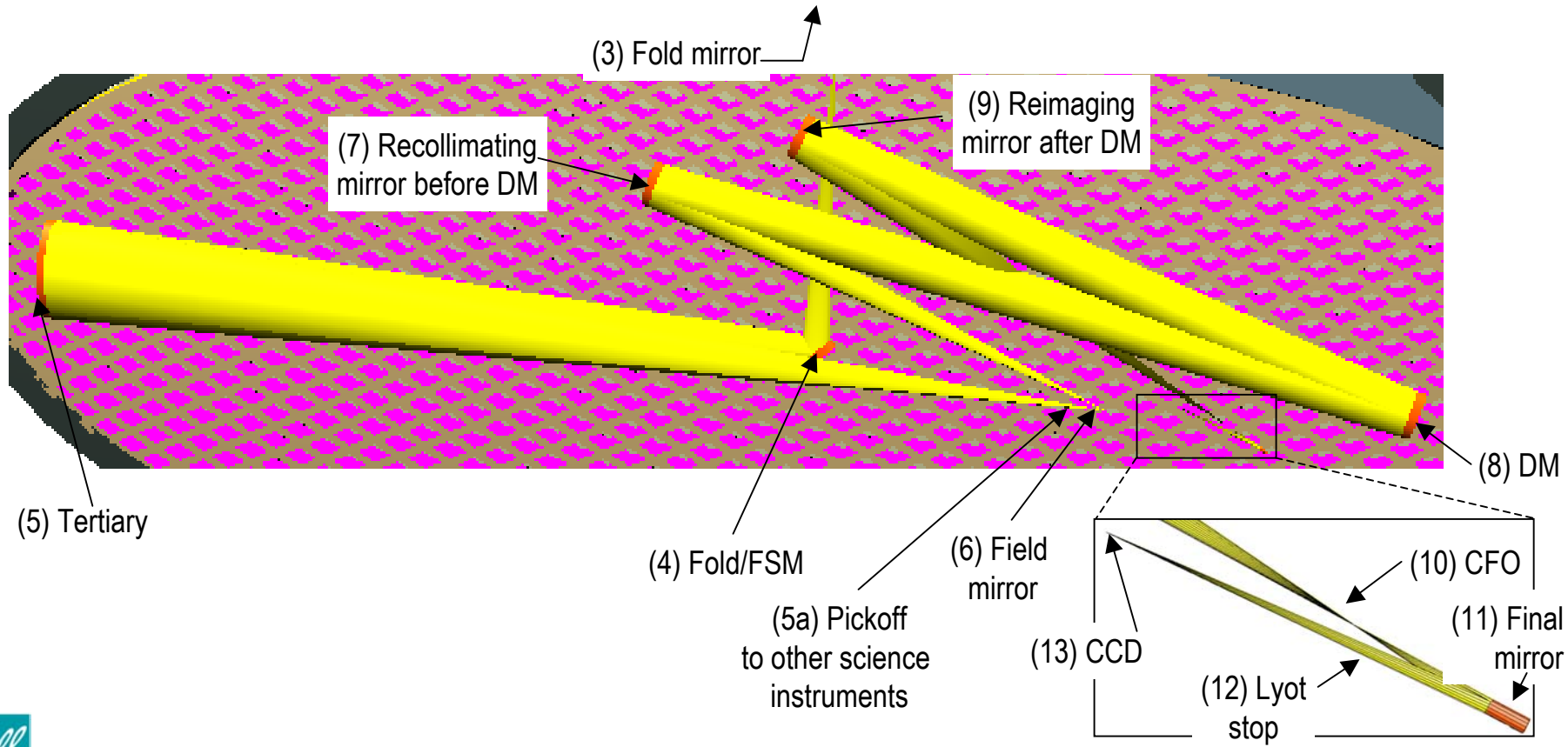

# Other Science Instruments

- Diagram on pg II-17 shows a pickoff at 2nd image
  - FOV > ±2 arcmin with aberrations < λ/140
    - Excellent starting point for any instrument package
  - Does not benefit from the main DM before that pickoff
  - Does benefit from primary mirror WFE corrections
  - Stray light from bright central object (planet-search candidate star) may limit sensitivity in this off-axis FOV
  - Current approach for planet spectroscopy is a sequence of observations through color filters
    - Worst-case measurement throughput — does not take advantage of simultaneous measurements
    - This is definitely an area for further study
- UV/Visible multi-object spectrograph: spectral resolution 100 - 10,000
- Wide-field camera: FOV 2 x 2 arcmin (central hole), 5 x 13 mas pixels

# Section 4.
# Detailed Optical Design & Issues

*Charley Noecker, David Spergel, Jeremy Kasdin, Jeff Wynn*

Optical Design
Optical System Issues

# Main Optical Design Issues

- Aperture shape
- Focal plane mask options
- DM placement
  - At a pupil image to within << $2*(\text{pixel size})^2/\lambda$
  - Before CFO (pending analysis of "after" case)
- Amplitude errors in the pupil
- Steering mirror and body pointing requirements
- WFE sensing

# Classical coronagraph design questions

- CFO beta vs. throughput vs. BW
  [beta ≡ (Gaussian radius)/(Airy radius) ]
  - Smaller beta allows smaller IWD, but requires heavier loss in Lyot stop
    - Trade SNR on planet vs. beta and Lyot size
  - Large optical bandwidth (planet search mode) means large range in beta; requires conservatism in beta at short-wavelength end
- Amplitude error compensation w/ DM
  - Sacrifice half the FOV
  - Spectral bandwidth limitations
- CFO mask manufacturing tolerances
  - Attenuation > 1e6 at center
  - Deviations from nominal profile at ~1 cycle per $\lambda/D$ must be very tightly controlled (1e-8?)
  - This is a critical technology development area

# Shaped pupil coronagraph design questions

- Truncated gaussian vs. prolate spheroidal/ Kaiser
- Kaiser parameter vs. PSF shoulders vs. throughput
  - SNR on planet
  - Allowed WFE sigma
  - IWD
- Rim shape
  - Tolerances
  - Manufacturing: width as wings taper to zero
  - Potential for actuated rim; amplitude contro
- Width of waist in PSF/ opening angle / multiple apertures
  - rotations needed to scan for planets
  - phasing sensitivity of sub-apertures
  - amplitude correction
  - CFO masking in broad spectral band

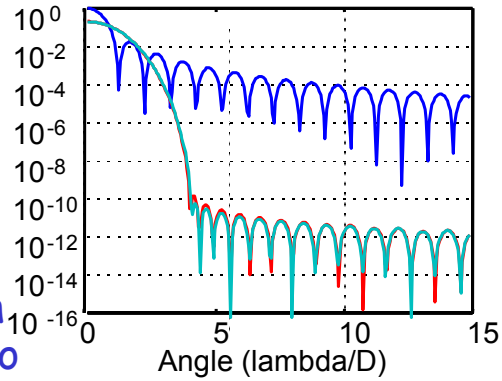


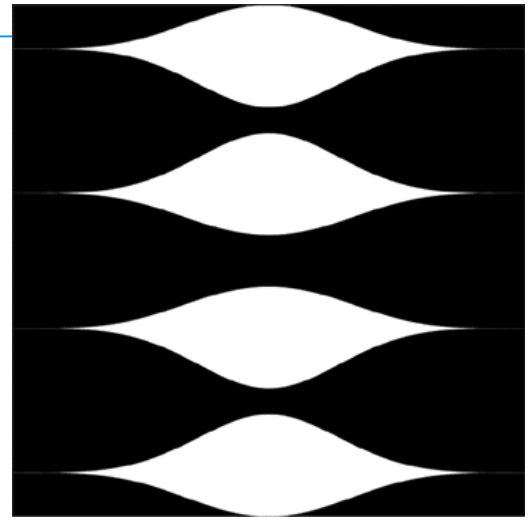

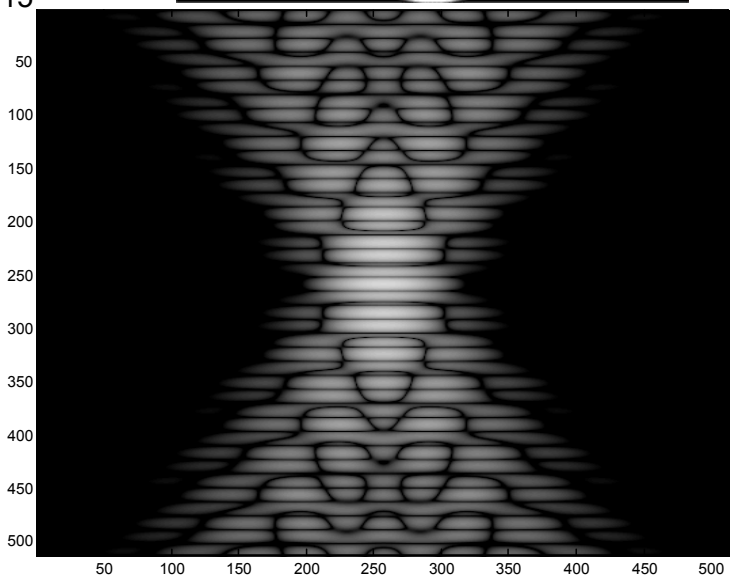

# Wavefront error control

- Layered control
  - Primary mirror — 300 actuators
    - Low spatial frequencies < ~1.5 cycles/meter = 15 cycles/diameter
    - Stroke ~ tens of microns
    - Resolution ~ 7 nm, in DM actuator stroke budget
  - Deformable mirror
    - Stroke ~65 nm
    - Resolution ~0.5 Å

# Wavefront errors specified within specific spatial frequency bands

| Spatial frequency band | Cycles across aperture diam | RMS at primary | RMS (nm) after DM |
|---|---|---|---|
| Low (LSF)<br>Figure error | 0-4 | 7.8 nm | < 1 nm |
| Critical (CSF)<br>DM-controllable ripple | 3-130 | 4.8 nm | 0.07 nm |
| Mid (MSF)<br>Ripple | 130-10k | 4.8 nm | |
| High (HSF)<br>Surface roughness | Above 10k | 1.5 nm | |
| | | 10.5 nm | RSS total |

- LSF band is weakly constrained -- its effects are suppressed by CFO mask
- CSF band is the tightest
  - Initial case must be within actuator stroke
  - Final case determines planet sensitivity
- Mid and high bands don't contribute directly at planet position

# Steering Mirror vs. Body Pointing

- The allowable body pointing error for the telescope is based on the accumulation of wavefront errors due to beam walk.
- Simplified analysis of wavefront errors under rigid rotation of the telescope
  - Repointing the telescope body leads to substantial beam walk across some mirrors
    - Using the FSM to maintain pointing on the CFO does not remove these errors
  - This beam walk changes the wavefront error contribution of those mirrors
  - The correction at the DM is then incorrect for the new wavefront
- The estimate assumes the root-PSD for each mirror is 10x better than the HST nominal measured root-PSD
- The results are given in the backup charts
- An allowance of 14 mas body pointing error seems strict enough to control WFE to tolerable levels

# Amplitude error compensation

- Phase correction (at DM) can compensate for amplitude errors
  - If perfect pupil field is perturbed by a cosine amplitude error plus a sine phase error,

$$E = A(xy)\left[1 + b\cos(k_0 x) + ic\sin(k_0 x)\right]$$

  - Then the focal plane field is

$$E_{fp} = a_{fp}(k_x, k_y) + b \cdot a_{fp}(k_0, k_y) + b \cdot a_{fp}(-k_0, k_y) + c \cdot a_{fp}(k_0, k_y) - c \cdot a_{fp}(-k_0, k_y)$$

  - The "b" and "c" terms each give scatter peaks on CCD at $(k_0, k_y)$ and $(-k_0, k_y)$
  - Phase correction can cancel amplitude error at one location <u>but not both</u>

- Bandwidth limitation
  - Amplitude error ~independent of $\lambda$
  - Phase correction scales as $1/\lambda$

  $\Rightarrow$ Errors in the correction accumulate away from center wavelength
- If $\delta A \sim 10^{-4}$ and the optical band full width $\delta\lambda/\lambda \sim 30\%$, the leakage is $(\delta A)^2 \, (\delta\lambda/\lambda)^2 / 12 = 7.5\text{e-}11$
- Passively, this $\delta A$ would be a challenge for a 10-mirror system
- An actuator (spatial light modulator) could make it easy
- The actuator should be
  - achromatic
  - gentle on wavefront and polarization
  - stable
- This is a tech development issue

# Amplitude correction candidates

- Intensity profile actuators
  - Photosensitive coatings
  - LCD-like (via polarization)
  - Pupil edge actuation (for shaped pupils)
    - Works only in a "stripe" of the PSF
  - Interferometric (example shown)
    - DM in one arm controls amplitude
    - Resulting phase effects corrected by another DM

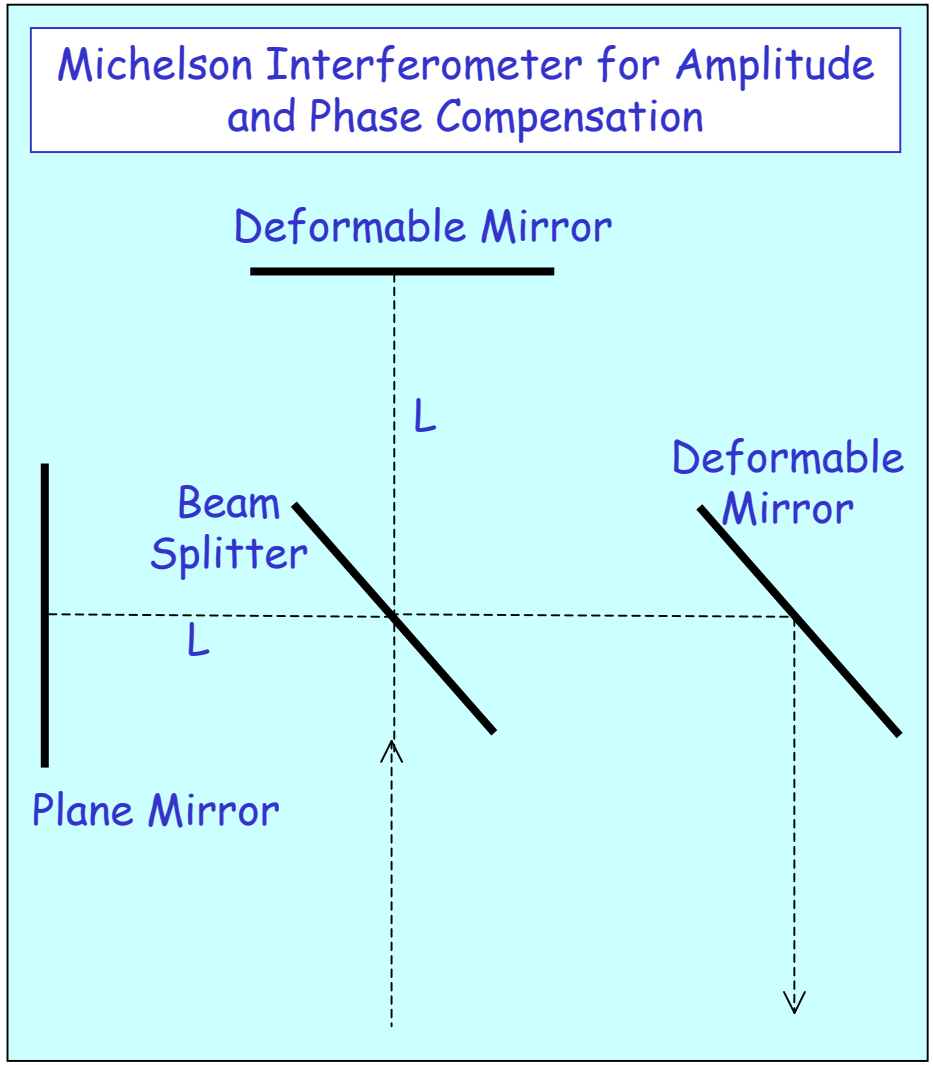

# Sample calculations and images

# Postulated wavefront PSD after DM correction

- Hand-edited root-PSD (blue curve)
  - Starting point is HST-like root-PSD, but 10x better
  - High frequency end of this is unchanged by DM control — left alone in editing too
- This root-PSD is used to make a WFE map
  - Its spectrum shown in red
- This WFE map is used with classical and shaped pupil types
- This can be used to test the sensitivity to WFE

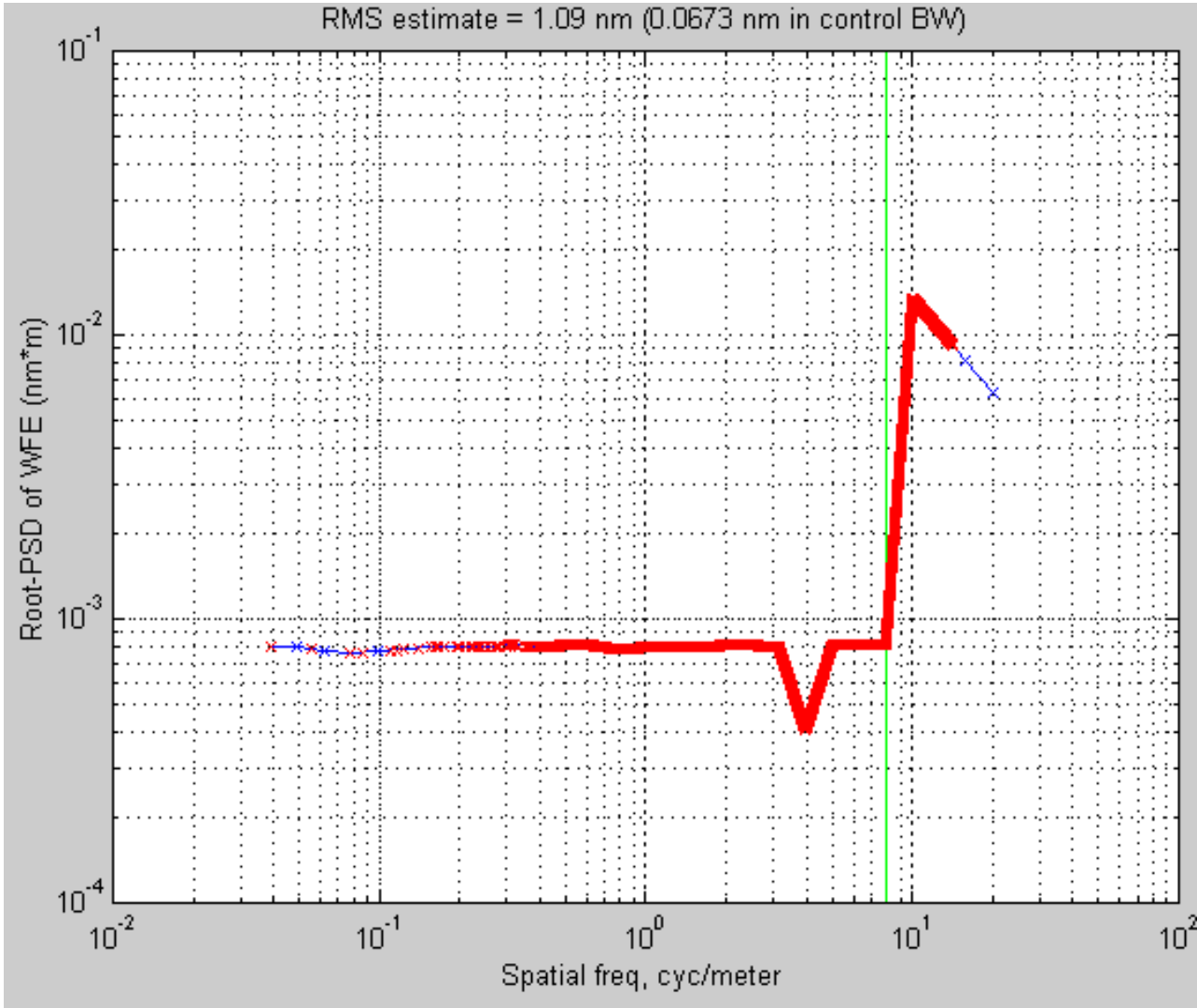

# Phase map in pupil

- Classical coronagraph's elliptical aperture
- Left image shows phase in star's WFE map (speckled)
- Right image shows phase in planet's WFE map (stripes)
  - Mainly a tilt from being 60 mas off-axis

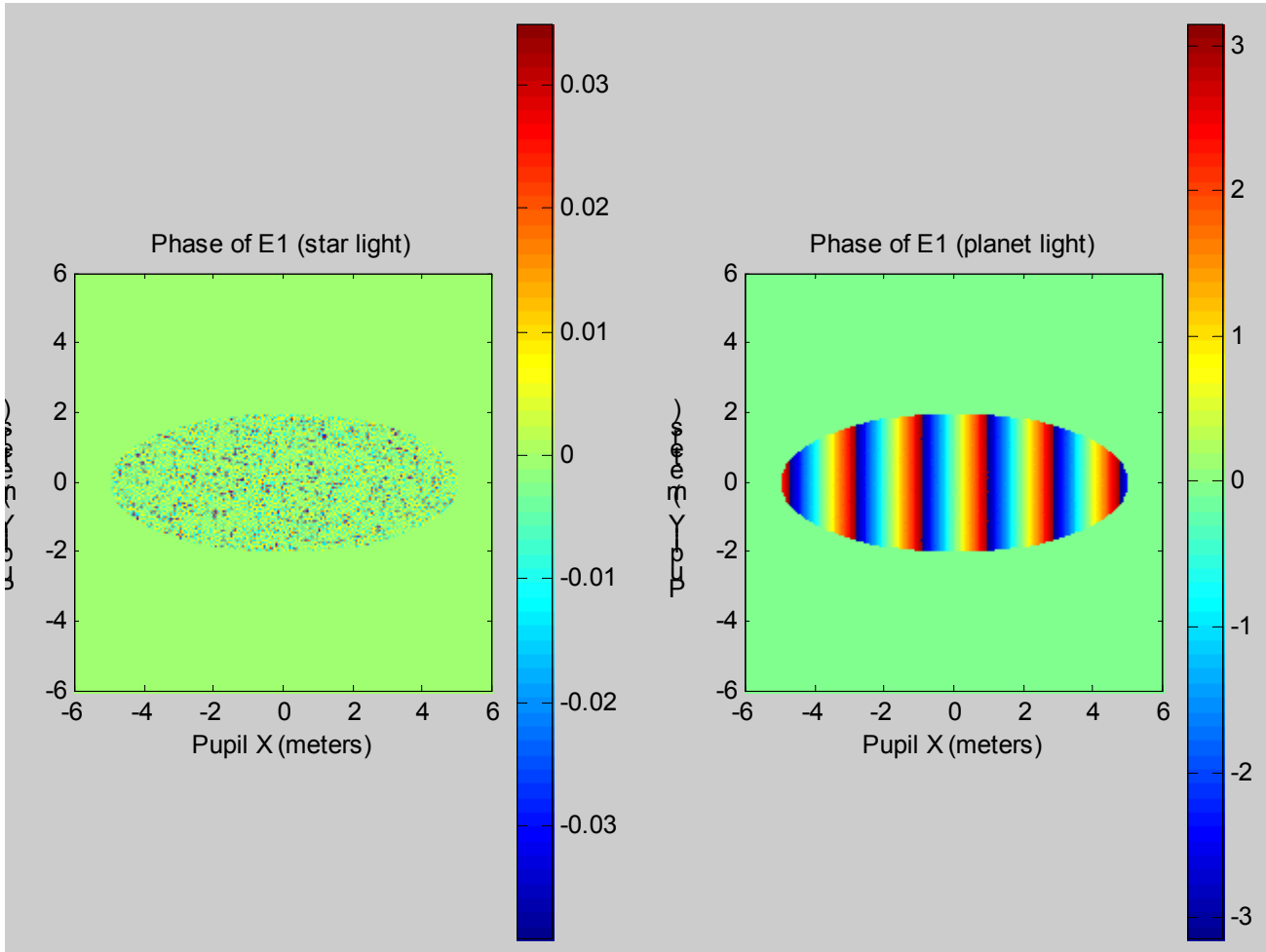

# Classical coronagraph — before and after CFO mask

- Star and planet PSFs before and after coronagraphic field occulter (CFO)
- Planet-star flux ratio has not yet been applied
- Upper right shows star central peak suppressed ~25x
- Lower right shows planet escaping the CFO (2x suppression)

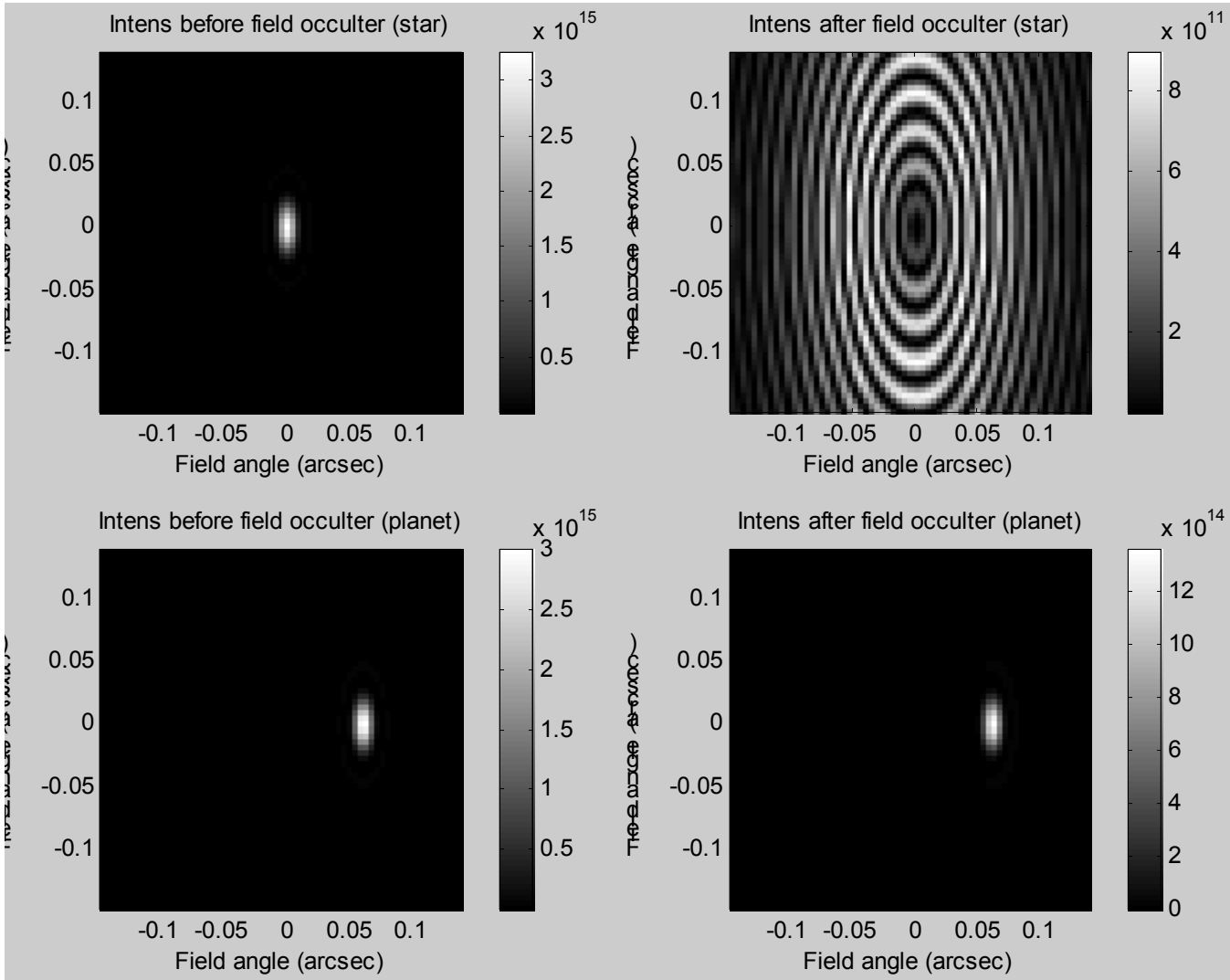

# Classical coronagraph — before and after Lyot mask

- Rings surrounding star's central peak carry light to a fuzzy ring at the next image of the pupil, shown here
- Scraping off this ring gains a factor 1000 or more in starlight suppression
- The remainder comes from WFE scatter
- Most of planet light is in central portion, which escapes the Lyot stop again (2x suppression)

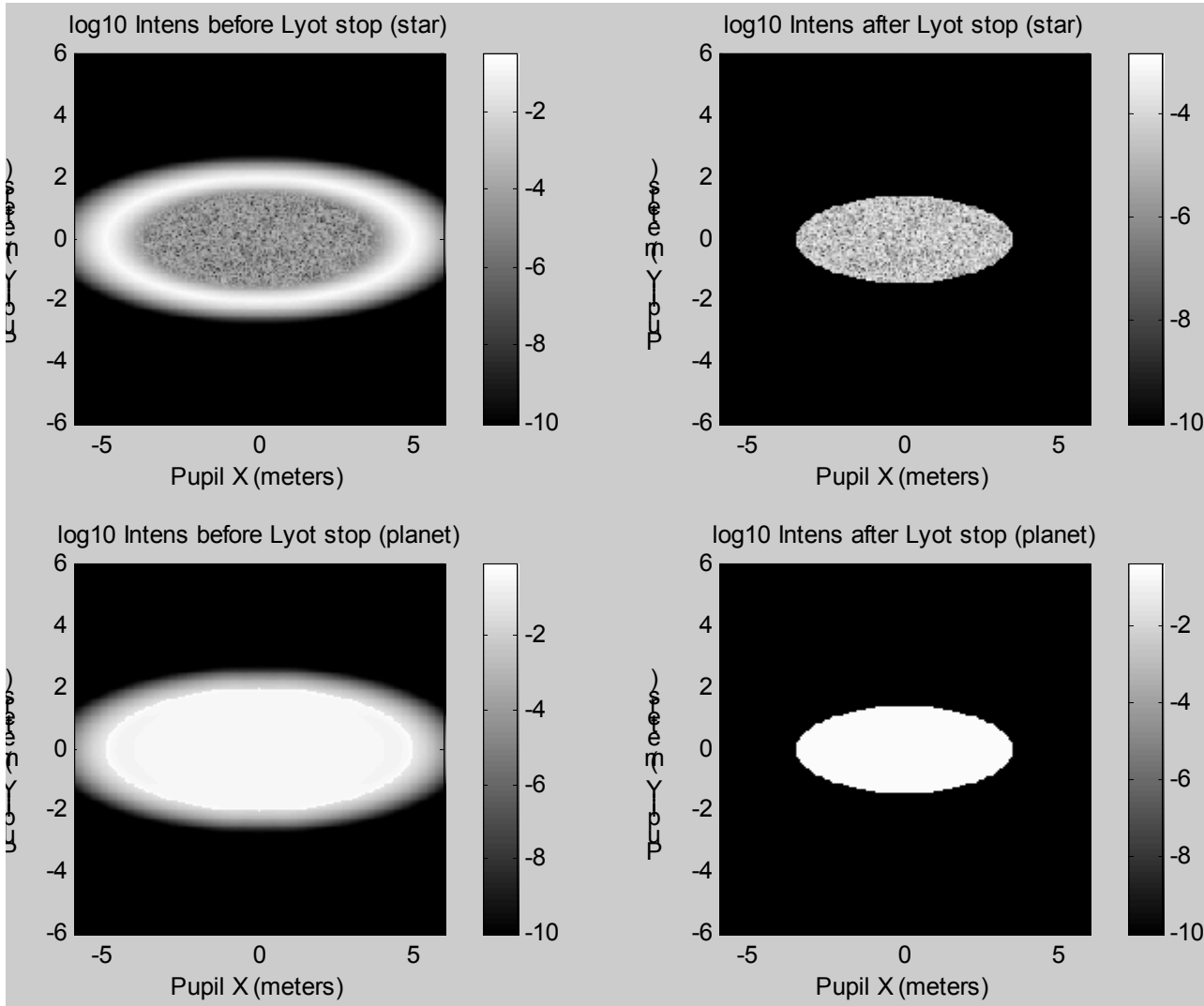

# Final image

- Log10 of stellar intensity at the CCD focal plane
- Color range limited at 1e-8 to 1e-12
- Pupil = 4x10m ellipse
- Gaussian CFO, radius = 3.3 $R_A$
- Lyot radius = 70%
  - ~2.8x7m ellipse
  - Throughput ~50%
- $\lambda$ = 500-550 nm
  - Outer 0.5 arcsec suffers from granularity in wavelength integral
- Star = 5700 K
- RMS WFE = 67 pm

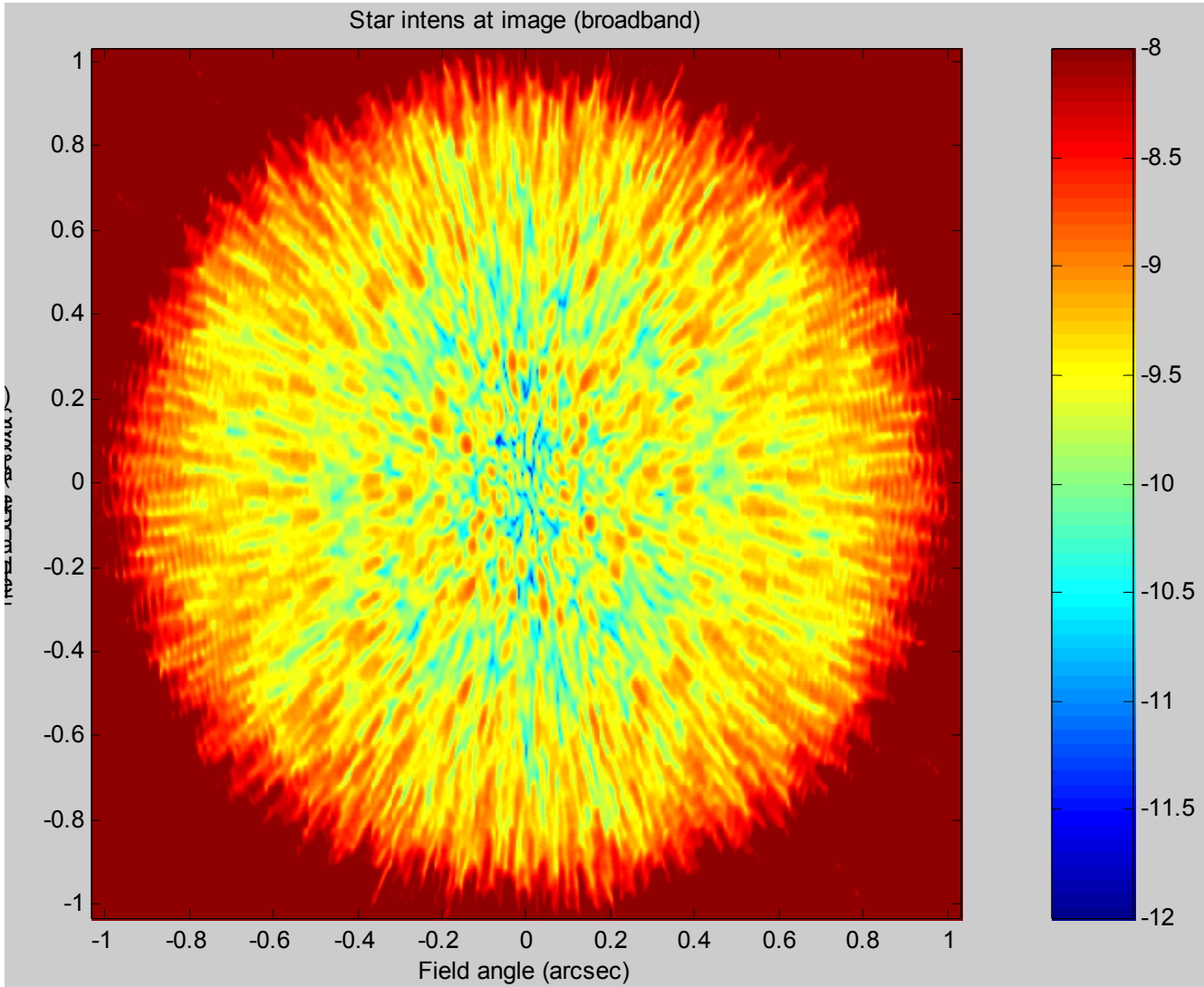

# Classical coronagraph typical throughput attenuation factors

| | Star | Factor change | Planet | Factor change |
|---|---|---|---|---|
| Start at pupil | 31.4 | | 31.3625 | |
| After field occulter | 1.28 | 0.041 | 13.95 | 0.44 |
| After Lyot stop | 0.00133 | 0.001 | 6.44 | 0.462 |

- These factors apply only to the implementation chosen here
- CFO and Lyot stop radii can be separately selected for particular goals

# Single shaped pupil aperture

- Pupil = Kaiser in 4x10m ellipse
- λ = 500-550 nm
- Star = 5700 K
- RMS WFE = 75 pm
- Planet = 1e-10 at ~60 mas offset

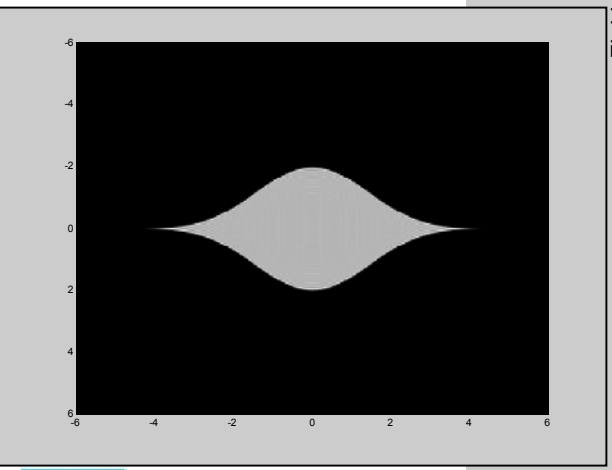

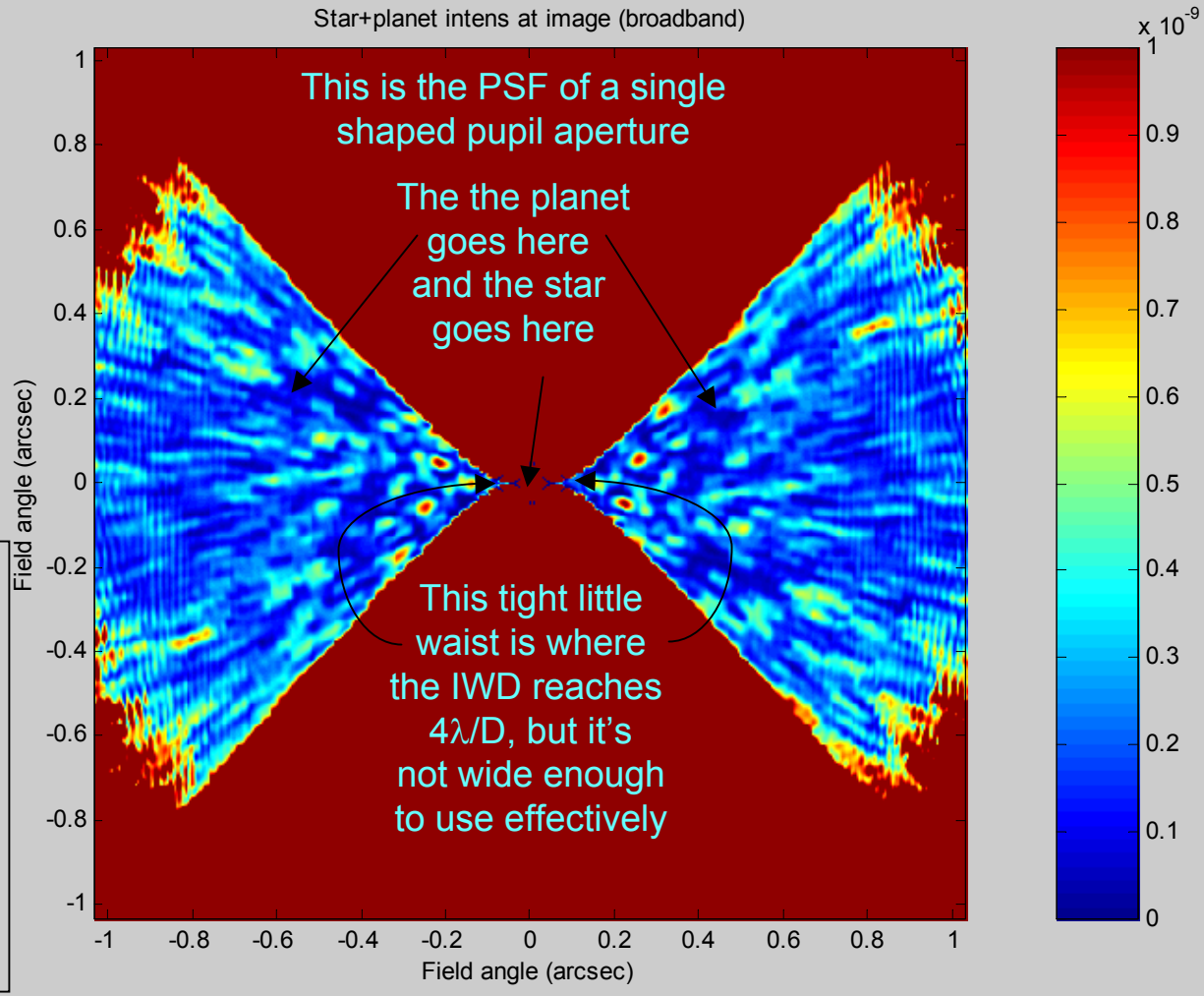

# Final image
# Dual shaped pupil coronagraph

- Pupil = dual Kaiser in 4x10m ellipse
- λ = 500-1000 nm
- Star = 5700 K
- RMS WFE = 80 pm
- Planet = 1e-10 at ~100 mas offset

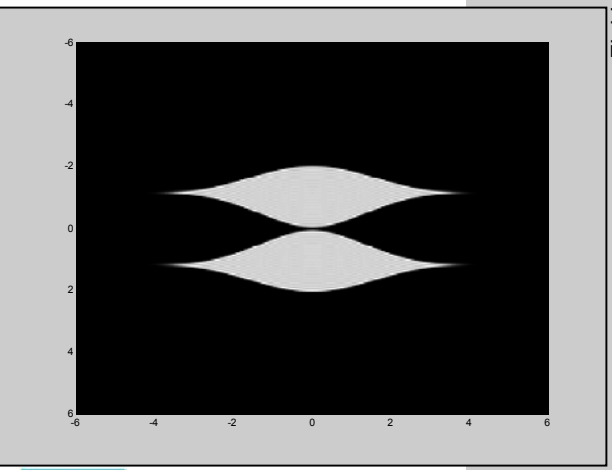

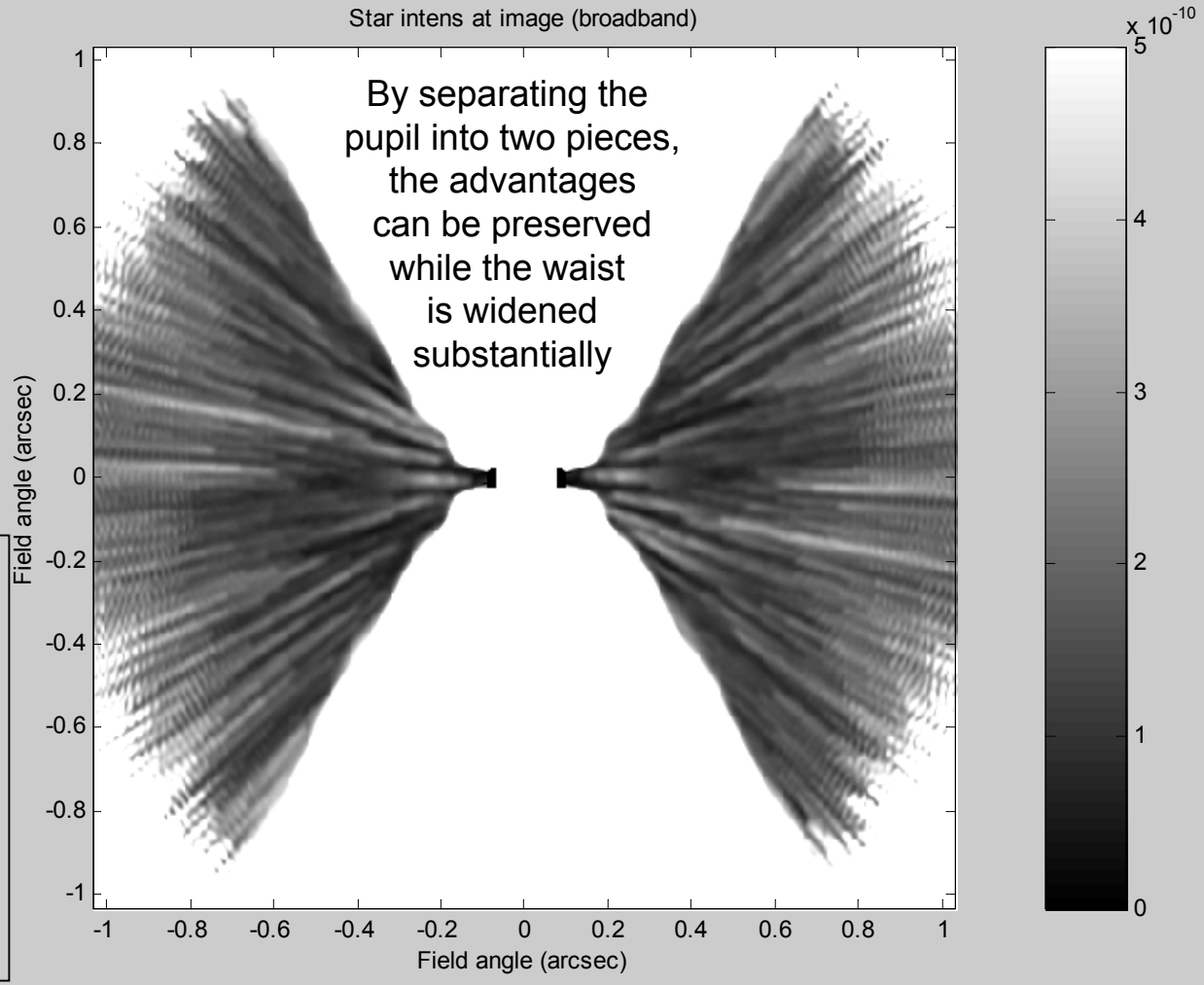

# Final image — Star and planet
# Dual shaped pupil coronagraph

- Pupil = dual Kaiser in 4x10m ellipse
- λ = 500-1000 nm
- Star = 5700 K
- RMS WFE = 80 pm
- Planet = 1e-10 at ~100 mas offset

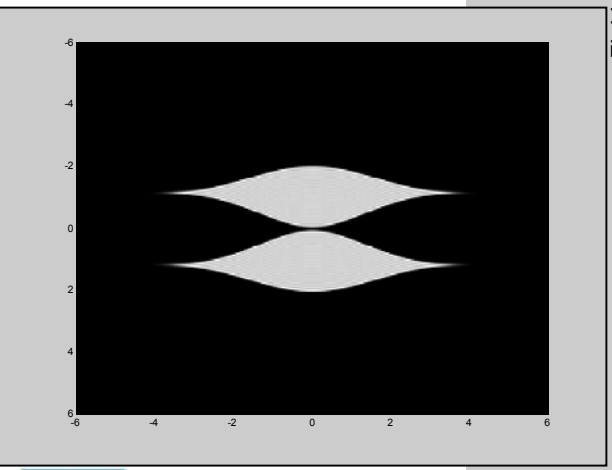

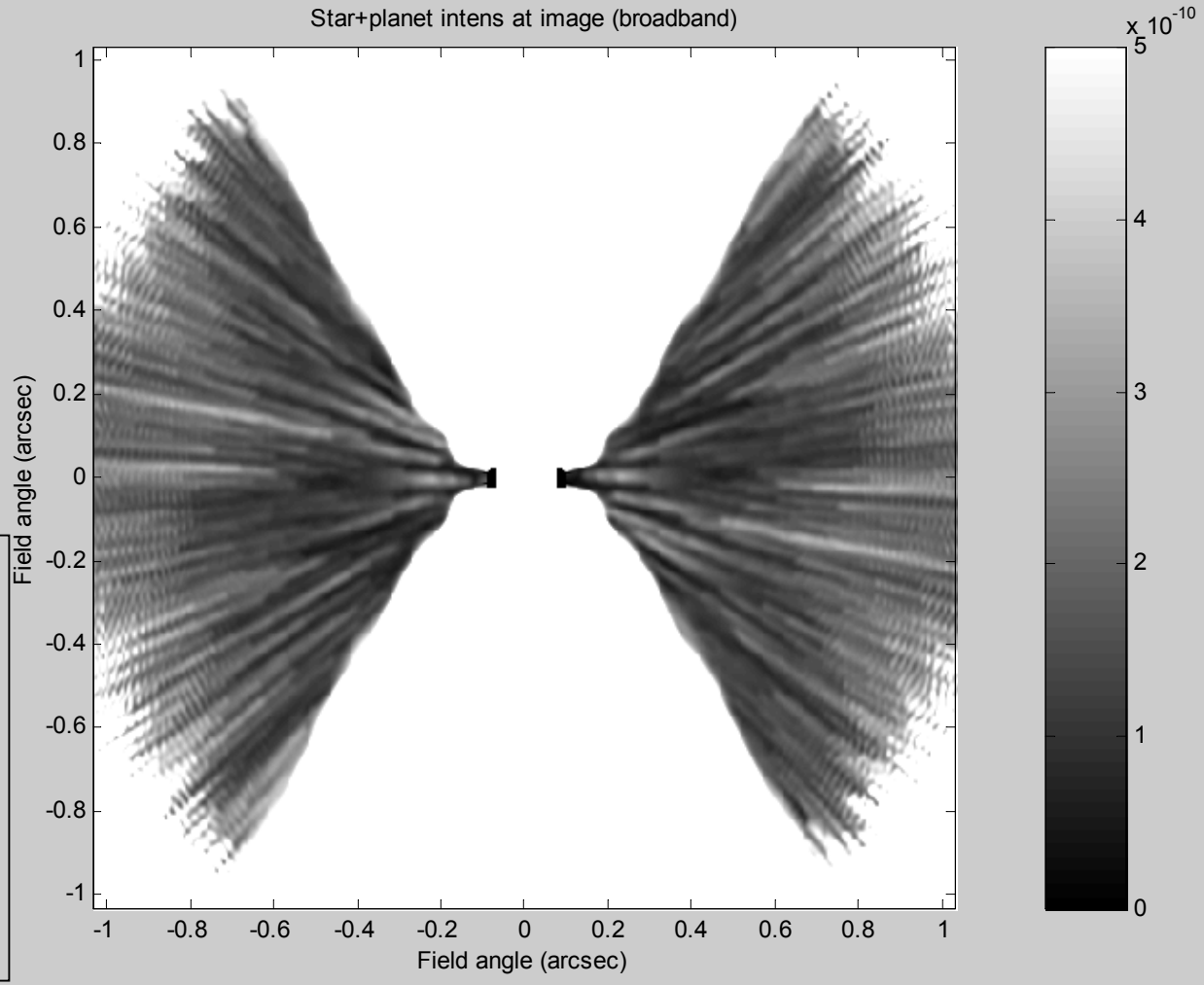

# SNR calculations

| TPF S/N calculation | Maj. Axis (m) | Aperture Minor Axis (m) | Wavelength |
|---|---|---|---|
| **Chris Burrows Nov 2001** | **10** | **4** | **5.00E-07** |
| Pixel Size (mas, parallel to major axis) | | Pixel (mas, parallel to minor axis) | |
| | 5.16 | 12.89 | |
| Ext. Photons/sec/A/cm^2/mag=0 | **950** | Photons/sec/cm^2/A/mag=0 | 165.07 |
| Bandwidth | **20%** | Photons/sec/cm^2/mag=0 | 1.65E+05 |
| Exposure time (sec) | **12000** | Photons/cm^2/mag=0 | 1.98E+09 |
| Aperture area (cm^2) | 3.14E+05 | Photons/m=0 | 6.22E+14 |
| Stellar Magnitude (Sun at 10 pc) | **4.7** | Counts | 8.20E+12 |
| Planet Offset (mags; = 1e-10) | **25** | Total planet counts | 820.34 |
| Q (ratio of planet to star residual) | **1** | Star counts per central planet pix. | 82.03 |
| Exozodi (mag/sq arcsec) | **22** | Exozodi counts | 32.78 |
| Dark current/sec | **0.001** | Dark current counts | 12.00 |
| Read noise | **2** | Read noise counts | 4.00 |
| | | Total background counts | 130.82 |
| FPA throughput (gaussian mask) | **0.5** | Proportion in central pixel | **0.1** |
| | | Central intensity | 1.26E+14 |
| Sharpness degradation | **0.5** | Central intensity/arcsec^2 | 2953.65 |
| Sharpness | **0.07** | Cent. Int./pix., no exit pupil mask | 0.196 |
| | | CCD Efficiency | **0.8** |
| Number of surfaces | **10** | Exit pupil throughput | **0.5** |
| Reflectivity/surface | **0.92** | Off mask throughput | 0.174 |
| | | **SNR** | 6.4 |

# Wavefront Controls - Burrows, Trauger, and AOA

- Shack Hartman sensor inadequate for TPF requirements
- Sensing and control based on phase diversity, using science CCD
  - Current baseline approach, based on CODEX analysis
  - Measure speckle amplitudes from CCD
  - Apply correction at corresponding spatial frequency
    - Choose 2 or more hypothesized phases
    - Collect new speckle images for each
  - Determine best-guess actual phase, apply correction
  - Lather, rinse, repeat
- Assume set/forget operation for the critical spatial frequencies

# Detector Technology -- Summary of Characteristics and Types

| CHARACTERISTICS | CCD | Si Hybrid | MCP | APD | STJ | Microbolo | InSb |
|---|---|---|---|---|---|---|---|
| Wavelength coverage (μm) | 0.1-1 | 0.1-1 | 0.01-1 | 0.1-1 | 0.01-5 | any | 0.4 - 5 |
| Pixel pitch (μm) | 6-25 | 17-30 | ? | ? | ? | ? | 25 -50 |
| QE (%) | >80 | >80 | >90 | >90 | ? | ? | 85 |
| Read noise (electrons) | 3* | 3* | 0 | 0 | ? | ? | 15 |
| Dark current (counts/s/pix) | 0.01 | ? | ? | ? | ? | ? | 0.01 |
| Overlight damage | N | N | Y | N | N | N | N |
| CR degradation | low | low | low | ? | ? | ? | low |
| Format size (2001) | 4K x 4K | 1K x 1K | 1K x 1K | ? | 10x10 | 100x100 | 4K x 4K |
| Energy resolution | N* | N* | N(?) | N(?) | Y | Y | N |
| Time stamping | N* | N* | Y | Y | Y | Y | N |
| Operating temperature (K) | 150 | 30 | 150 | 150 | 0.1 | 0.1 | 77 |
| Power supply | 5 V | 5 V | 1 KV | 5 V | 10 mV | 1 mV | 15 V |
| Technology readiness | high | moderate | high | low | low | low | high |

* Modified CCDs and hybrid devices that support non-destructive read modes can in principle have less than 1 e/read effective read noise and can therefore be used to detect individual photons
  Modified CCDs can time-tag photon arrival to within a frame read-time
  Since there is no read-noise penalty, low dark-current devices can be mated to integral field spectrographs to determine the energy of each photon

Backup charts

# Mirror coating trade

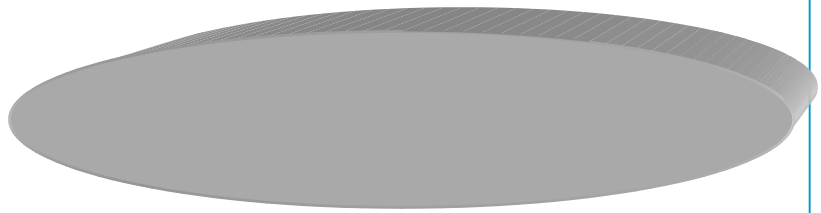

- Silver
  - reflectivity ~98% per surface
  - Gives 80% throughput after 10 mirrors
  - Cuts off dramatically at < ~400 nm
- Aluminum (preferred)
  - reflectivity ~ 92-96% per mirror across the visible band
  - Gives ~50-60% throughput after 10 mirrors
  - This reflectivity extends into the UV
- With silver mirrors, UV capability would be virtually eliminated
  - Would still have a mighty good visible wide-field camera capability (at least 2x2 arcmin with 13x32 mas pixels)
- With silver mirrors, coating degradation is a technical risk
  - Many people have had trouble with "measles" (patches of degraded coating)
    - could prove disastrous to coronagraph performance
  - Of course, Ball knows how to procure great silver mirrors
  - Probably nobody else will believe this can be done with billi[illegible]ollar reliability

# Contaminant effects fall outside the critical spatial frequency range

- Both molecular contaminants and settled particles will contribute mostly in the high spatial frequency range
  - MOLECULAR: multi-molecular drops ~1-10 nm high
  - PARTICLES: dominant particle sizes ~0.1–1.0 μm
- Contributions from each particle or drop fall off as diameter$^4$
- Coverage ~ few percent is tolerable
- Micrometeorite craters are similar

# Contamination threats to image quality

- CONCERN: Small changes in contaminant features on the optical surfaces during an observation period will degrade the light suppression
- RESPONSE:
  - Changes in distributions of both particulate and molecular contaminants will be nil or minute during periods of up to several days
  - Micro-meteor impacts with the telescope lightshade etc. pose the only credible threat to image quality during an observation. Such an impact would generate particulate and some molecular debris which would settle and adsorb onto proximate surfaces

# Meteor impacts and effects

- Meteor impacts on the telescope system (light shade etc) will be common
- These meteors are concentrated in clouds, intercepted annually
  - impact rate ~20x for ~5 % of year
  - Much less for ~95 % of the year
- Quantity/distribution of impact debris on optical surfaces depends on proximity of optics to the impact points and on the impact direction

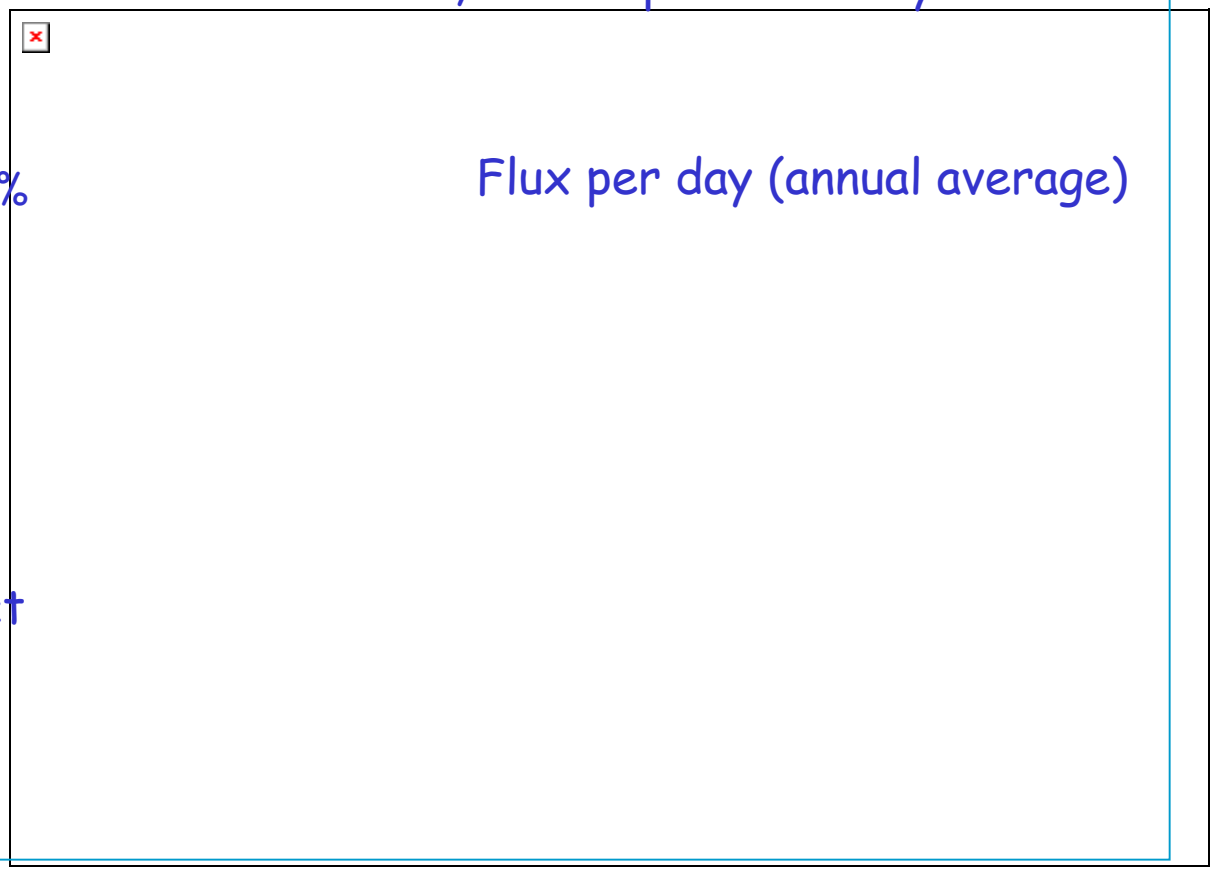

# Estimated contaminant quantities on TPF optical surfaces

- It is possible to achieve surface cleanliness on the optical surfaces of the TPF telescope at these levels:

| | At launch | Steady state on orbit |
|---|---|---|
| Molecular deposit quantities | ~ 0.5 - 1 nm | ~ 0.5 - 1.5 nm |
| Molecular contaminant rates | — | < 0.004 nm / day |
| Particle distributions | Level 100 - 200 | Level 100 - 200 |
| Particle redistribution rates | | |
| Quiescent periods | Nil | Nil |
| During meteor impact | — | TBD |

# Molecular contaminants

- Molecular contaminant deposits will either be random distributions of multi-molecule drops or uniform thin films
  - Energy relationships between admolecules and surfaces tend to favor drop formation
- The size distributions of the multi-molecule drops will be outside the spatial frequency ranges (see figure next page)
  - For molecular contaminant deposits in quantities equivalent to a few mono-molecular layers, the multi-molecular drops will have radii which probably will not exceed about 10 nm and thicknesses on the order of 3 to 10 nm
  - These drop thicknesses are on the same order as the figure errors of the defined spatial frequency ranges, though the spatial frequencies of the drops are far greater
- The growth rates on molecular contaminants will be extremely low, resulting from outgassing from source materials and can be controlled by materials choices, vacuum bakes, and best cleanroom practices

# Predicted size distributions of molecular contaminants

# Particulate contaminants

- Settled particles will also generally be outside the spatial frequency ranges (Figure 3)
- The exceptions are fibers and large particles, whose dimensions place them in the extreme end of the HSF range
  - However, we would expect a very low number, if any, of such fibers and particles on optical surfaces such as those of the TPF. This must be controlled by use of best cleanroom practices
- Small settled particles will be quite stable on the optical surfaces. Large shock forces are necessary for their redistributions, and there are no such sources on TPF

# Size distributions of small particles

# Primary Mirror Construction
## Jeff Wynn

Primary Mirror Construction
Technology Development


TAKE PICTURES.
FURTHER.

# Primary Mirror Construction

- The monolithic primary mirror will be constructed from segments that draw from AMSD technology
- AMSD areal density is 15 kg/m$^2$ for mirror/actuator system (TPF allocates 35 kg/m$^2$ )
- Core and faceplate segments will be fused together to form the monolithic PM blank
- Existing Kodak facilities and capabilities will be utilized to produce segments
- New Kodak facilities will be needed to process and test the full primary mirror

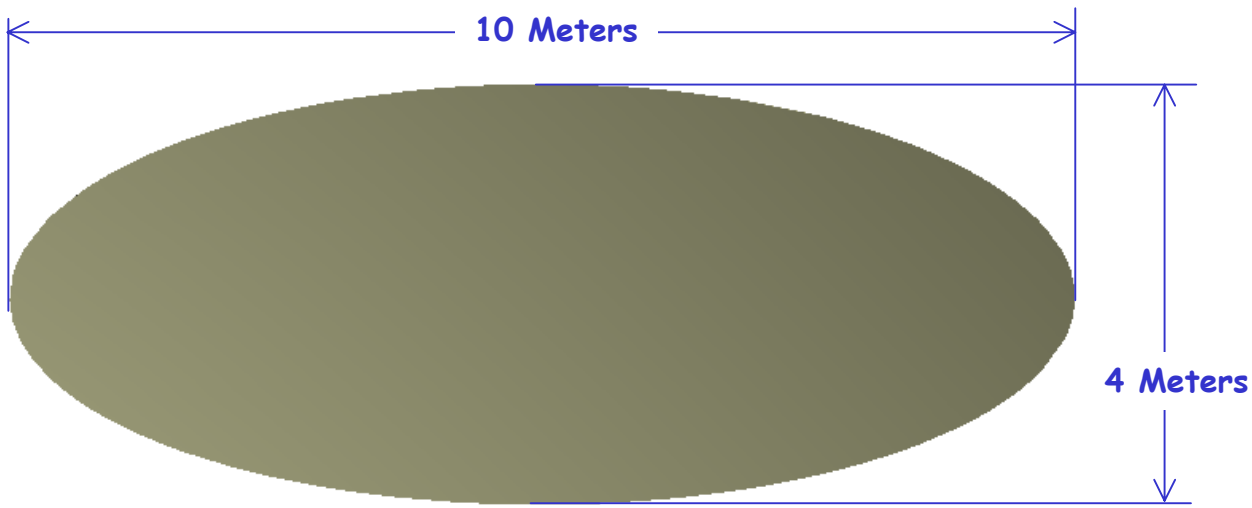


TAKE PICTURES. FURTHER.

# Segmented Construction of Optics

- 30 cm ULE blank
  - Segmented core
  - Segmented back plate
  - 19 mm deep core
  - Low Temp Fusion of segments
  - Proof of concept blank
- The TPF monolithic PM will have a segmented front and back plane

Kodak

TAKE PICTURES.
FURTHER.

# Lightweight Optics - Core Generation

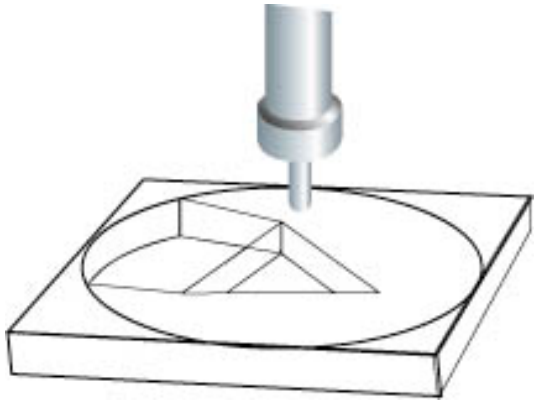

Waterjet cutting reduces time required to fabricate lightweight mirror blank

Core strut thickness of 0.02" (0.5 mm) demonstrated

TAKE PICTURES. FURTHER.

# Mirror Construction Elements

ULE Glass Core Element

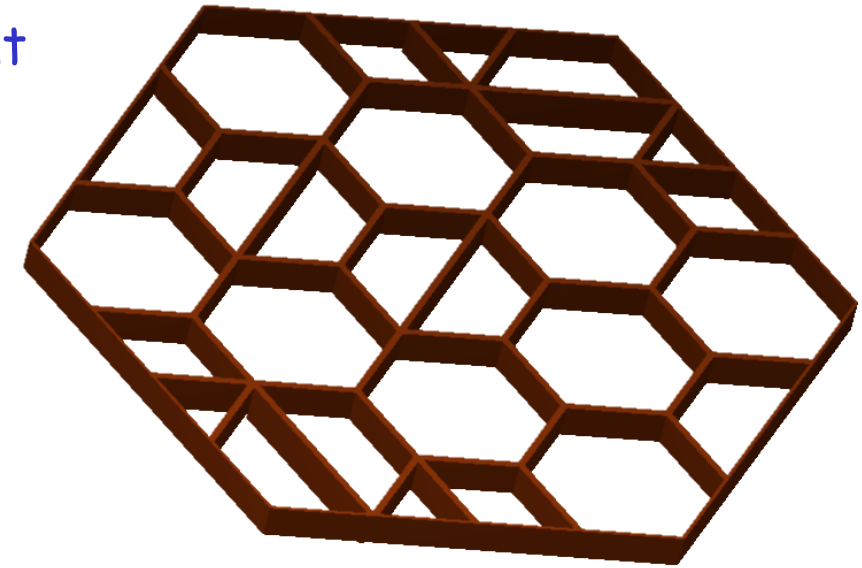

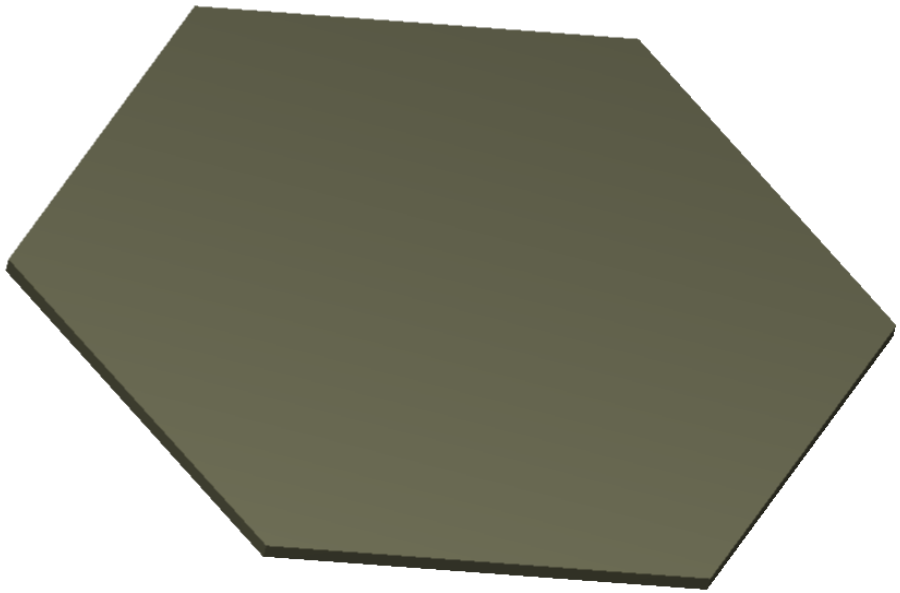

ULE Glass Face-sheet Element

Geometry Shapes and Sizes will be Traded

TAKE PICTURES. FURTHER.

# Mirror Blank Fabrication
# Low Temperature Fusion Technology

State of the Art Lightweight Mirror Blank Fabrication Processes with Corning Glass, Inc.

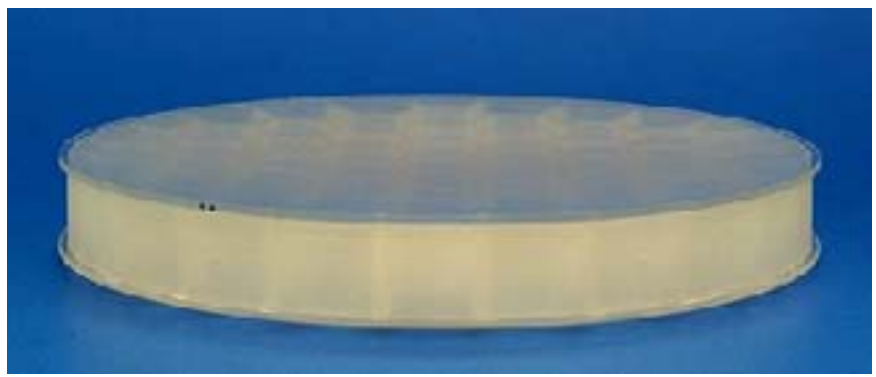

TAKE PICTURES. FURTHER.

# Basic Assembly Approach

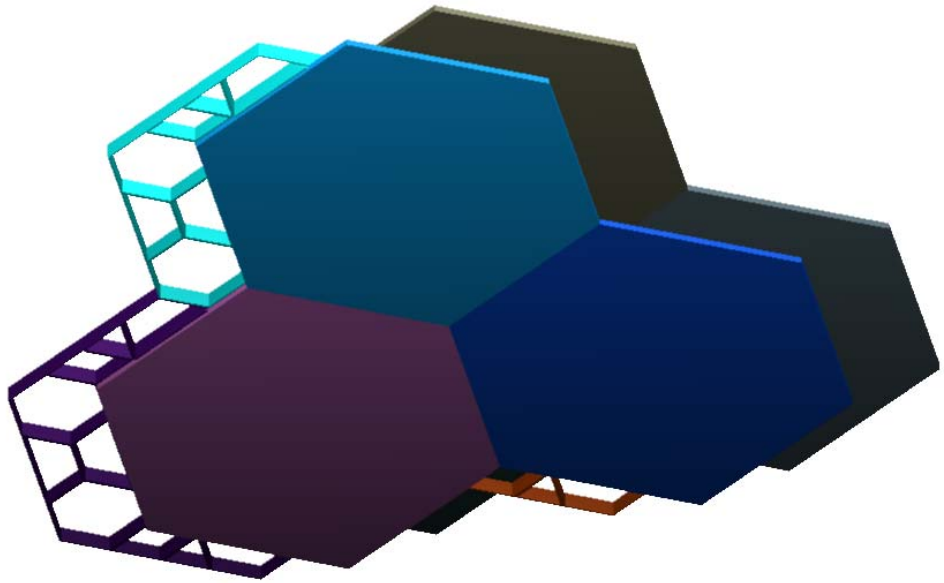

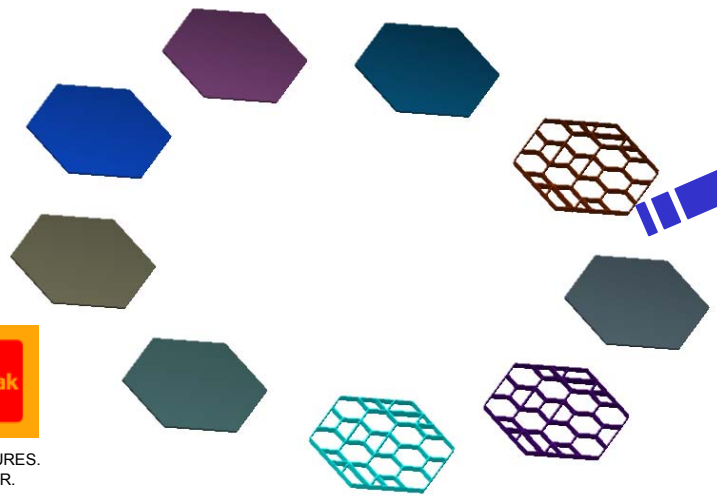

Elements Assembled into Large Apertures

Kodak

TAKE PICTURES. FURTHER.

Ball

# Offset Face-Sheet Pattern

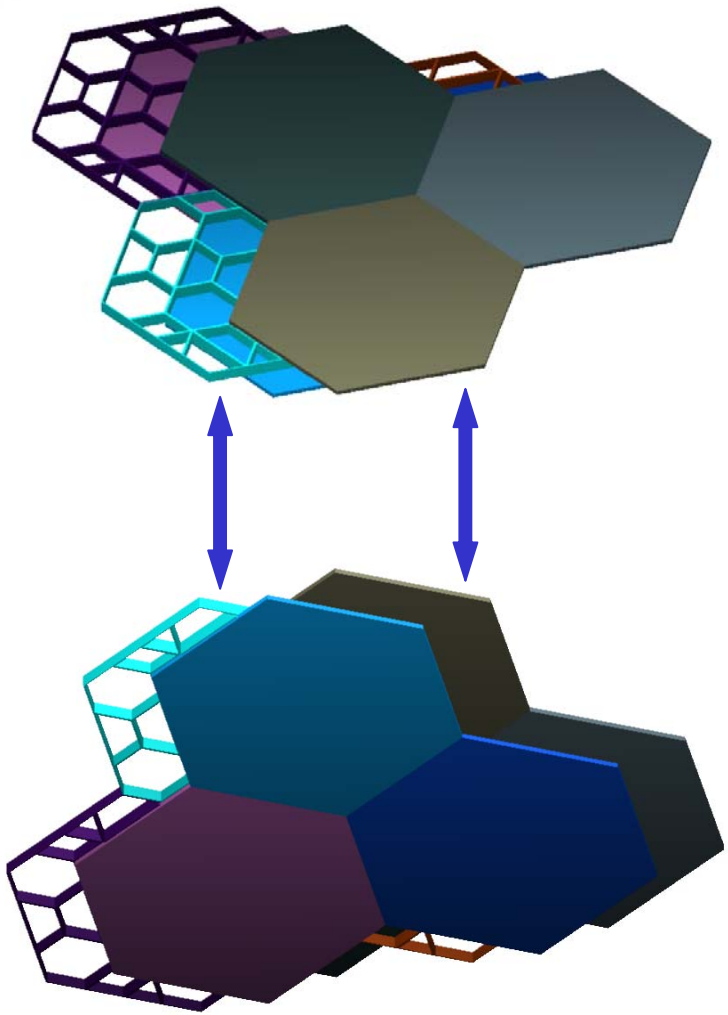

Front and Aft Face-Sheets assembled in offset pattern to minimize figure errors of the completed large assembly

Low Temperature Fused and Low Temperature Slumped

TAKE PICTURES. FURTHER.

# Completed Assembly

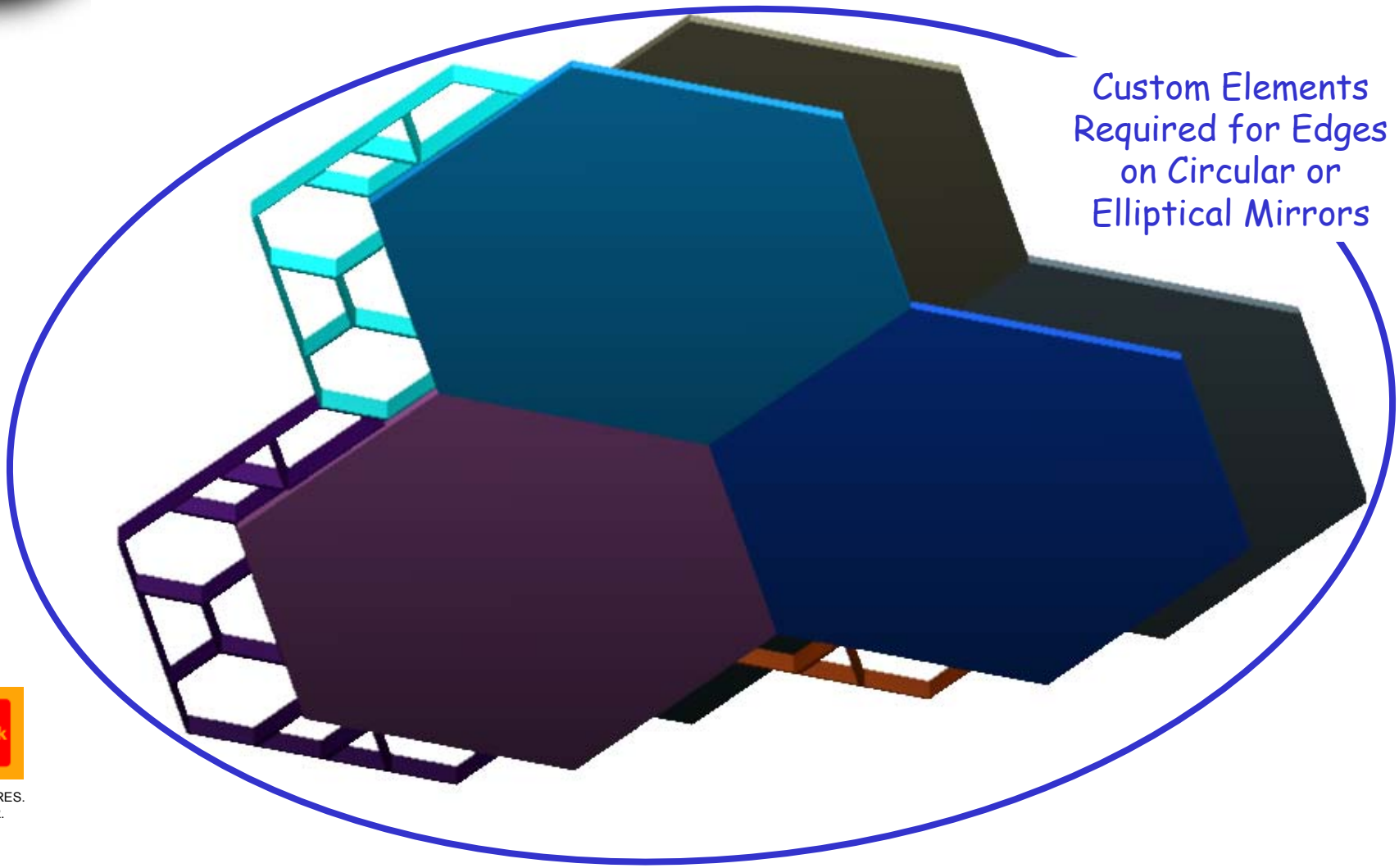

# TPF Mirror Finishing

- A new Small Tool Polishing (STP) Facility and Ion Figuring Facility will need to be provided with multiple heads to finish the large surface area of the monolithic PM
- The deterministic ion process will be used to achieve the difficult wavefront requirements

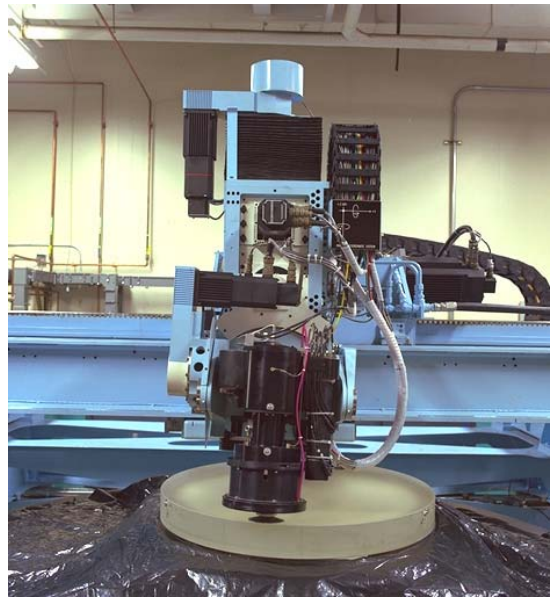

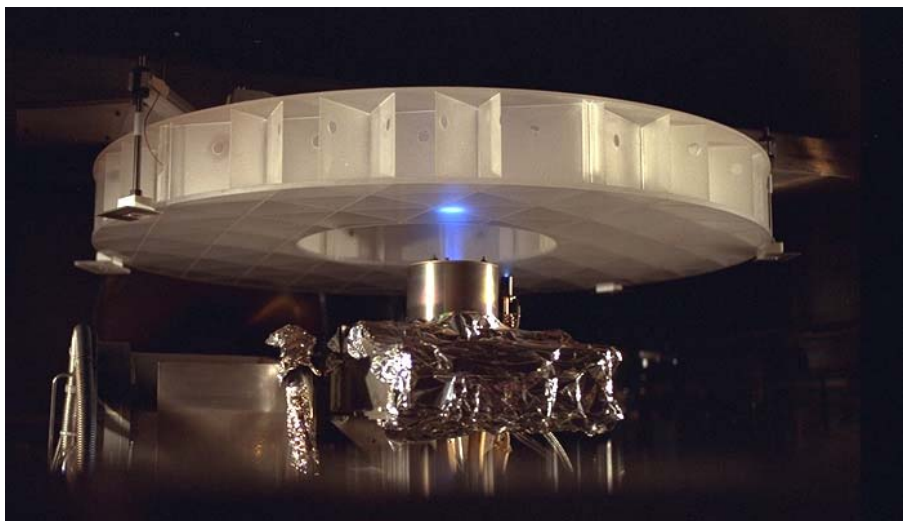

# TPF Primary Mirror Technology Development Plan

## OBJECTIVES

**Proof of Principle**
Produce 1/2 Meter Flat

- Develop processing technique using a flat lightweight optic with segmented face sheets.
- Demonstrate low spatial frequency surface control with actuators

**Segment Demonstration**
Produce 1+ meter powered segment

- Repeat above objectives on larger lightweight optic with power.

**Sub Scale Development**
Design, and build 1/4 scale Primary Mirror (PM)

- Achieve TPF requirements on subscale PM

**Full Scale Development**
Design and build full scale Primary Mirror

TAKE PICTURES. FURTHER.

# Technology Development Plan -- Proof of Principle

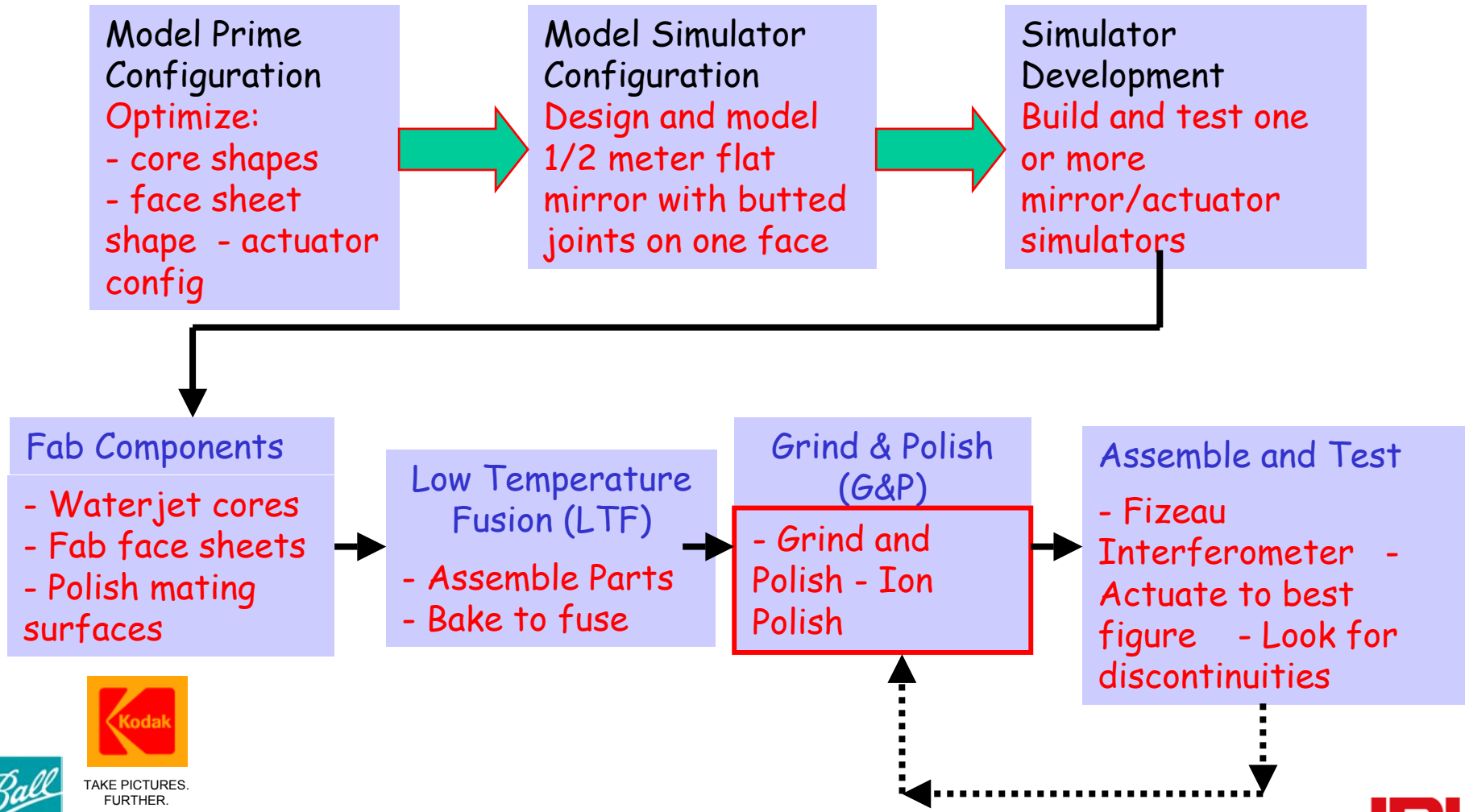


TAKE PICTURES. FURTHER.

# Technology Development Plan
# Segment Demonstration

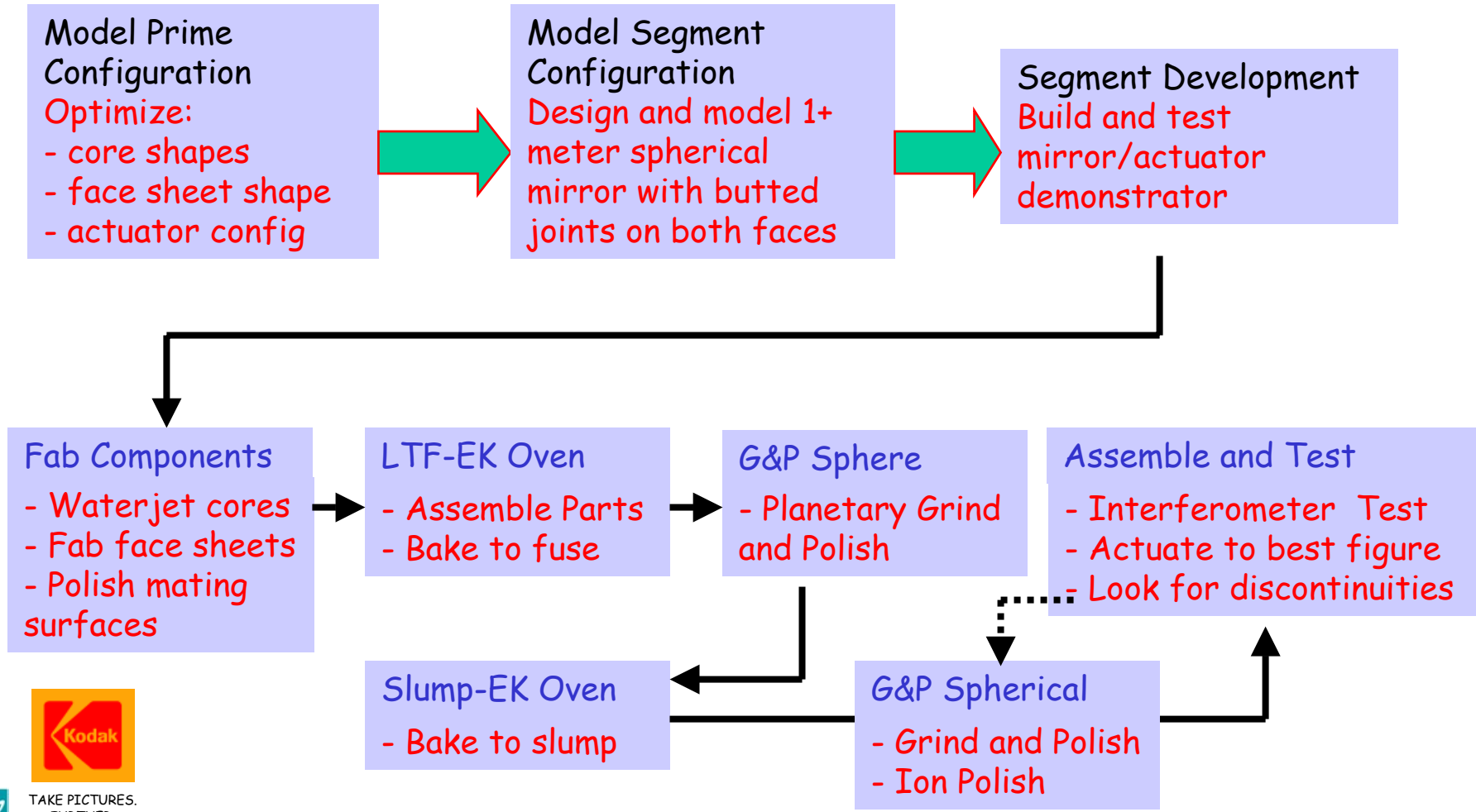


TAKE PICTURES. FURTHER.

# Technology Development Plan
# Subscale Demonstration

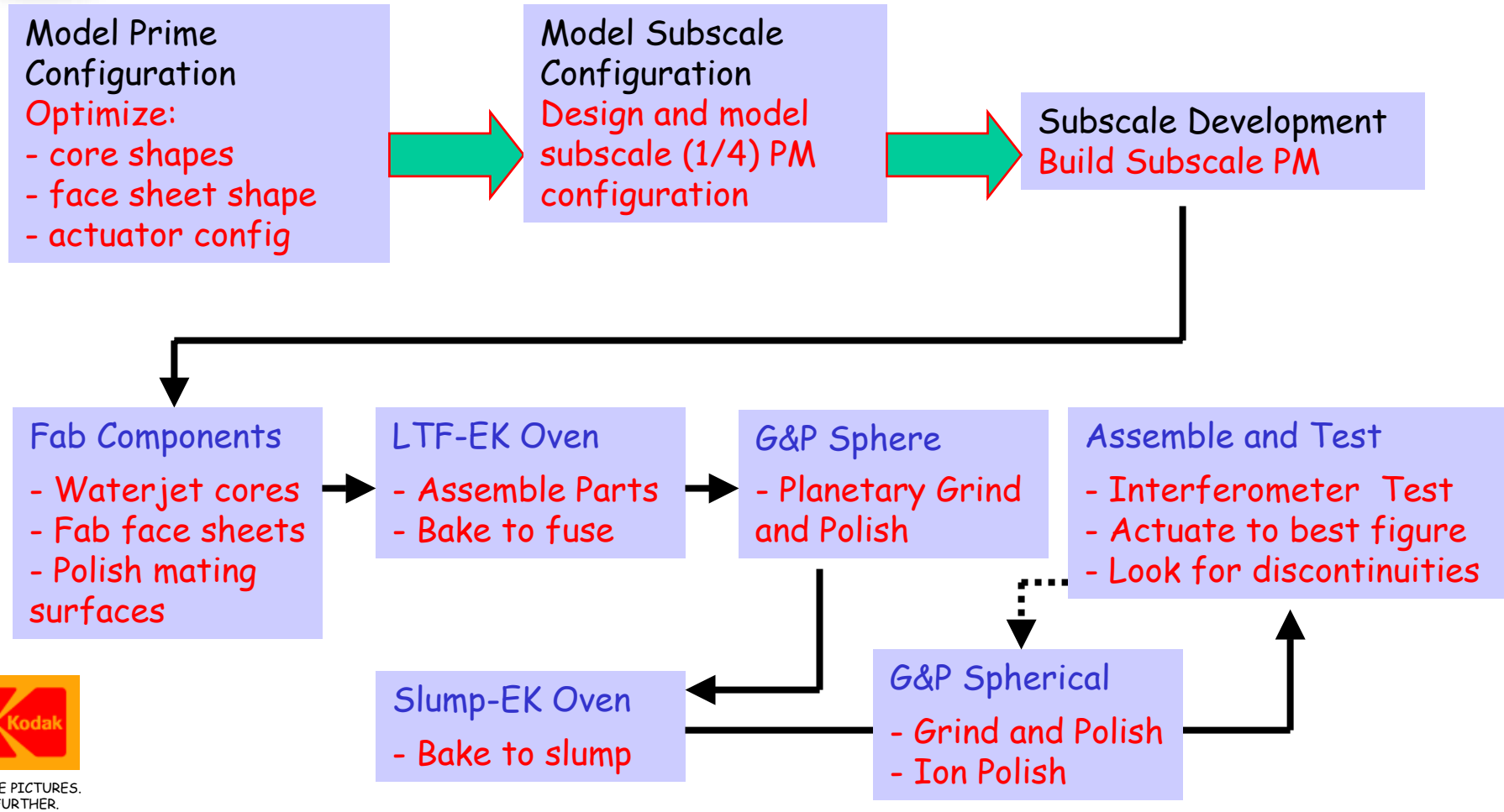

# TPF Primary Mirror Full Scale Development

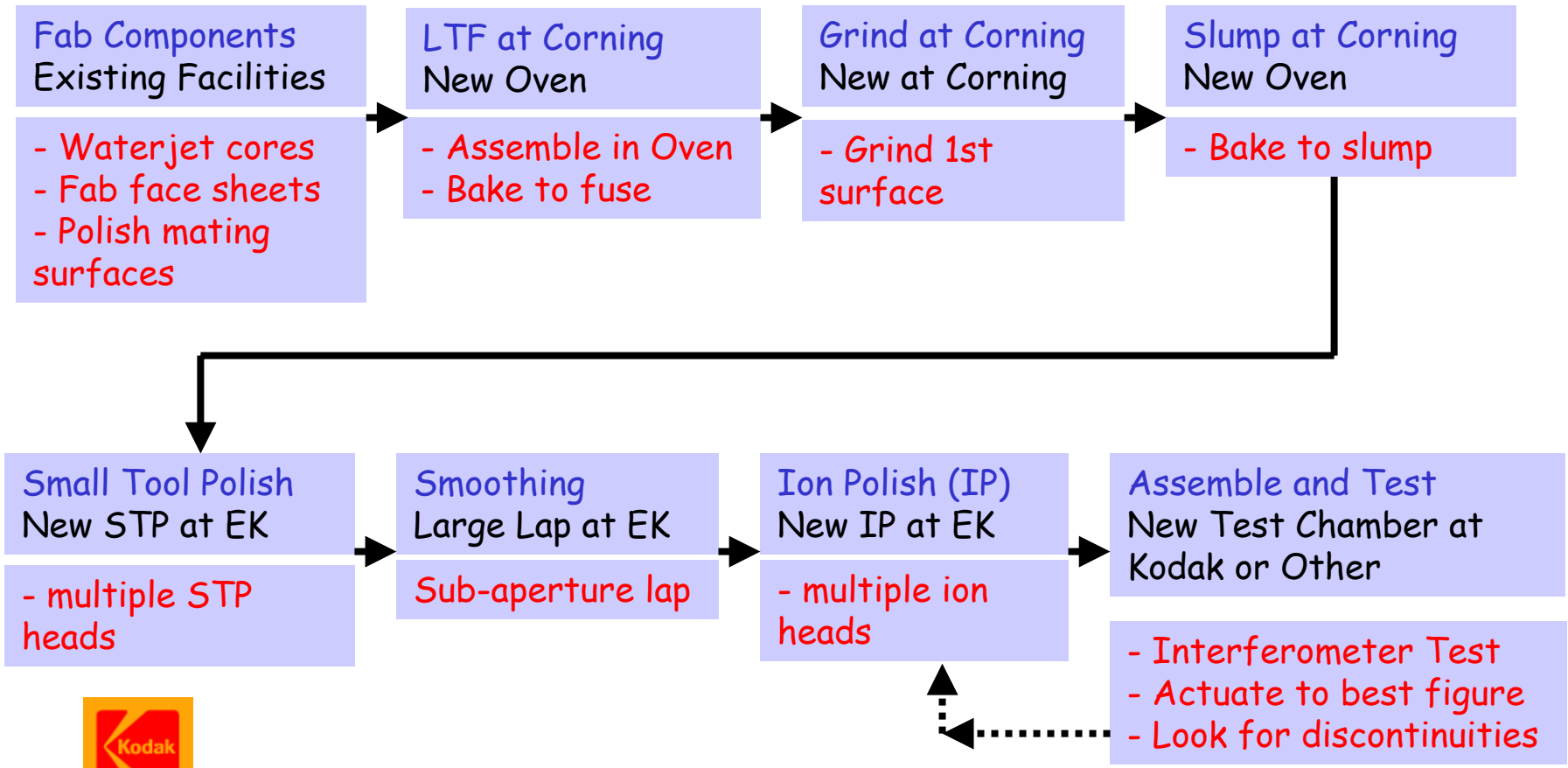


TAKE PICTURES. FURTHER.

# Kodak Glass Semi-Rigid AMSD For NGST

## Backup Material for TPF

TAKE PICTURES.
FURTHER.

# Eastman Kodak AMSD Status as of 10/2001

## Glass semi-rigid design

- ULE facesheet (1 mm thick)
- 3.4 mm thick core composed of 19 individually waterjetted ULE subsections
- Facesheet, core, and backplate fused to achieve sandwiched glass construction
- Design consists of 22 actuators at 19 contact points (6 rigid body in 3 bipods, 16 force actuators); for AMSD rigid body actuators will not fabricated
- Composite reaction structure

## Fabrication status

- Original facesheets and cores fabricated and integrated using low temperature fusing
- Handling operation revealed some areas not fully fused; another ULE mirror assembly is ready for fusion

TAKE PICTURES. FURTHER.

# Glass Mirror System Overview

- Lightweight stiff ULE mirror (sandwich construction)
- Stable composite reaction structure
- Single design for AMSD ambient & cryo

3 stiff displacement actuators
- kinematic mirror mount
- 3 DOF mirror rigid body control

16 soft force actuators
- mirror radius & figure control
- gravity off-loading

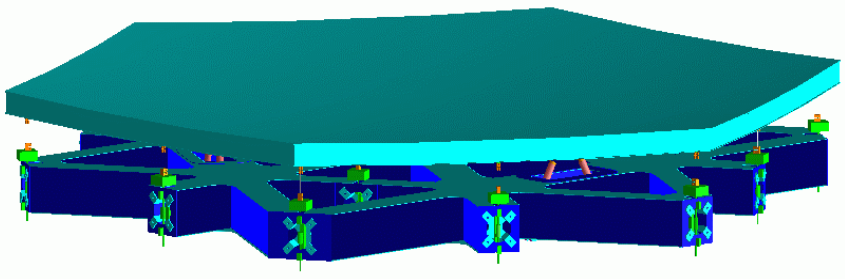

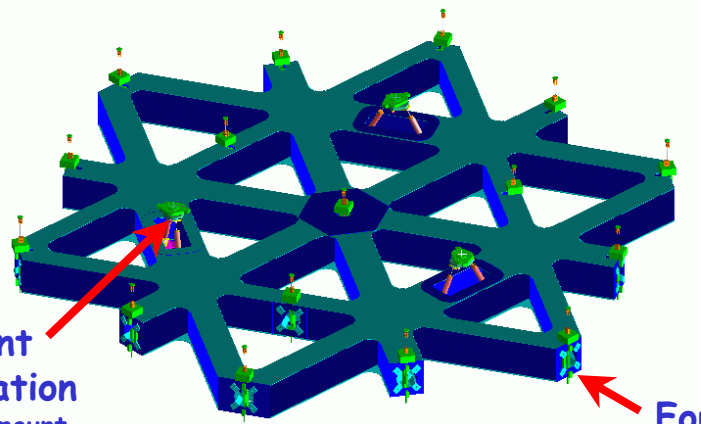


TAKE PICTURES. FURTHER.

# Mirror Description

- 1.4m x 3.40cm
- <12 kg (<8 kg/m2)
- fn = 151 Hz free
- Construction
  - all ULE glass
  - segmented core
  - AWJ cut core
  - low temp fusion
  - low temp slump
- 21 parts total
  - 2 face plates
  - 13 full-hex core seg
  - 6 half-hex core seg.

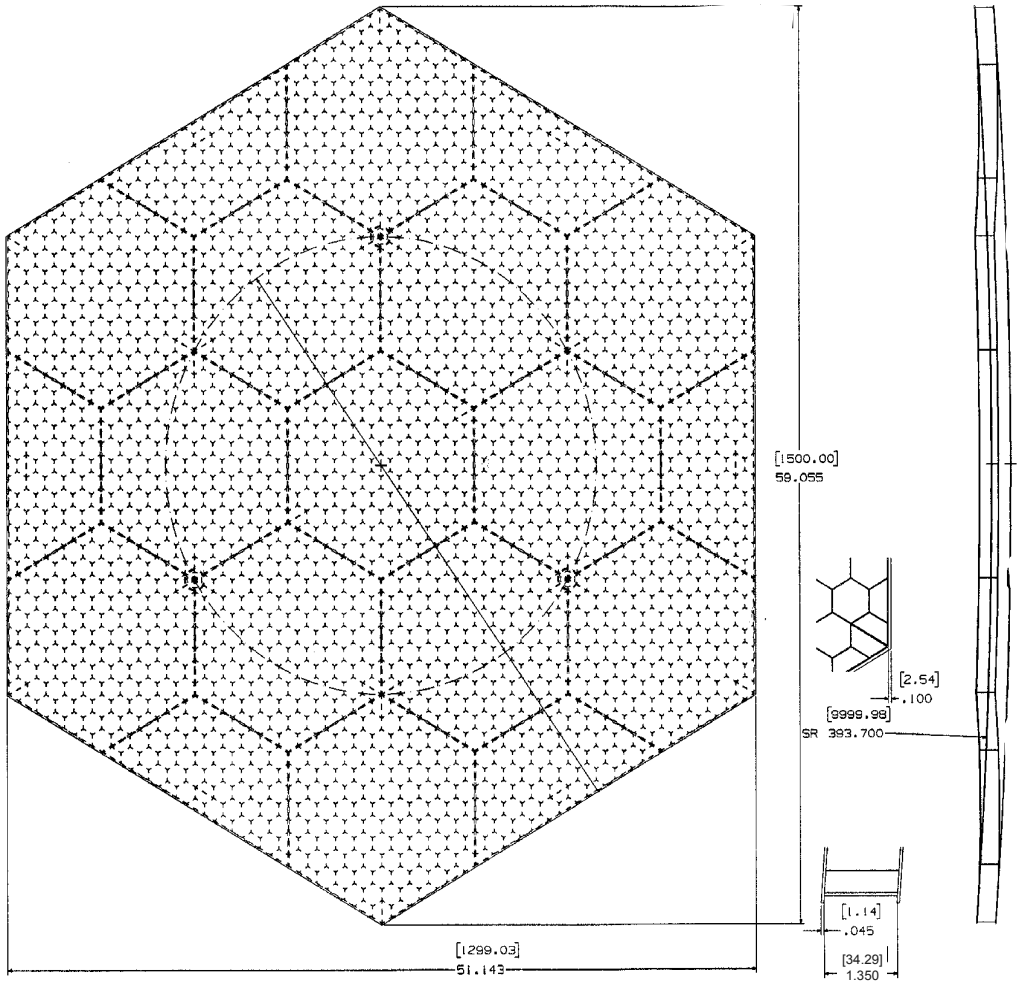


TAKE PICTURES. FURTHER.

# General Program Status

- Mirror blank component processing went very well
  - Processes developed that will allow the generation of mirror blanks very quickly
- Low temperature fusion (LTF) appeared to go well
  - Highest break strength values ever recorded on T-Box samples
  - Better than 99% fusion of the joints
  - Minimal devitrification
  - Overall LTF process was not successful
    - Mirror shows "debonding" in some areas
    - Additional small delaminations appearing over time
  - Investigation into the problem has identified the most probable cause
- Replacement ULE mirror ready for fusion at COI

# AMSD Mirror Fabrication

Mirror core segments and top and bottom facesheets fabricated

Combined with low temperature fusion technique

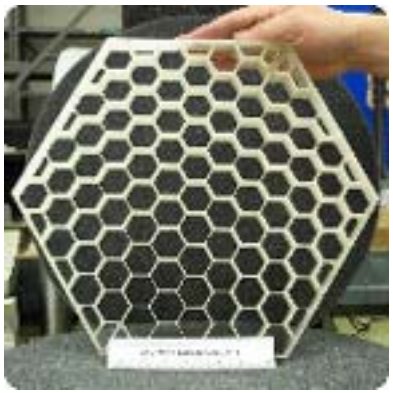

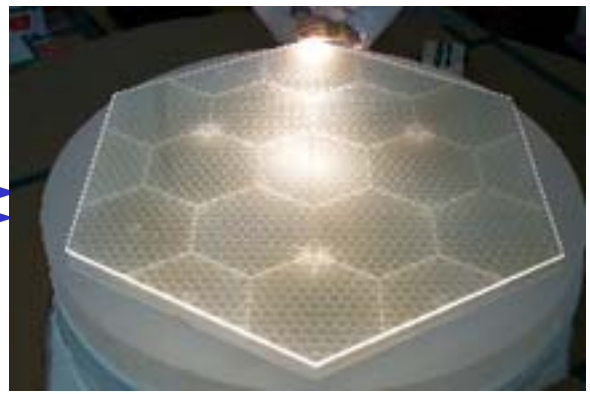

TAKE PICTURES. FURTHER.

# AMSD Program Summary

- Even though Kodak experienced an LTF failure that caused the loss of the first ULE mirror, no technology issues have been identified
- Most probable cause has been identified
  - Samples have been fabricated that demonstrate a robust process
- Kodak is moving forward with a replacement mirror program that supports the decision date for NGST primary mirror selection

# Section 5.
# Modeling Approach & Results

Mike Lieber, Charley Noecker

Model Descriptions
Results of Modeling and Simulations

# Overview of TPF Performance Modeling(1/2)

- **Both focused models and fully integrated system modeling(ISM) used for design development and performance evaluation**

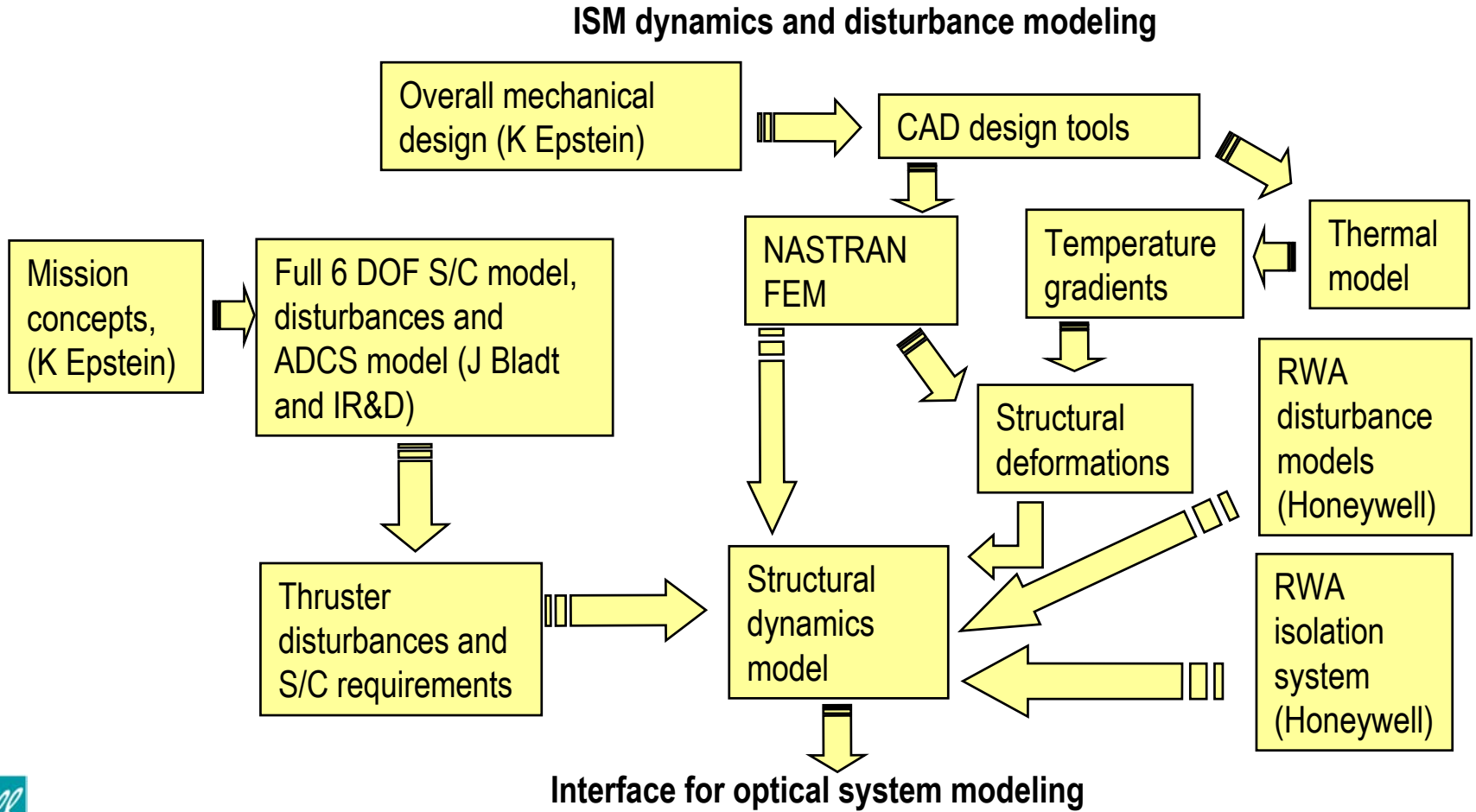

# Overview of TPF Performance Modeling(2/2)

**Phase I Architecture Definition and Science Requirements**

Science Requirements and phenemenology Bob Brown & Team

Orbit and Sky Coverage Ball (D Ebbets)

Architecture definition, Charley Noecker

**Departure point for modeling presented in current phase**

Further characterization of candidate star/planet systems (D Ebbets)

Radiometric models of star/planet systems

Code V optical design (B. Woodruff)

ISM of optical system

Sensitivity issues, quasi-static and dynamic disturbance effects, end-to-end system issues

Focused optical models

Multiple pupils, spectral and scatter issues, pupil configurations, numerical methods, optical model development, wavefront quality, sensitivity issues (C Noecker)

Detailed design, analysis and optimization Spergel pupil (D Spergel, J Kasdin)

Optical system consultant (C Burrows), wavefront quality and diffraction analysis, DM issues,

# Integrated Modeling of TPF - Simulink/Matlab Environment

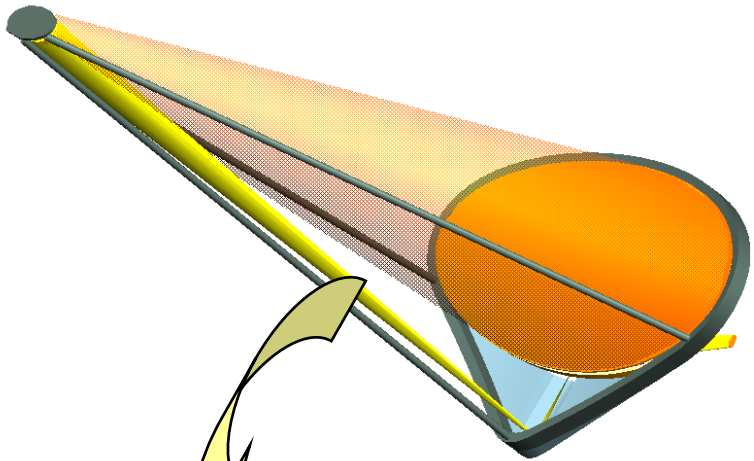

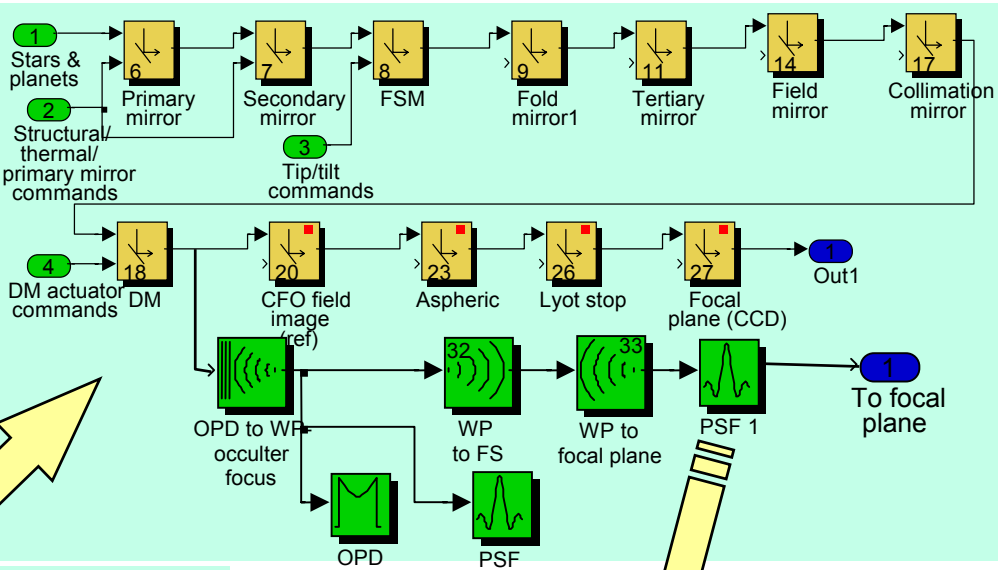


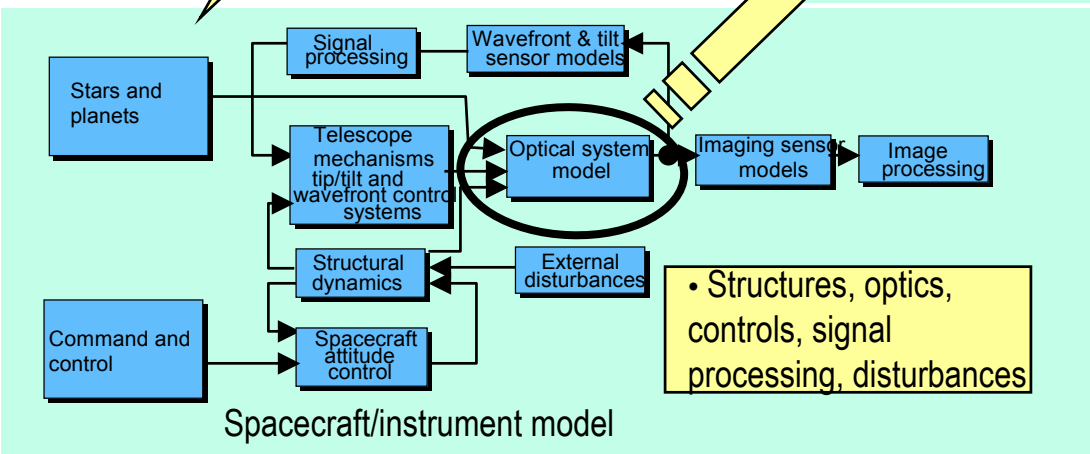


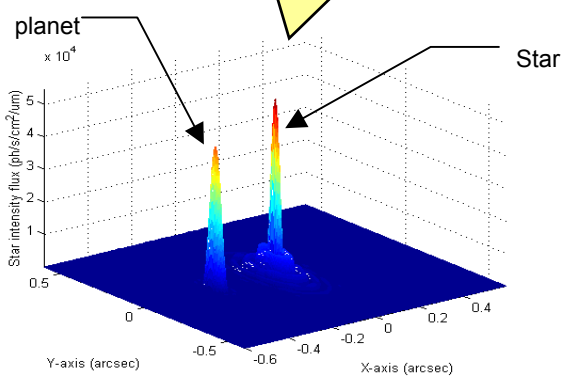

# Optical layout for integrated model

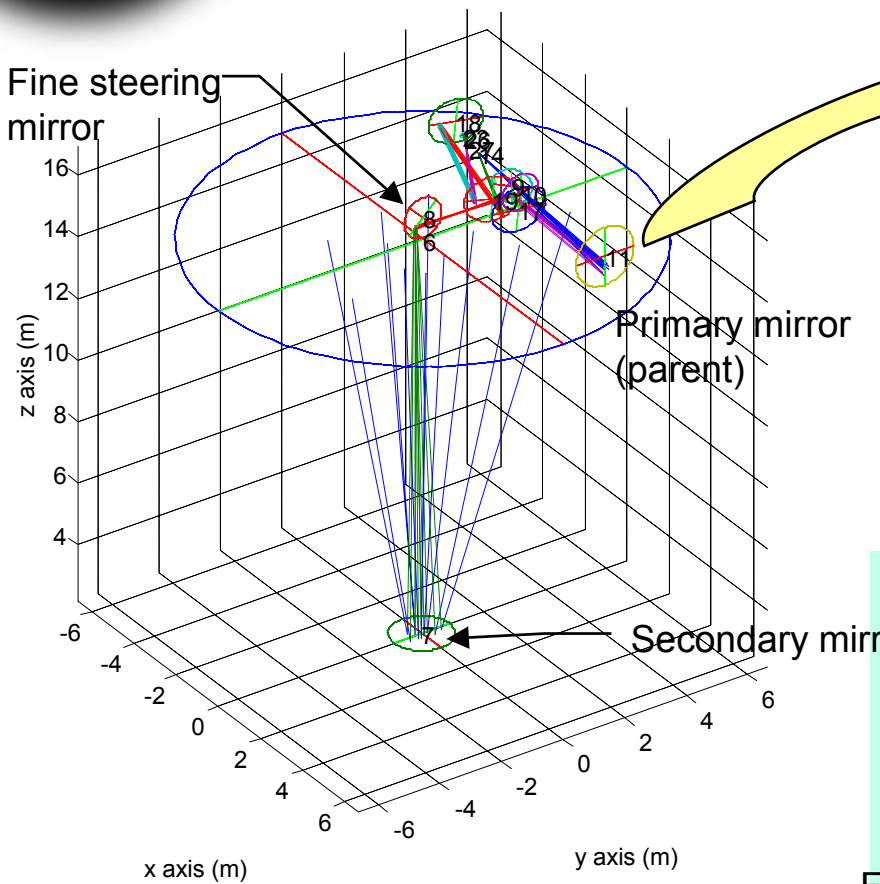


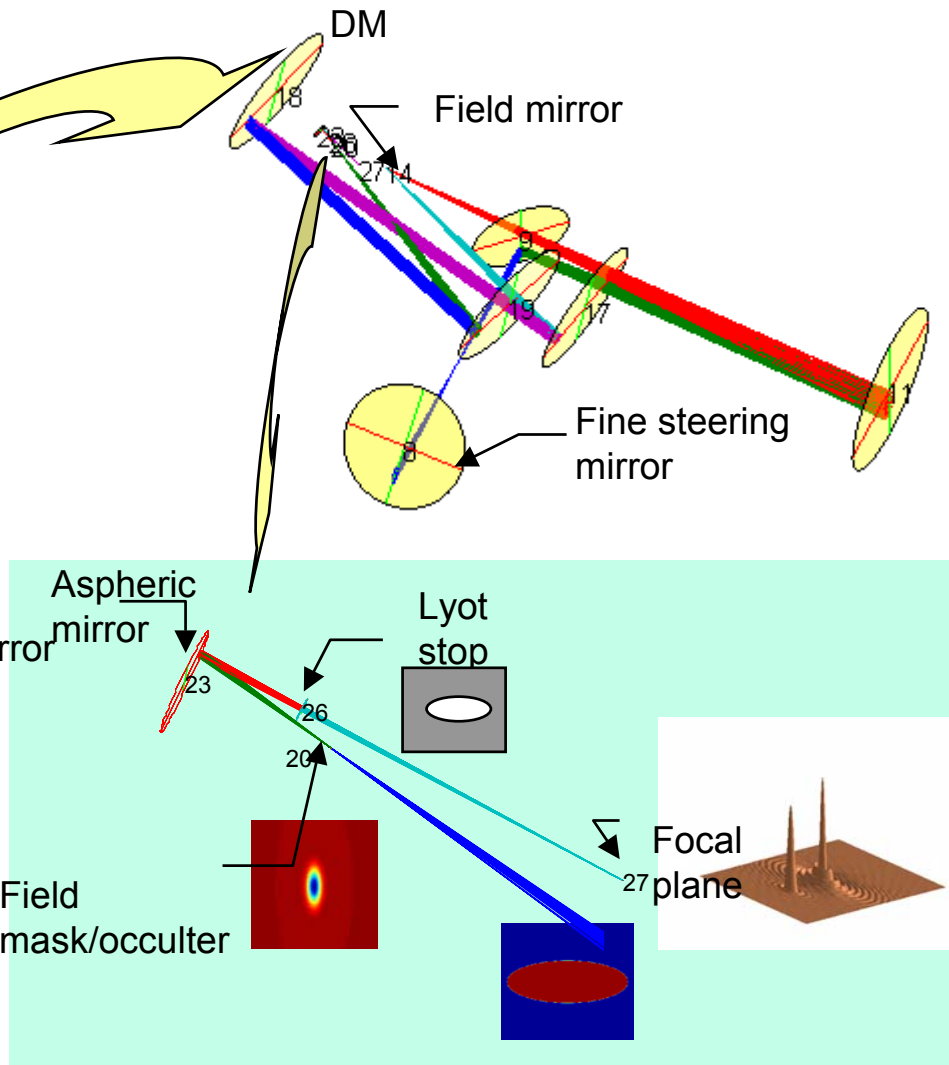


•Ray tracing, sensitivity matrices, diffraction calculations

# Baseline Evaluation of Shaped Pupil Concept

- Shaped pupil creates broad valley for planet discovery
- Epsilon Eri - earth size planet at 1 AU, with 4.16e10 and 4.81 ph/s/um for star and planet respectively
- Optimization trade between Spergel pupil tail extent, fundamental noise floor and IWD.
- Omits effect of wavefront ripple

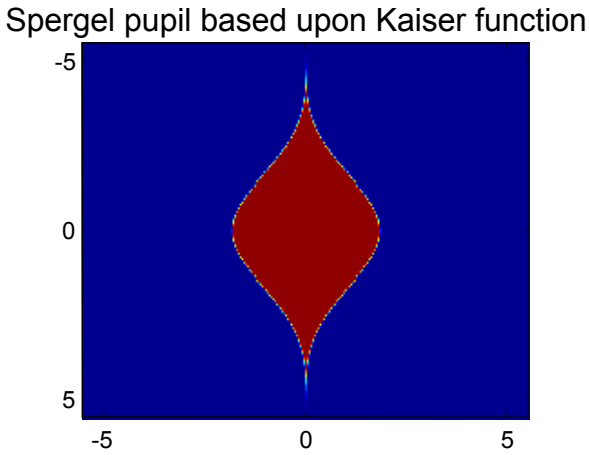


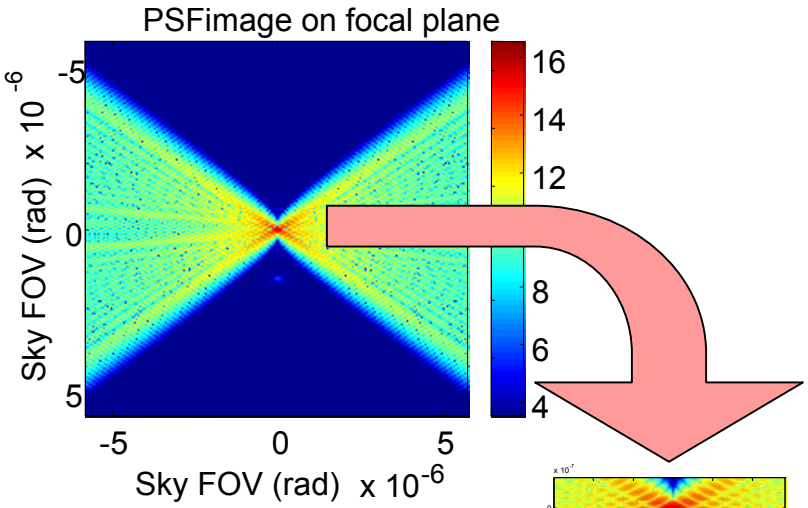


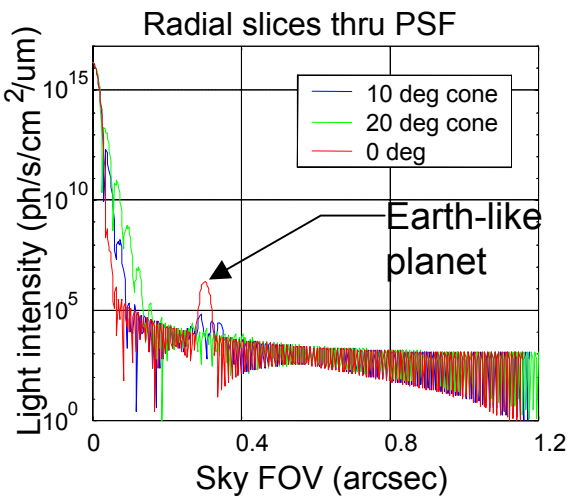


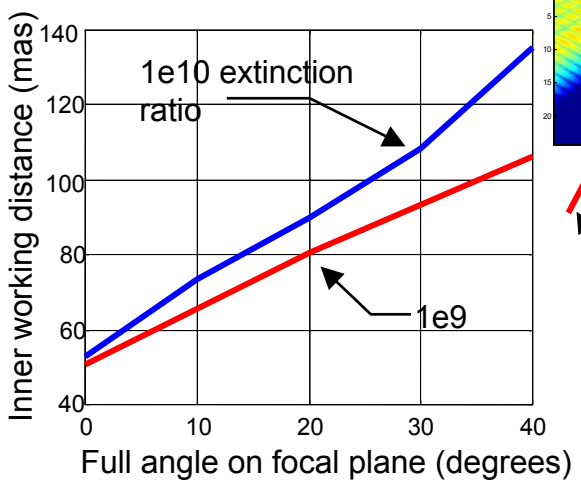


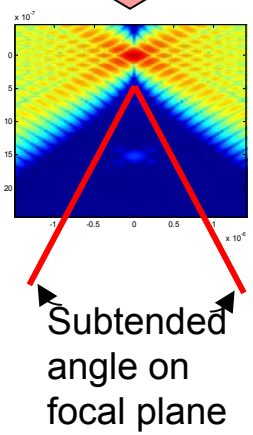

# Baseline Evaluation of Elliptical Pupil Concept

- Elliptical mask 4x10m (31 m^2 area) with Tau Ceti as input star
- 1-Gaussian mask at field stop - 4 sigma radial
- Lyot stop 1/2 dimension of pupil image

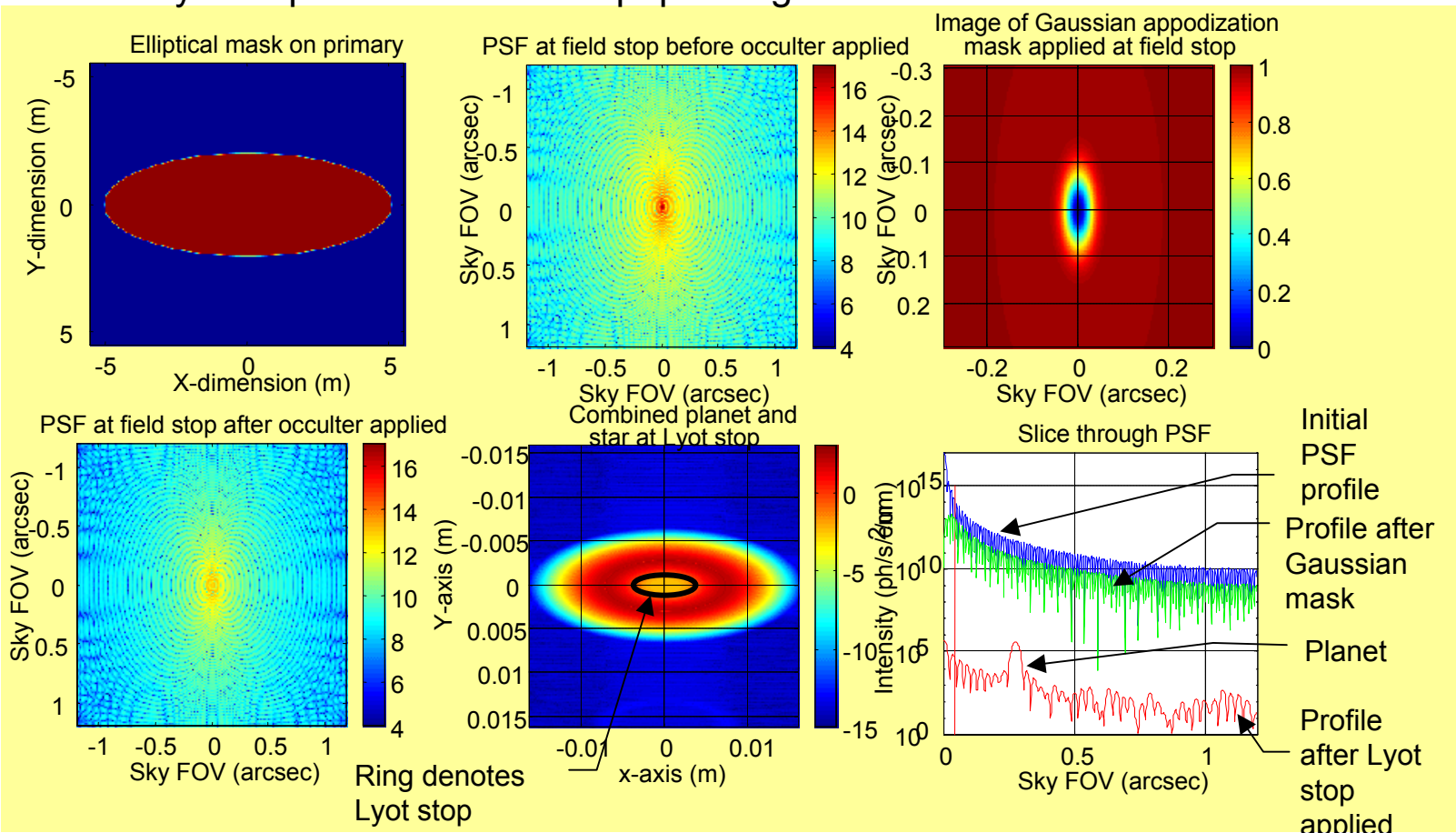

# Classical Coronagraph Throughput depends on desired IWD

- CFO mask/ Lyot stop combination is optimized for planet SNR at a chosen IWD
  - Small IWD ⇒ small CFO
  - To maintain constant Q, must decrease Lyot stop throughput
- 0.1nm RMS residual thermal distortion assumed

Change in light transmission versus IWD with matched Gaussian mask/Lyot stop

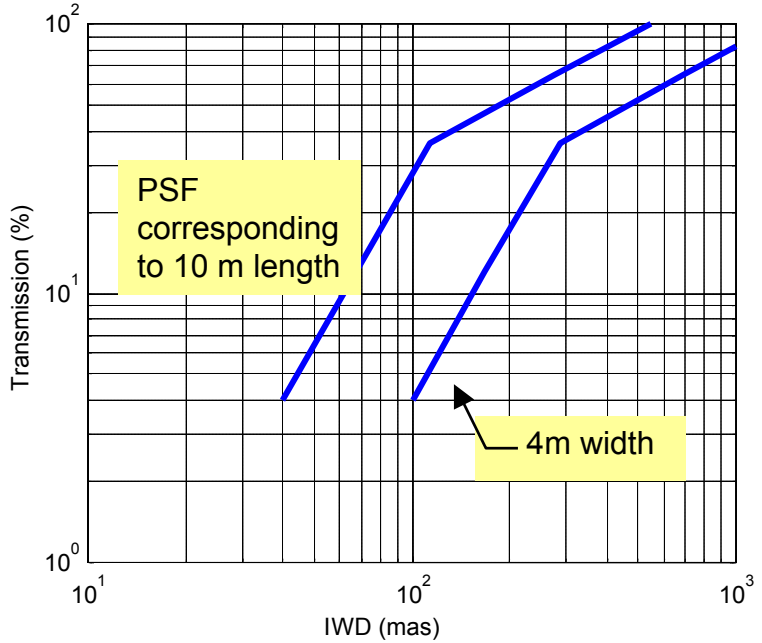


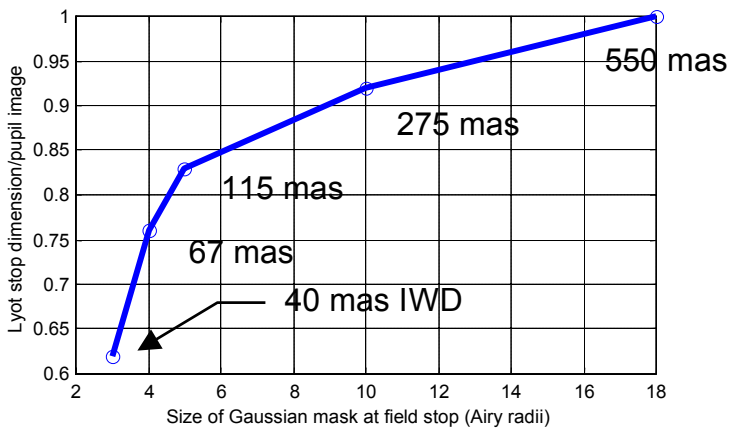


- For the classical coronagraph, throughput suffers for the closest IWDs
- For shaped pupils, the IWD is largely fixed by pupil length

# Classical coronagraph sensitivity to star pointing errors

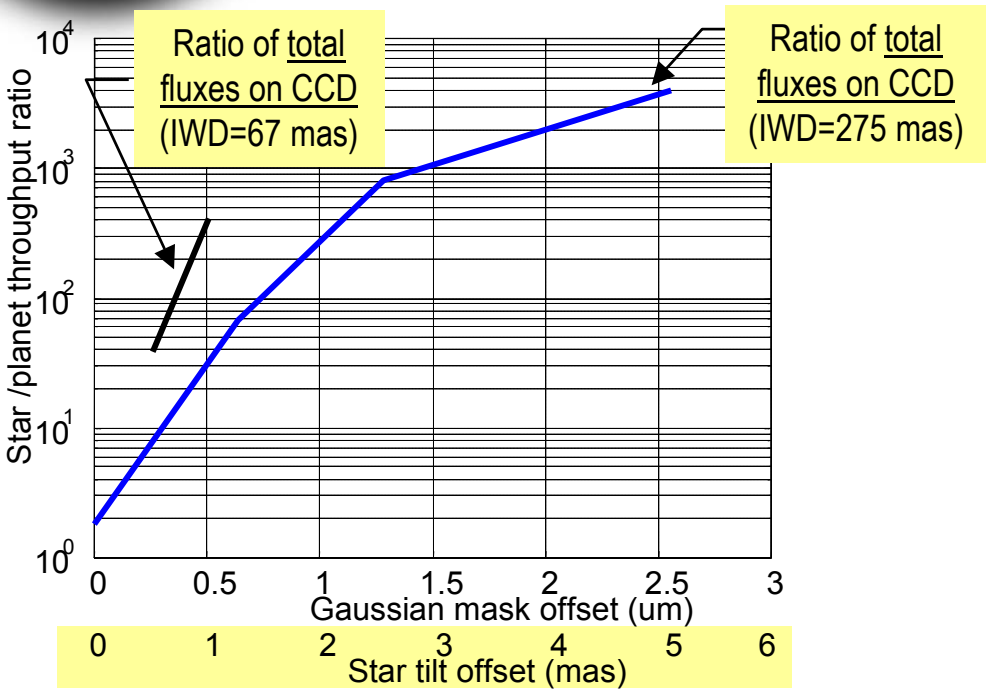


- Analysis also shows Q degrades from 2.5 to 1 at
  - 1 mas for the 67 mas case
  - 3 mas for the 275 mas case
- Current 1 mas pointing requirement may be insufficient

- Line plots show the ratio of total starlight to total planet light across the focal plane as a function of mispointing from the CFO.
  - This is a measure of residual aperture diffraction
  - Black: CFO/Lyot tuned for 67 mas IWD
  - Blue: CFO/Lyot tuned for 275 mas IWD
- Leakage sensitivity to offsets is higher for 67 mas
- Shaped pupil is much less sensitive to small star and mask displacements (monochromatic)

# Thermal Deformation Tolerances

- Thermal distortions can spread starlight onto planet pixel, decreasing "Q"
- Wavefront map from thermo-mechanical model shows mainly low-order aberrations
  - Calculated magnitudes are suspect
  - But the aberration composition should be typical of thermal distortions
  - Very low spatial frequencies
- Tolerance is sub-nanometer for a CFO/Lyot with IWD < 100 mas
- Shaped pupil seems more forgiving

Representative wavefront of a highly thermally deformed surface

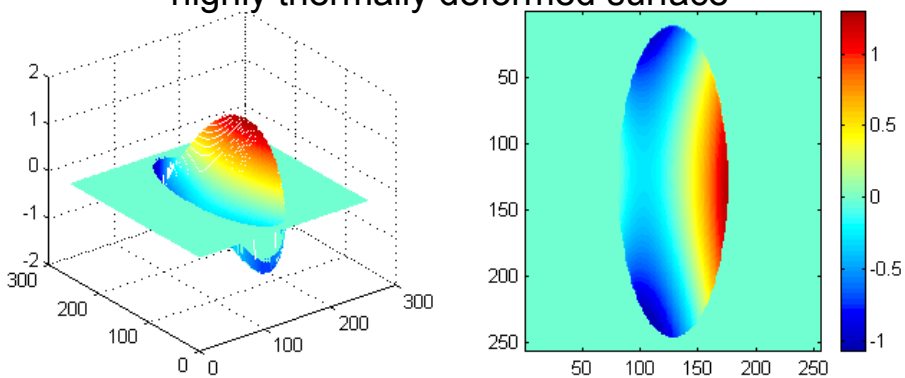

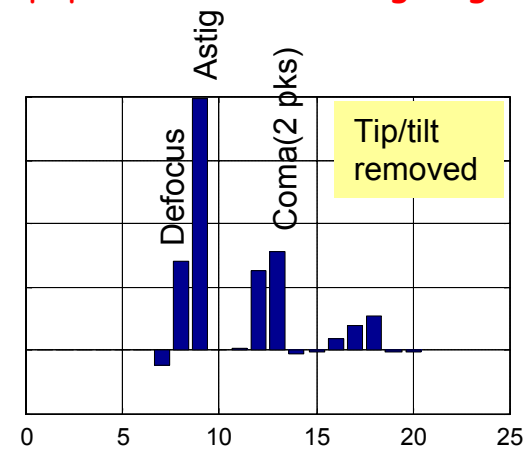


RMS value for a WFE with this aberration composition that decreases Q from 2.5 to 1, for IWD-optimized coronagraph parameters

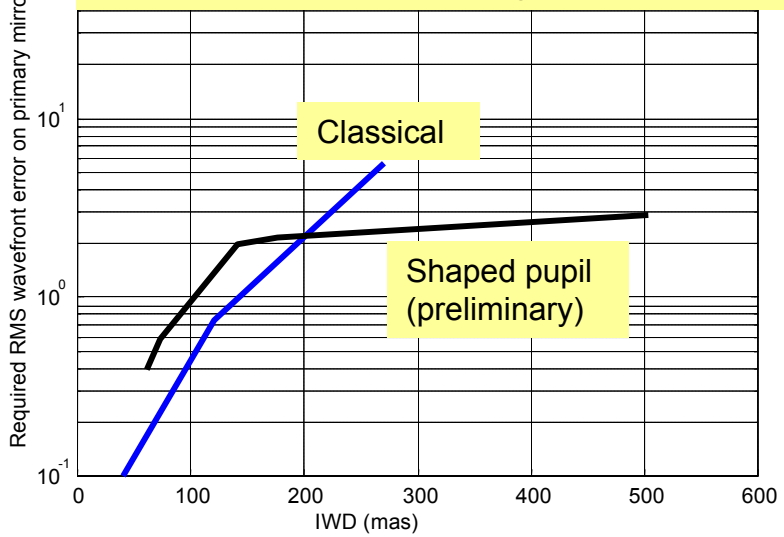

# Thermal effects on wavefront errors

- First order finite-element thermal model of primary mirror
  - With full sunshield
  - Divided mirror into 500 elements
  - Examined effects of large azimuth slews (no change in star) separated by 8 hour integrations
- Results
  - Front-to-back temperature difference changed by 1.2 mK over 8 hours
    - Coherent across full mirror, with rms ripple of ~0.1 mK
  - We calculate 0.03 Å peak-peak ripple on front surface due to glass only
    - Assumed ULE glass with CTE of $10^{-8}$/K
- The mirror backing structure has not been included yet
  - Will add a large low-frequency contribution to deformation
  - Design has not been optimized to control thermal deformations

# Impact of vibrations on pointing

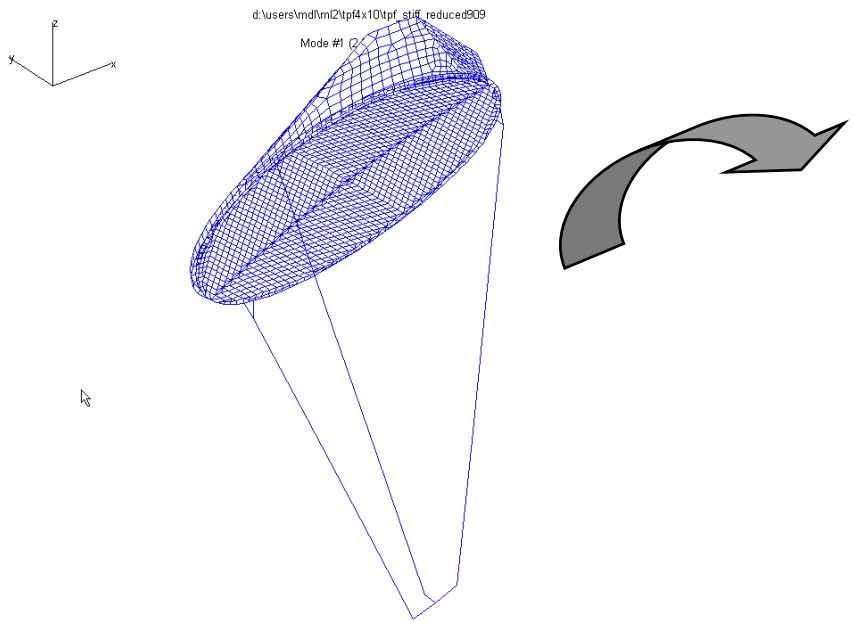


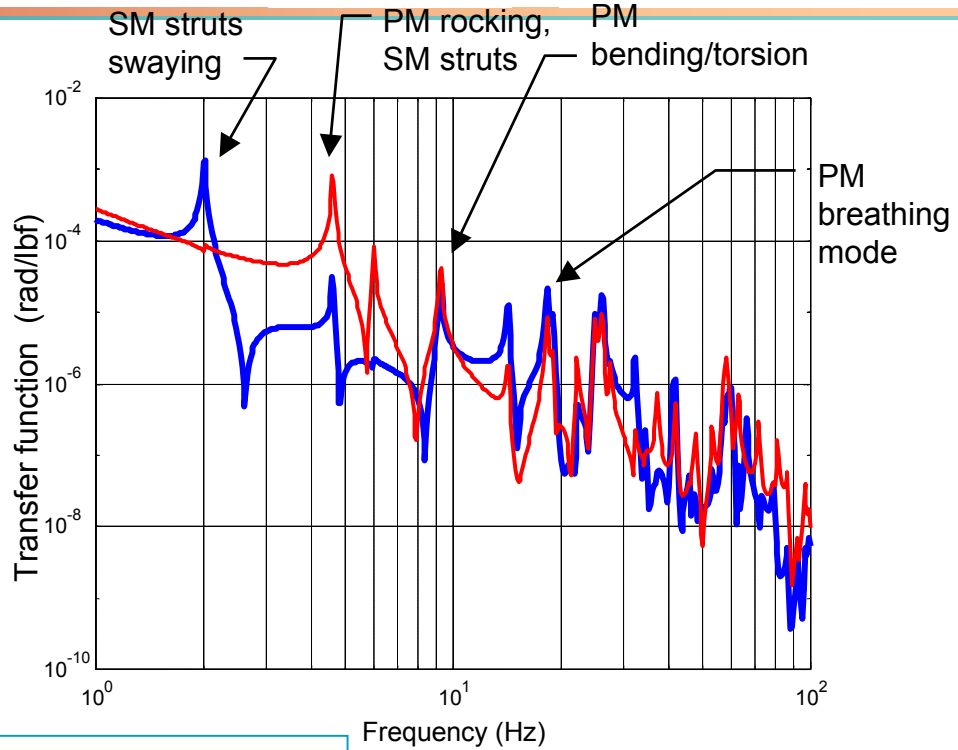


- Transfer function from reaction wheel forces to x and y tilt at focal plane
  - only strongest component is shown.
- Includes 42 structural modes out to 100 Hz
- Assumes damping of 0.5% for all modes

# System Level Consideration of Best Approach to Disturbances

- Design the system to minimize disturbance at source
  - generally more complex and costly to correct a disturbance after it enters system
  - Well-balanced reaction wheels and soft isolation
  - Sun shields designed to minimize WF disturbances during imaging
- Multiple-layer control systems for high-dynamic-range disturbance rejection
  - Body pointing for coarse pointing + FSM for fine pointing
  - Primary mirror for coarse wavefront correction, DM for fine correction
- Follow control engineers' mantra:
  If you can, measure directly what you are trying to control, e.g.
  - Position sensors for position problems
  - Direct image-plane tip/tilt measurements, rather than structure-mounted sensors

# Reaction Wheel Disturbance Modeling

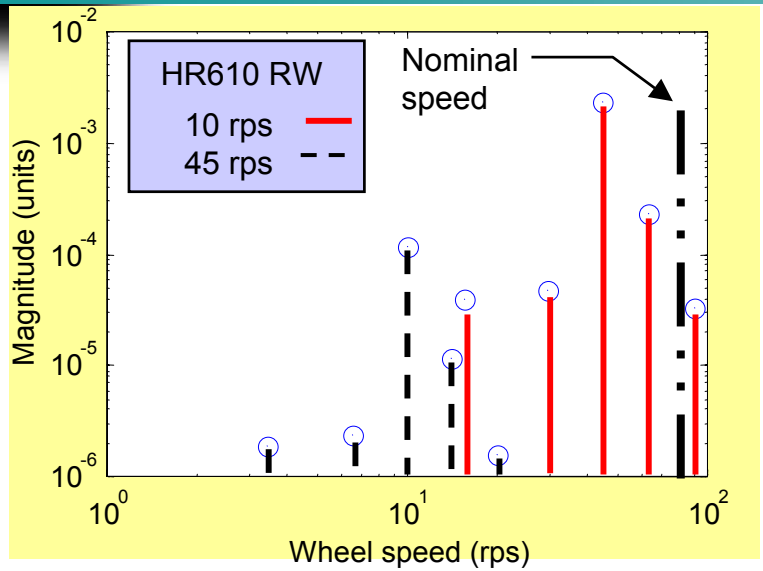


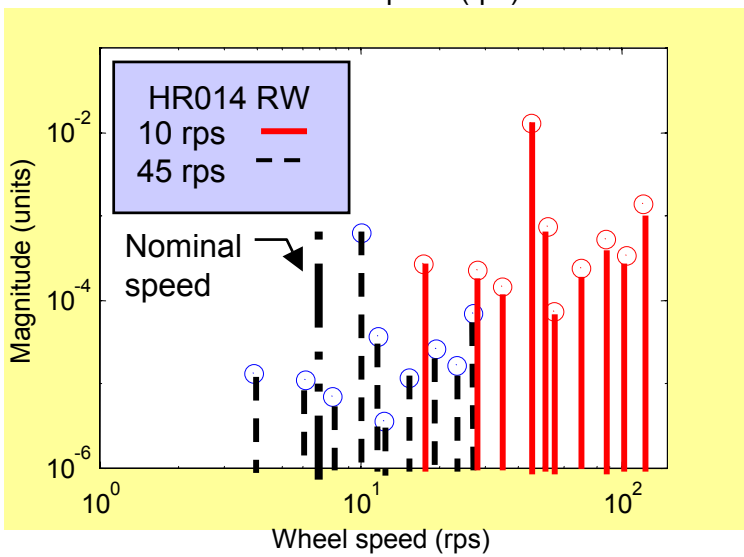


- Cluster of 5 wheels on single pallet
- Wheels are balanced to HST levels to minimize out-of-balance induced forces and torques.
- Forcing components increase by (wheel speed)$^2$.
- Internal resonance at 90 Hz included
- Radial forcing harmonics shown in figures for small fast wheel (HR0610) and large slow wheel (HR 014). Fundamental wheel harmonic provides dominant disturbance.
- Disturbance is applied to a node of the coupled structural/optical model

# Wheel Isolation Greatly Reduces LOS Jitter at High Frequencies

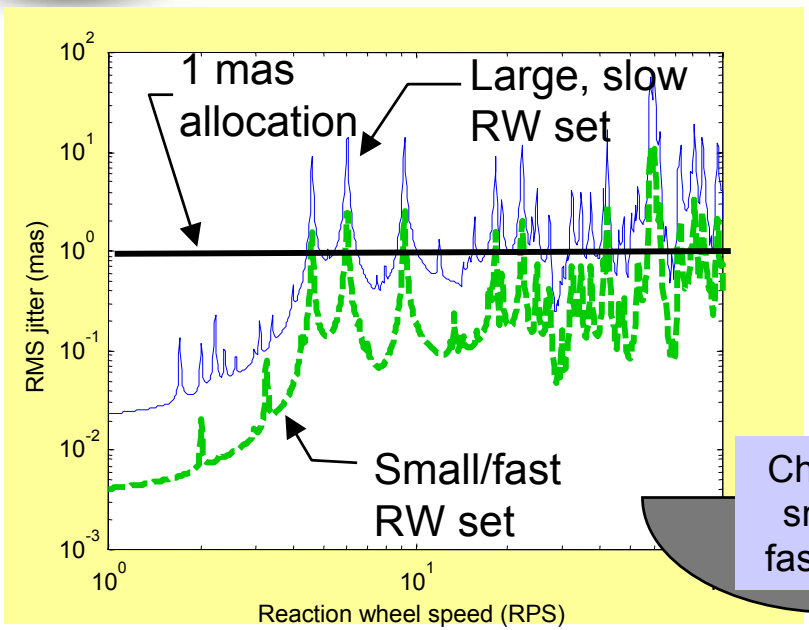


Choose small/ fast RW

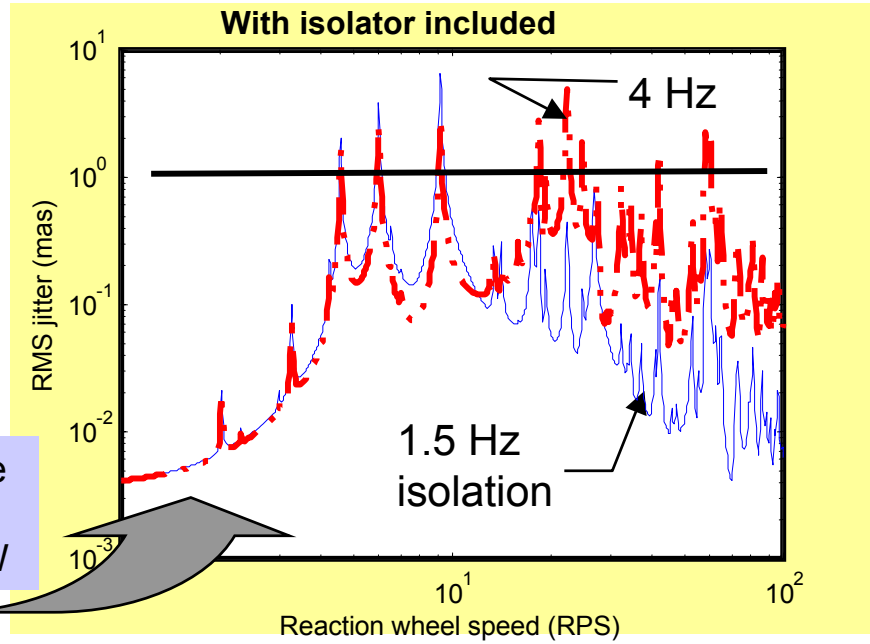


- Line of sight jitter is below the 1 mas RMS requirement over most speeds.
- Small/fast wheel produces less jitter than the larger wheel
- HST-class wheel with 1.5 Hz isolation will meet requirements except at a few resonances.
- These results are open-loop – they don't engage fine steering mirror pointing loop

# Isolated RWA Array

4/4 RWA Array

Beta = 30.5

Gamma = ± 20, ± 160

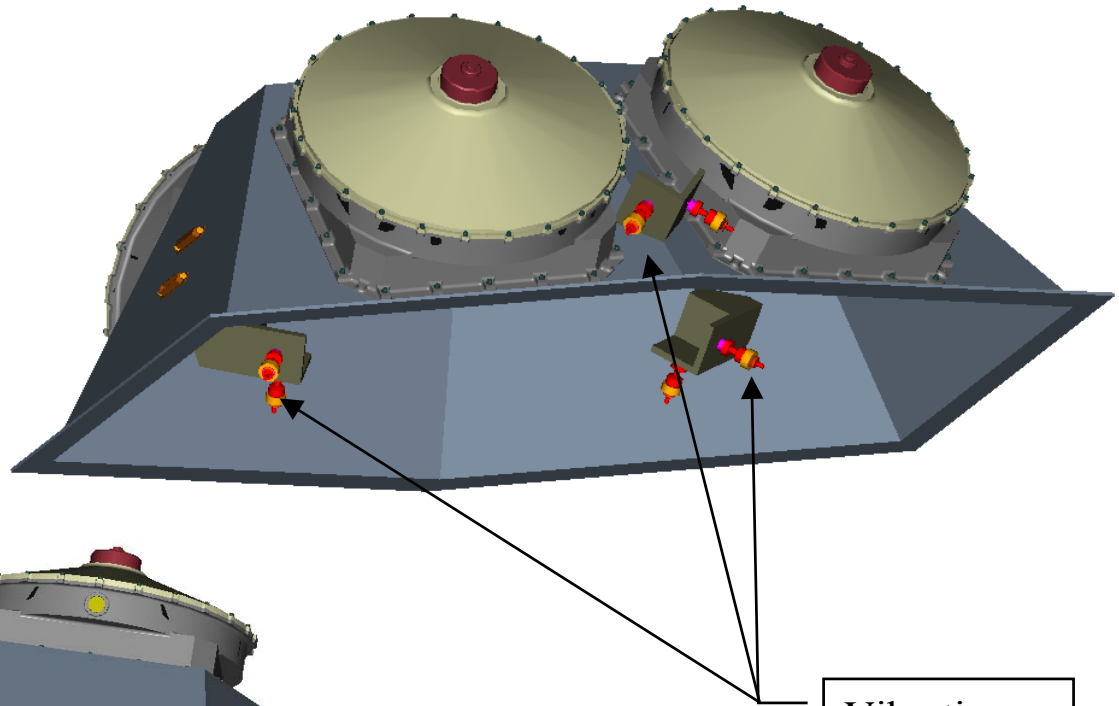

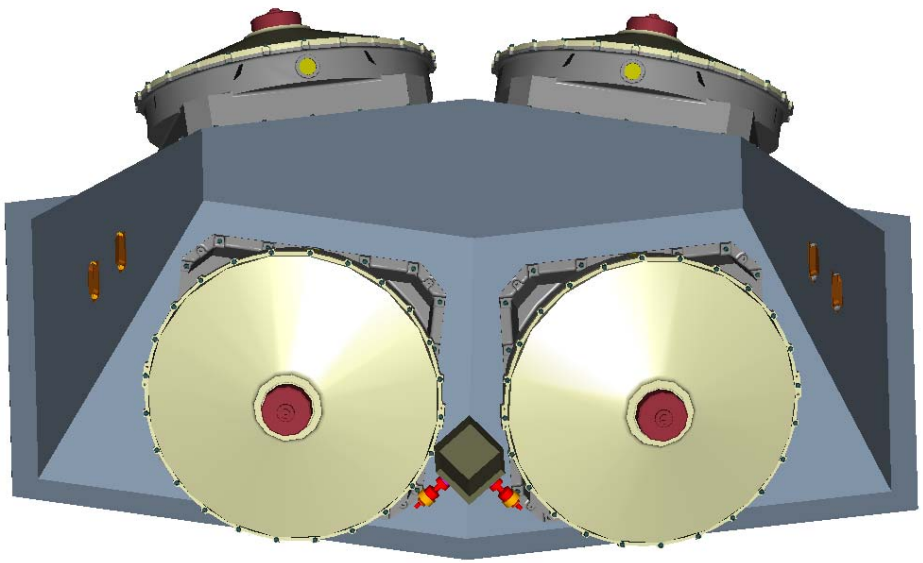

Vibration Isolation Hexapod

Strut heritage to MVIS design (built for AFRL in 1998)

- passive 1.5 Hz
- active can be added as option

# Isolator design tool 1.5-Hz transmissibilities

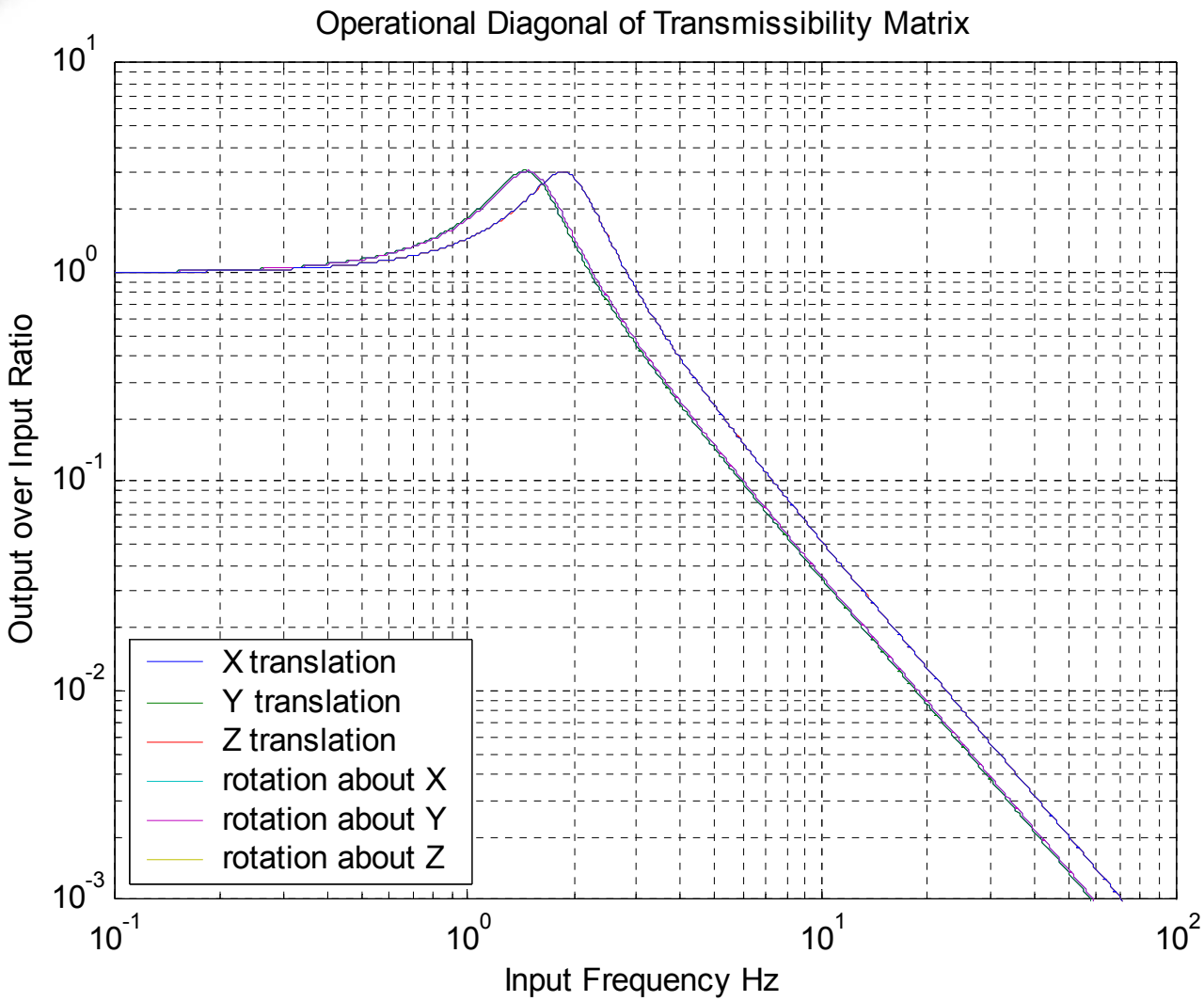


Backup charts

# Dynamic mirror distortion due to wheel harmonics is expected to be tolerable

- Without isolator:
- Worst-case primary mirror deformation (41 Hz)
- Gives spatial/ temporal RMS = 8.4nm (~17 nm WF error)

- With 1.5 Hz isolator:
- Worst-case primary deformation (4.6 Hz)
- Spatial/temporal RMS 0.05 nm (~ 0.1 nm WF error)
- Doubling wheel speed expected to suppress by > 10x

**Movie of primary mirror deformation**
**no RWA isolation**

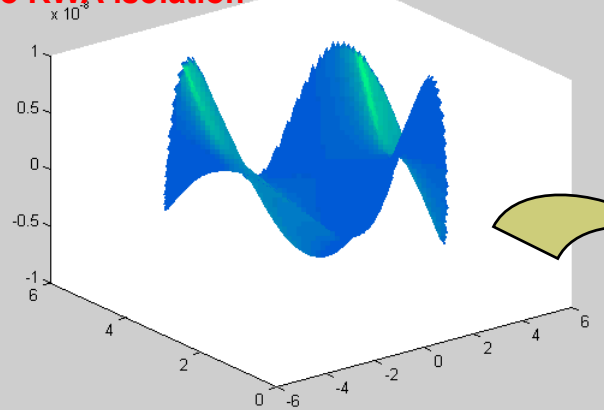

**Movie of primary mirror deformation**
**with RWA isolation**

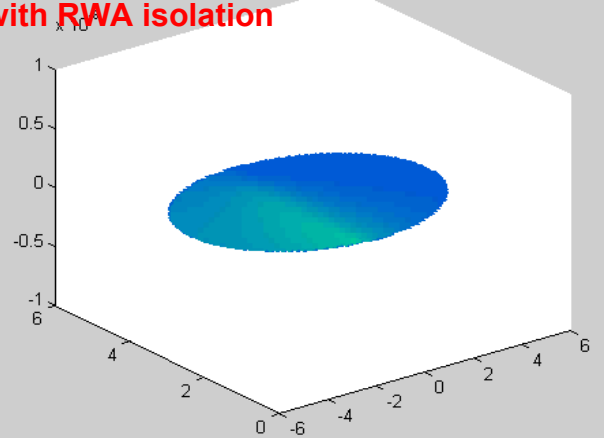

**Movie of star/planet PSF**
**no RWA isolation**

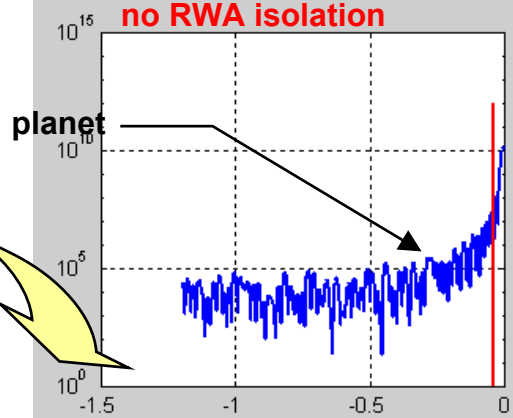


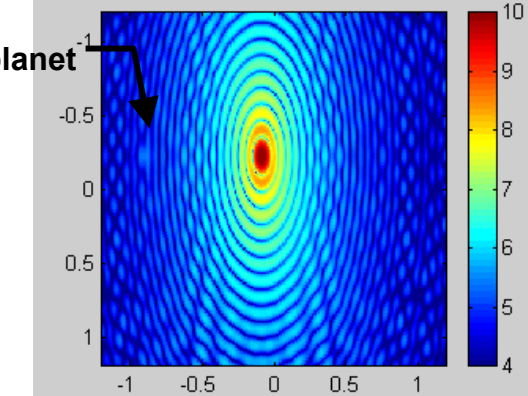


Note : Tip/tilt component removed - deformation only.

# ADCS And Thruster Models

- Full 6 DOF spacecraft model, based on IR&D development
  - 5 wheel system
  - PID controllers,
  - Torque management,
  - Slew profiling,
  - Thrusters,
  - Quantization models,
  - Solar pressure disturbances
- Model predicts effect of ADCS control on imaging performance
- Plot shows example using FEEP thrusters
  - total external torque over 200 s span

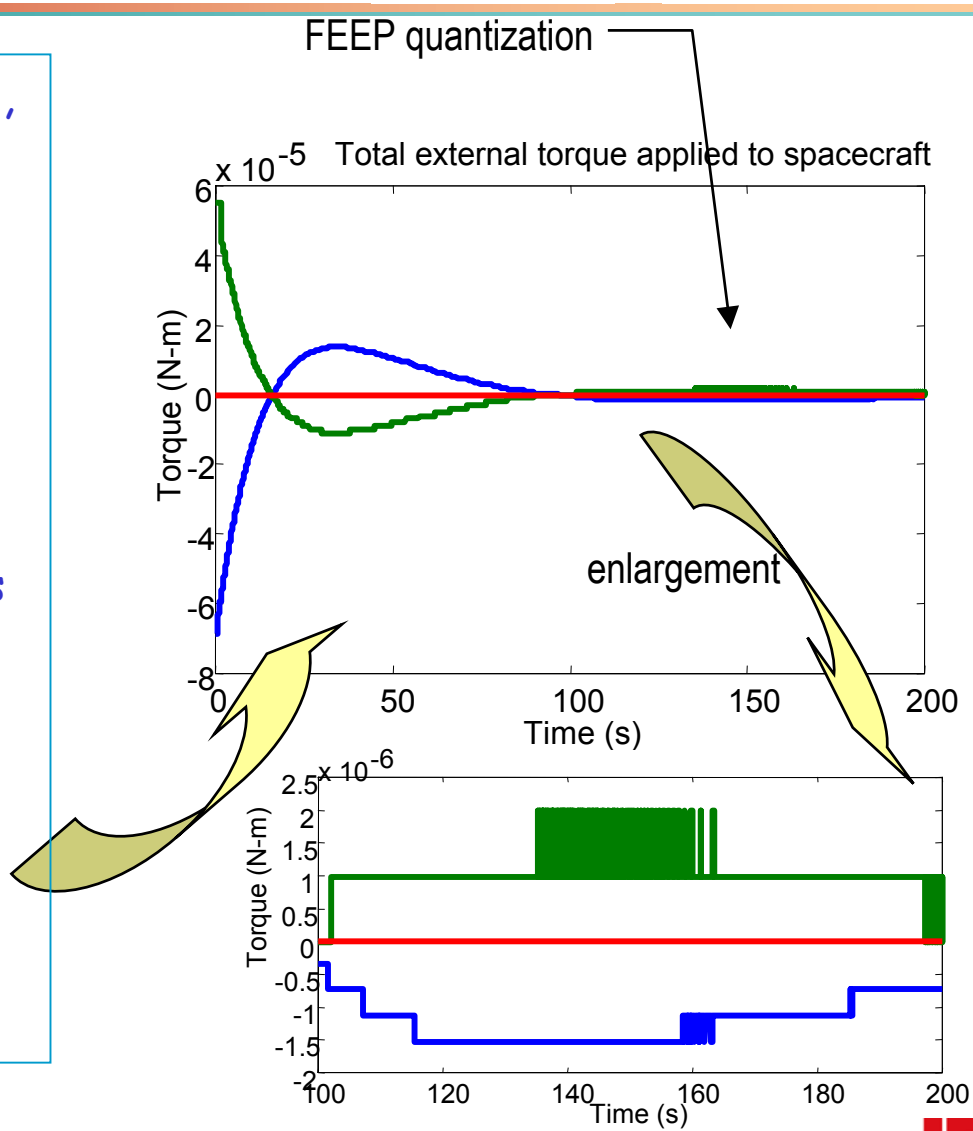

# Impulsive Disturbances — how much can we tolerate?

- Study of sensitivity to impulses
  - Thrusters
  - Microsnap
- Double sided pulse
  - 1 msec up, 1 msec down, then zero
- Examine tip/tilt response vs. force level
- Show resulting star leakage into planet pixels
- Tolerable impulse ~ few mN-sec
  - Comparable to StarLight mission thruster minimum impulse
  - $10^5$ times FEEP minimum impulse
  - 1 mN-sec is equivalent to dropping a paper clip from 2" height

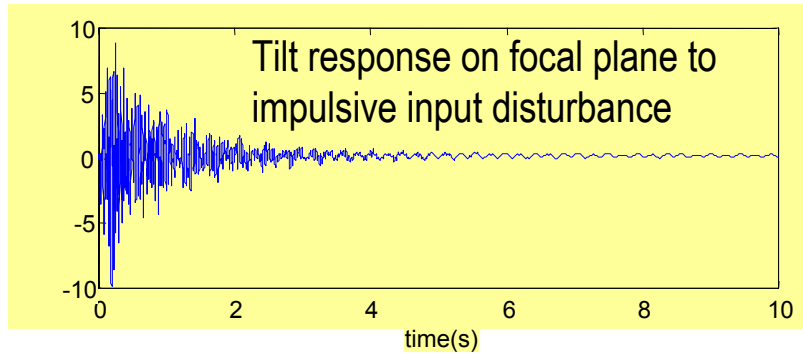


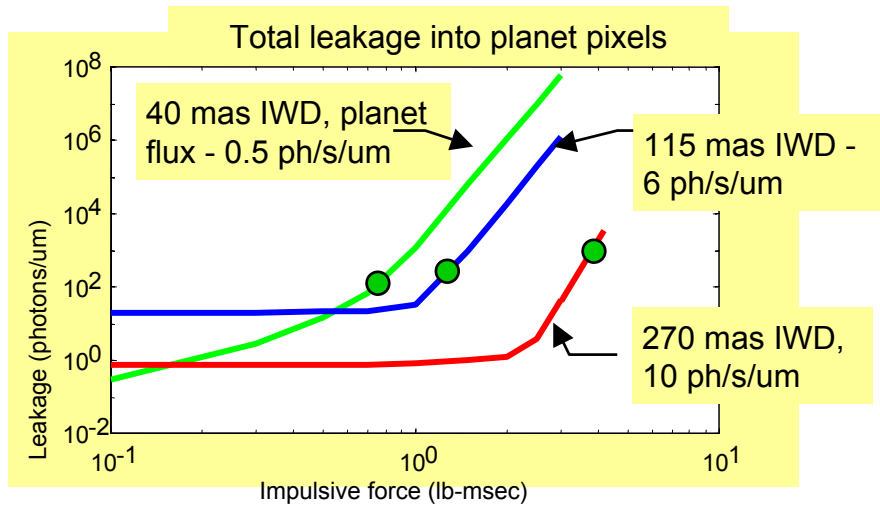


a

# Conclusions about Dynamic Wavefront Error

- The models indicate that we can get adequate vibrational stability with reaction wheels with very little restriction on operation
- Further work can solidify our understanding of the issues
- Even if this wheel/isolator system were not acceptable during observations, thrusters and other options could do the job with negligible vibration
- Remaining concerns include
  - Thruster pulses (for some types under consideration)
  - Microsnap (e.g. sudden release of stress stored in joints)
  - Any other devices on the spacecraft whose low-level vibration normally can be ignored

# Colorful Speckles

- We compute a series of images at the CCD focal plane across the full band of wavelengths
- We "core down" through that stack of images at a fixed angular position on the CCD
  - Patterns shift mainly by rescaling with angle $\propto \lambda$
  - They also change slowly in amplitude
- We examine the spectral content of the starlight background in each pixel

# Spectrum of scattered light is highly variable (1)

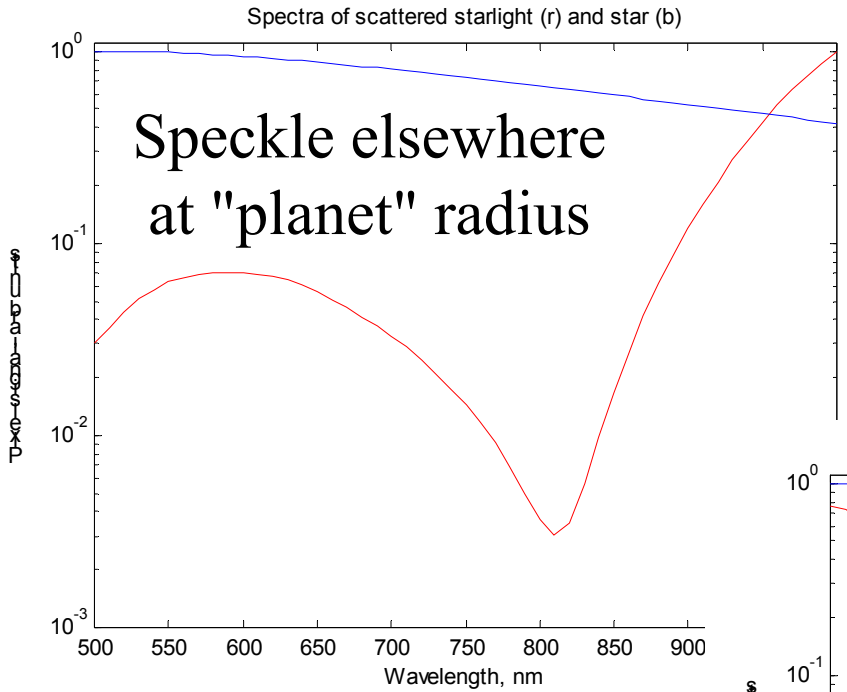


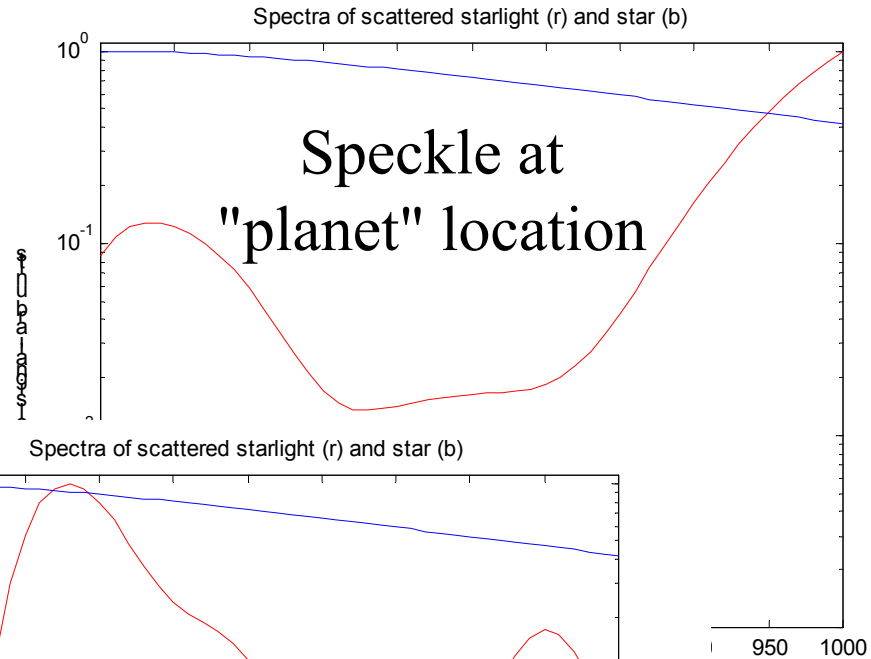


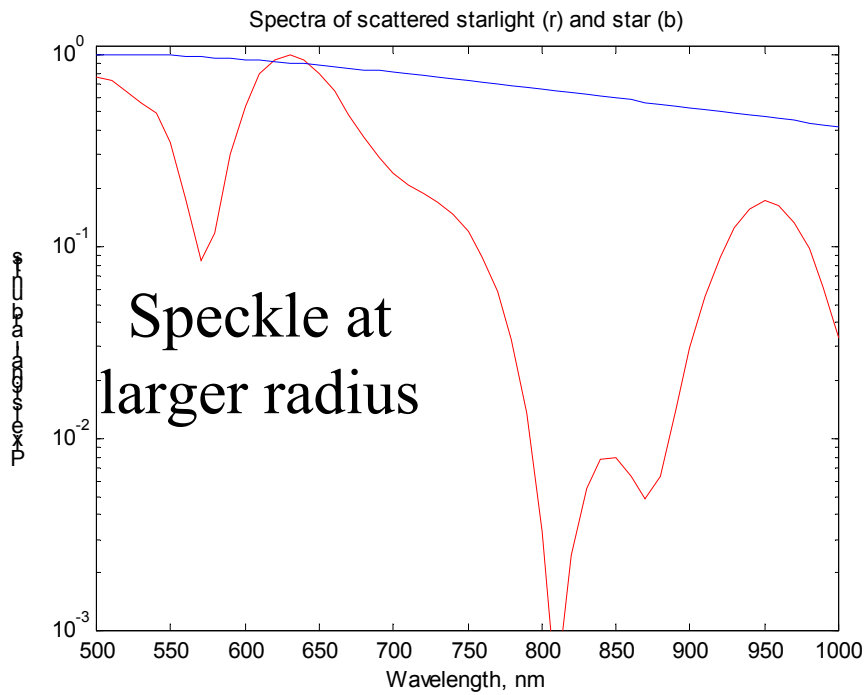


- Small field occulter (β=5)

# Spectrum of scattered light is highly variable (2)

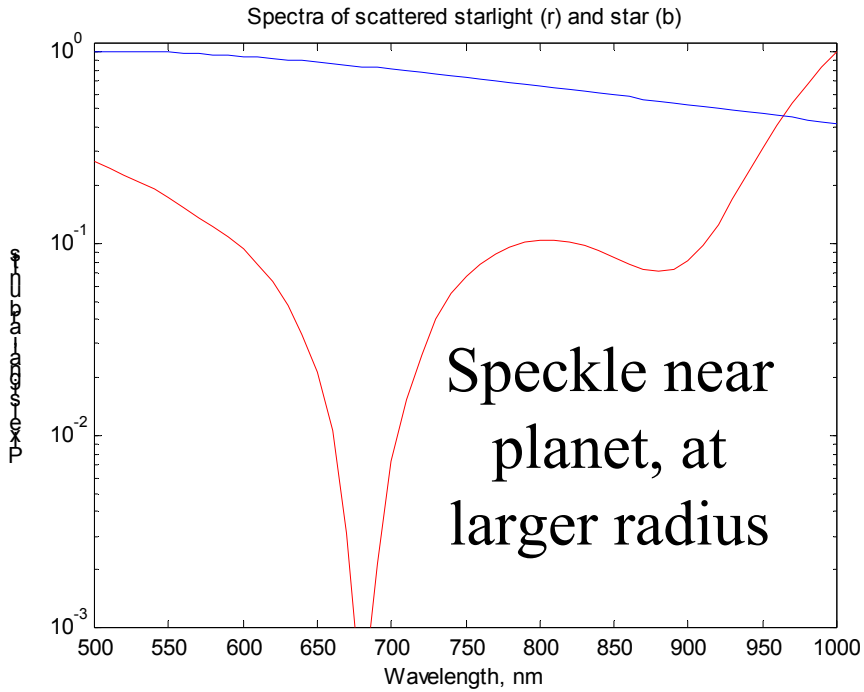


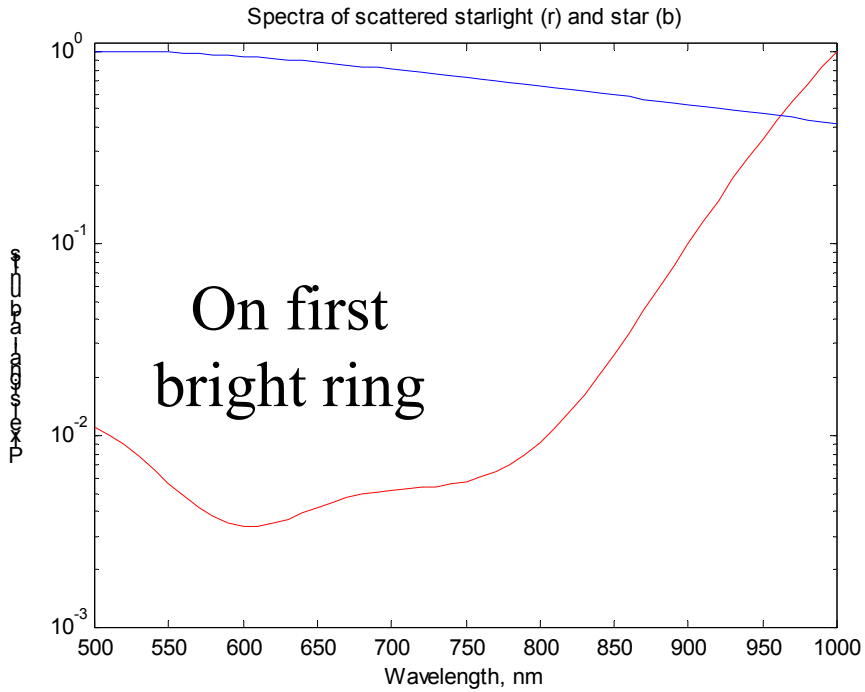


- Small field occulter (β=5)

# Spectral content of speckles

- Speckles can obfuscate in two ways
  - Obscuring planets during search
  - spectral interpretation
- Sharp narrow dips particularly interesting
  - Probably an interference effect between two leakage amplitudes:
    - Residual aperture diffraction
    - Wavefront scatter
  - Could be variable due to interference phase variation
    - Sensitive to what? How much?
  - Not dramatically mitigated by larger field stop (following charts)

# Spectra for wider field occulting mask (1)

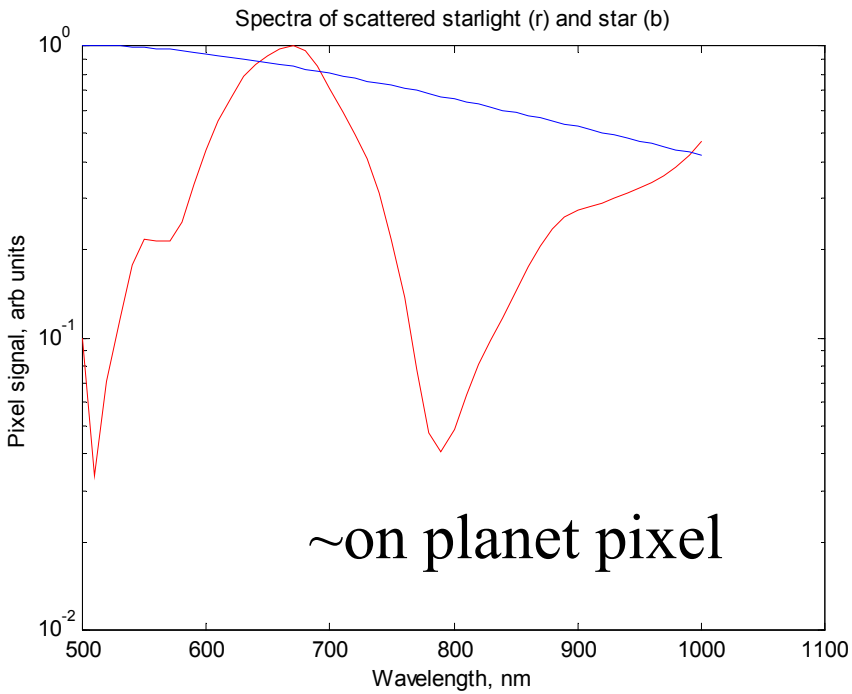


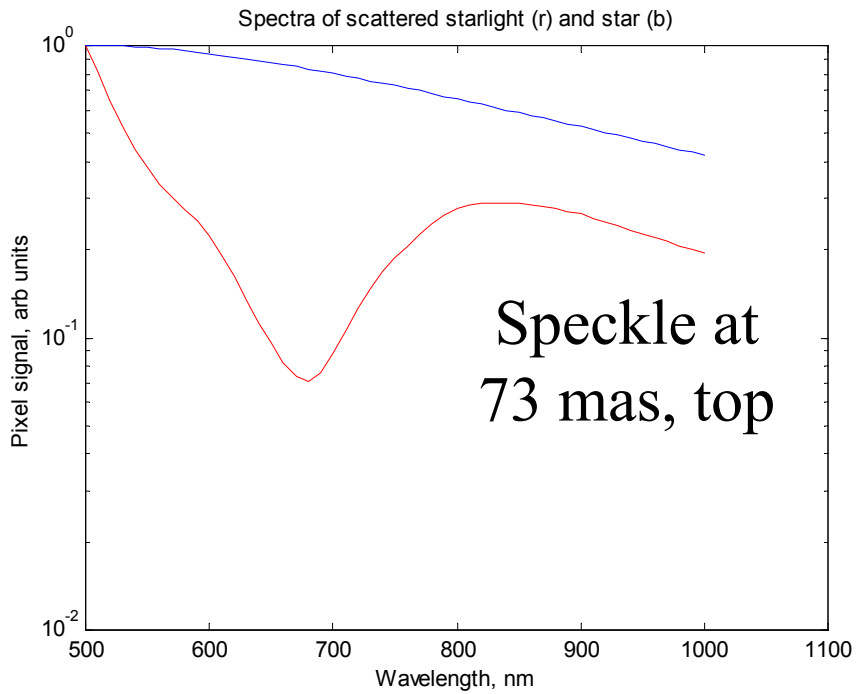


- Larger field occulter (β=6)

# Spectra for wider field occulting mask (2)

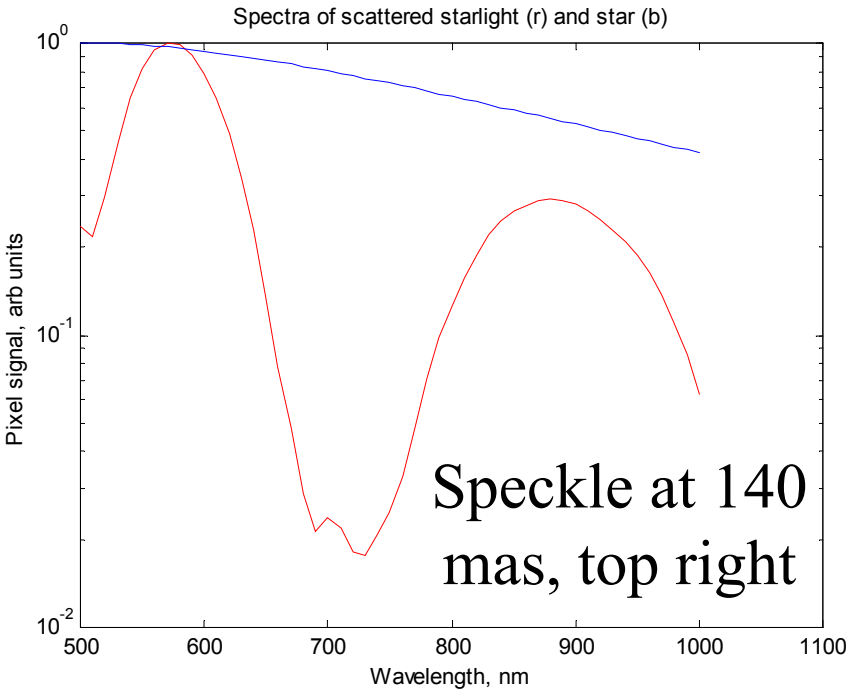


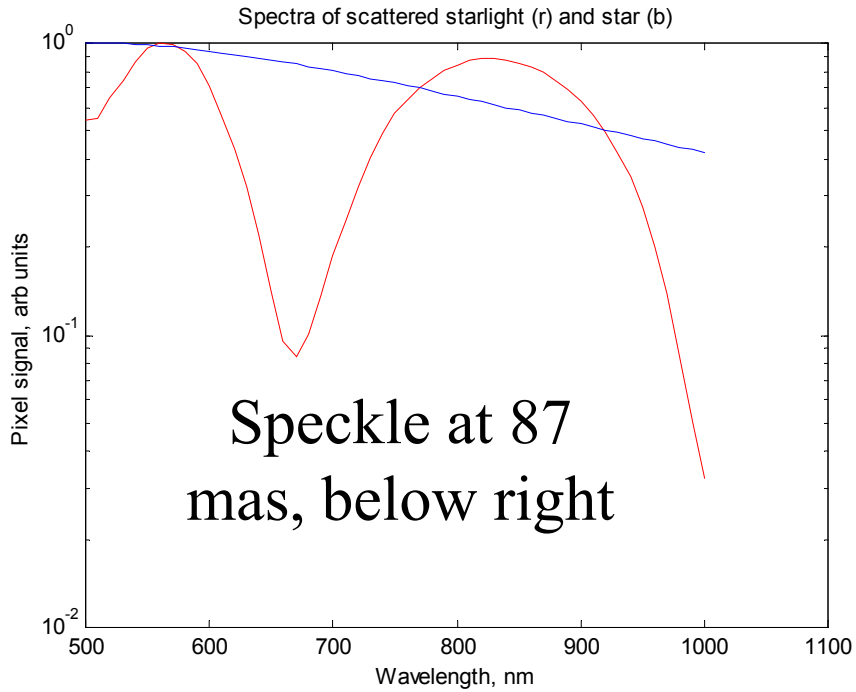


- Larger field occulter (β=6)

# Scattered-starlight spectra show factor-of-100 variations near planet

- Ensemble of spectra for 63 points in a 28x36 mas region surrounding "planet" at 100 mas

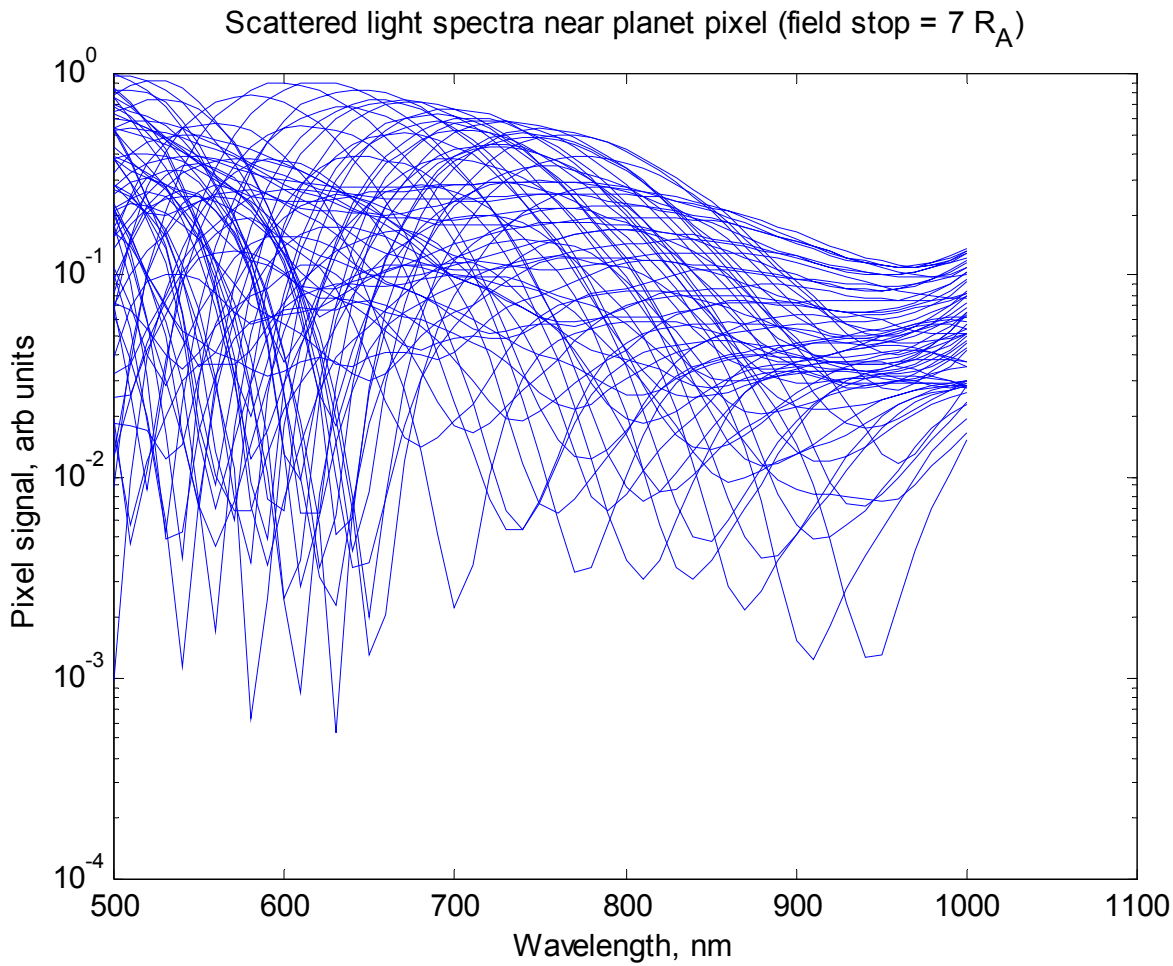

# Conclusions about colorful speckles

- These spectra of the background signals show that factor-of-100 variations with wavelength are common across a few tens of percent bandwidth
- Pixel to pixel variations are often dramatic as well
- The sharp notches that occur in some lines suggest an interference between two amplitudes, such as aperture diffraction and wavefront scatter
- These features will tend to complicate interpretation of planet spectral observations taken against this background
- We have not looked in detail at the problem of extracting planet absorption line signals from realistic data with these backgrounds

# Effect of color leakage

- For planet searching, it is advantageous to use the shortest wavelengths possible
- We must consider specifically the means of selecting that passband
  - All colors from the star will make it to the CFO in large numbers
  - PSF is wavelength-dependent, and CFO selects spatially there
  - When the CFO is small for tight IWD, less-valuable red wavelengths will sneak past the CFO more readily than the more-valuable blue ones (following figures)
- Color filters after all the masks can help screen out red photons
  - This becomes an important "line of defense" for close IWD
- At the end, all remaining light is detectable at some level by the CCD
- Following figures show the PSF of the 2-aperture Kaiser with color throughput factors:

| | <500 nm | 500-550 nm | 550-1000 nm | >1000 nm |
|---|---|---|---|---|
| Reference | 0 | 1 | 0 | 0 |
| Bad case | 0 | 1 | 1e-3 | 0 |
| Good case | 0 | 1 | 1e-6 | 0 |

- CCD responsivity curves not included

# Reference: Zero color leakage

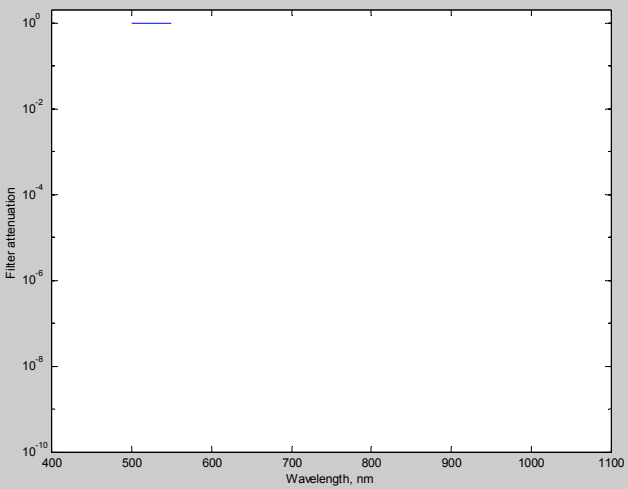


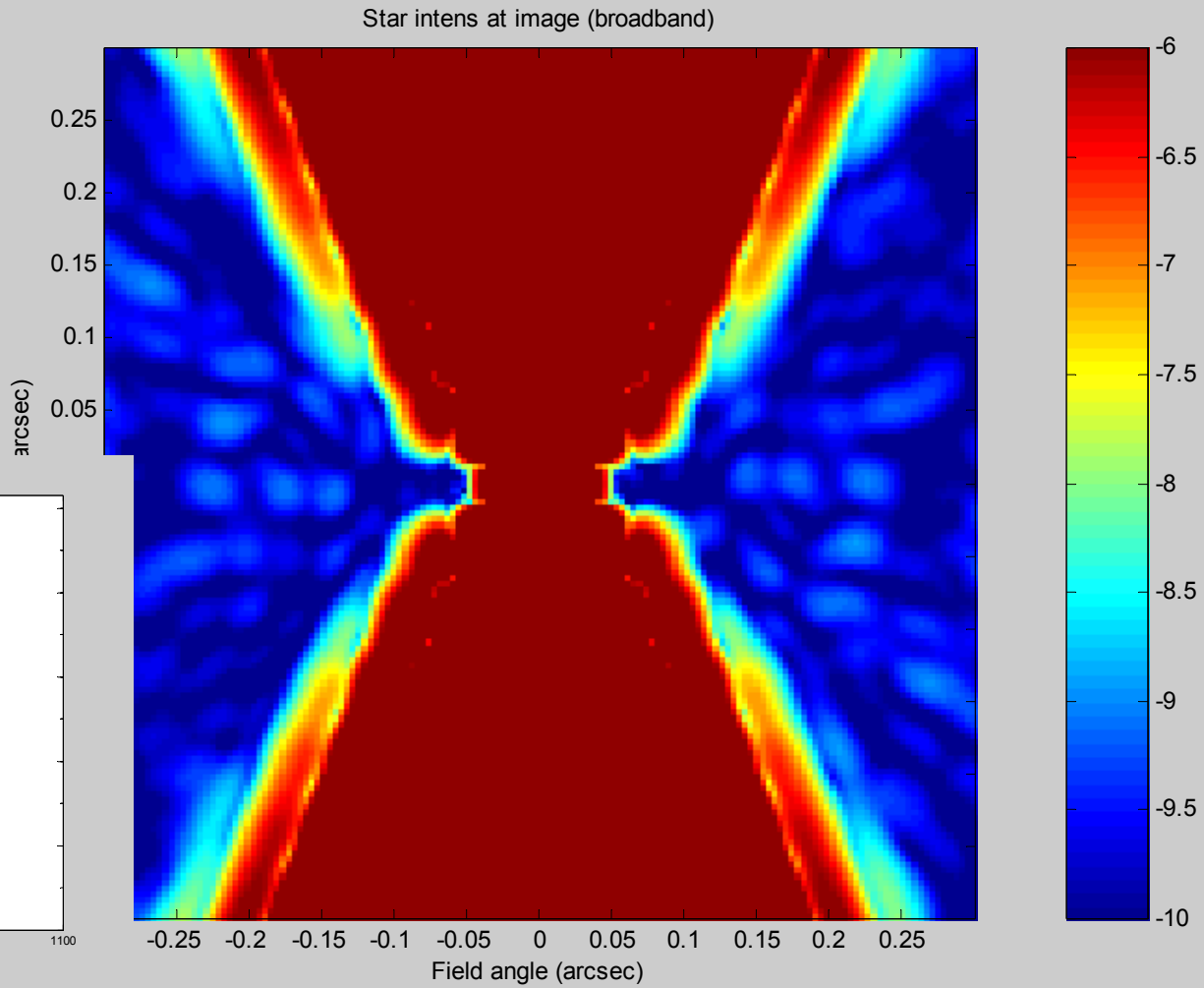

# Bad case: 1e-3 color leakage

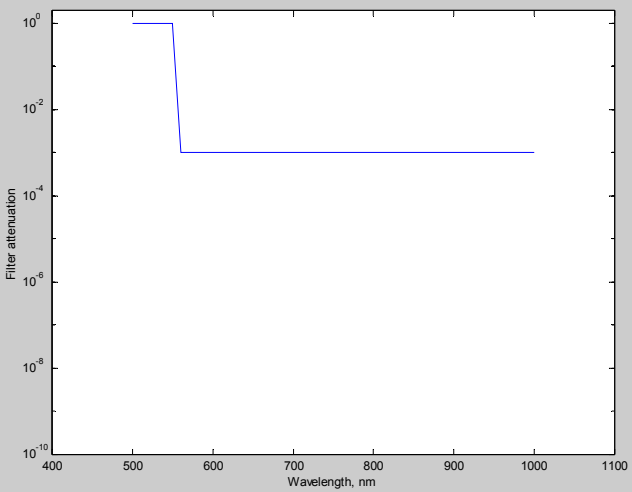


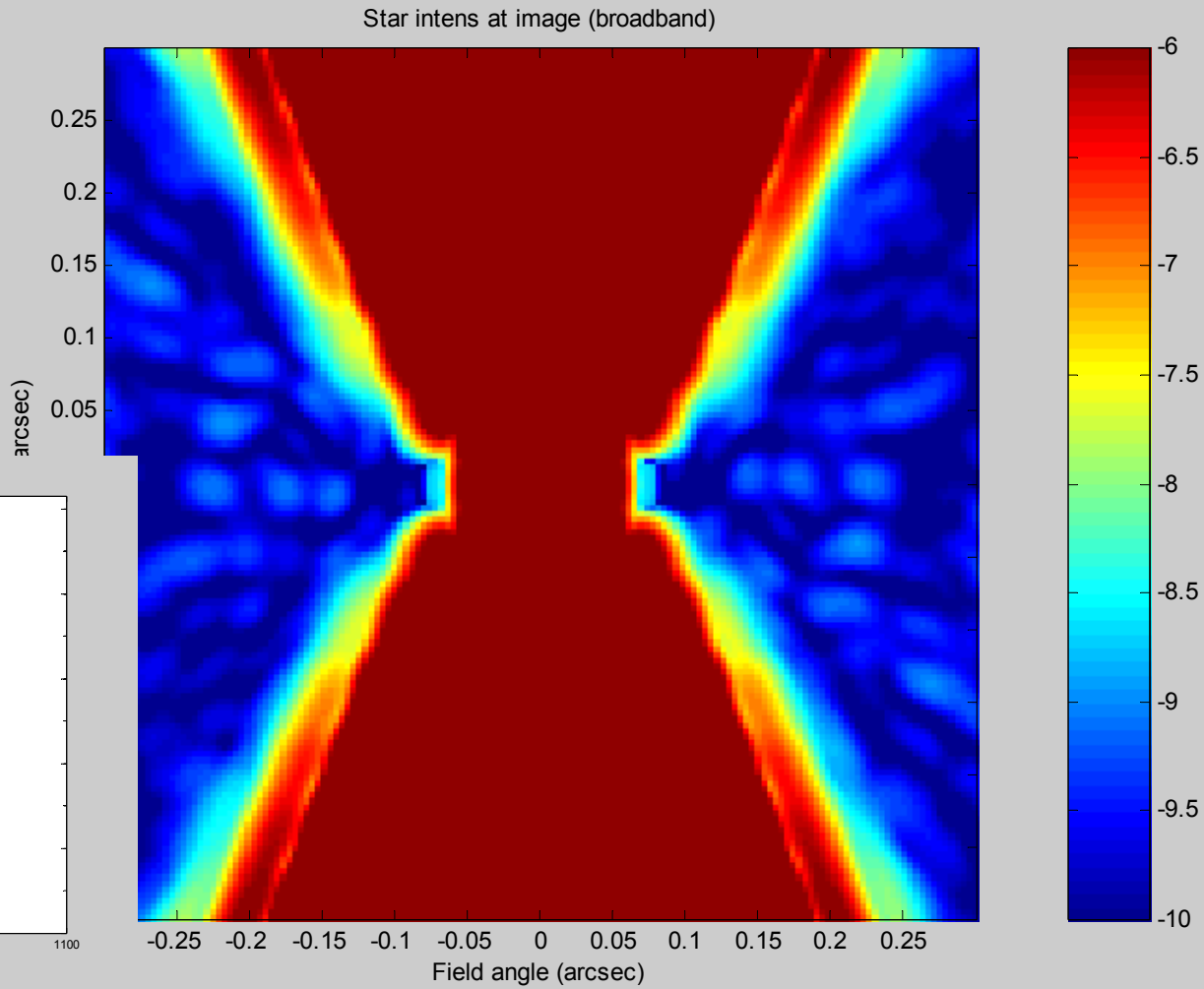

# Good case: 1e-6 color leakage

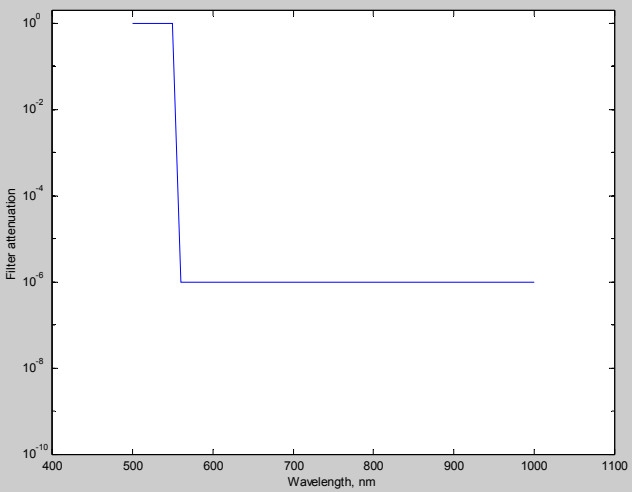


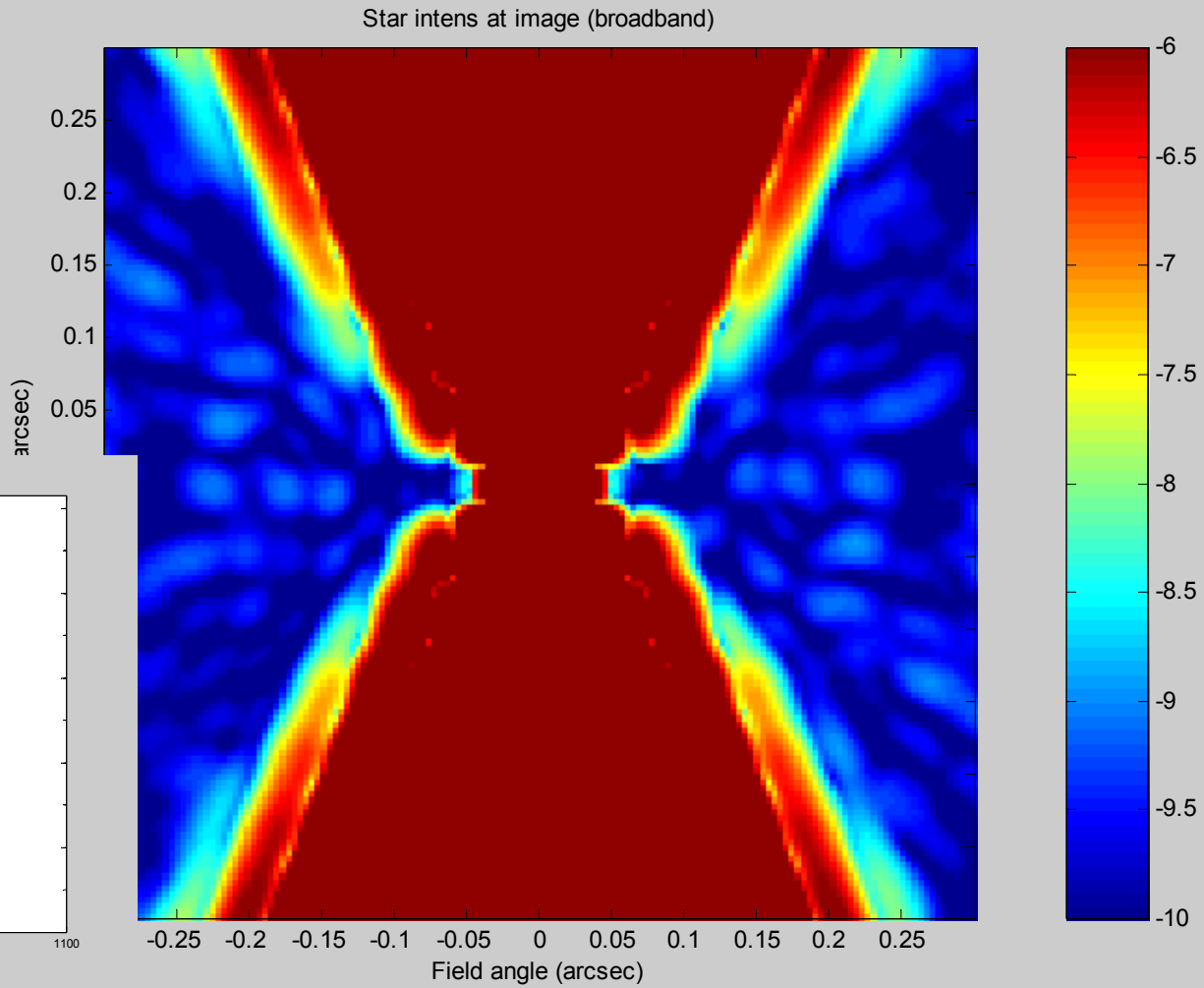

# Conclusions about color leakage

- A filter which suppresses long wavelengths by only 1e-3 will demand a dramatic increase in IWD vs. our early monochromatic calculations
  - IWD is defined by the longest wavelengths, not the shortest
- A filter which suppresses long wavelengths by 1e-6 would be more tolerable
  - These filters are manufacturable, and have been used on HST
  - Still increases IWD by ~20% -- might need to develop 1e-7 filters for improved IWD
- Pointing issues may arise again for the shaped pupil systems
  - At least requires some conservatism in choice of hourglass CFO and blue-pass filter
- NB: this also impacts the classical coronagraph, in a similar way
  - Sensitivity could be entirely different

# Fraunhofer vs. Fresnel diffraction modeling

- We assume the DM is at an image of the primary mirror
  - Must be at the image to within << $2\,dx^2/\lambda$ = 16 m, where dx is the DM actuator spacing
  - This cannot be satisfied for every optical surface
- If the PM is not perfectly focused on the DM, beam walk can occur
  - Shifts the wavefront correction map vs. the wavefront error map
- If another mirror (not at a pupil image) wrinkles the wavefront or clips the beam, significant variations in amplitude distribution at the DM will result
- Amplitude correction in the pupil can help correct for these effects

- In modeling, we have used a combination of raytracing and Fraunhofer propagation
- But Fresnel propagation is needed to account for these effects at the secondary, tertiary, etc. to high fidelity
- If we assume a successful amplitude correction system, we need not do this
- To check the adequacy of a specific amplitude correction system, we would need to model this to high fidelity using Fresnel propagation

# Section 6.
# Optical System Summary

Charley Noecker

Optical System Performance
Optical System Recommendations

# Areas Requiring Further Study

- Finish thermal-mechanical modeling
- Options in optical system design
  - location and type of elements
  - mask design
- Detailed DM model
- Partitioning of DM/PM wavefront control system
- Wavefront sensing and phase retrieval
- Amplitude correction
- Fresnel propagation
- Color leakage studies
- Tradeoffs with isolation, FSMs and wheel quality
- Structural materials and stiffness effects on design
- Inclusion of full detector models and signal processing models

# Summary of Modeling Results

- We have a fully integrated model of the coronagraphs, incorporating structures, optics, controls, and disturbances
- Dynamics of the optical system appear to be within reach of the requirement
- Thermal analysis of the optical system is incomplete
- The model demonstrates suppression of low-spatial frequency wavefront errors as desired, but still leaves some tight requirements
  - We get the least suppression when we tune the system for the closest IWD
- Tuning the CFO and Lyot stop for a chosen IWD leads to loss of system throughput
- The background light from the star can show strong spectral variation
- The leakage of red light past the CFO can increase the IWD unless it is carefully filtered out
  - True for both classical and shaped pupil

# Response to Nick Woolf (1 of 2)

- White paper "Scattered Light in Coronagraphs" by N. Woolf
  - Uses similar theory (minor discrepancies)
  - Similarly requires Q~1
  - Considers only low spatial frequencies,
- Differences
  - We calculate RMS over full range of relevant spatial frequencies (to ~1 arcsec)
  - We are insensitive to low f (resulting scatter mostly lands within CFO, not on planet image)
  - Our PSD requirement ~matches Woolf's
- Woolf considered too small a range of spatial frequencies; hence derived wavefront RMS is smaller
  - Doesn't show noise advantages afforded by large DM

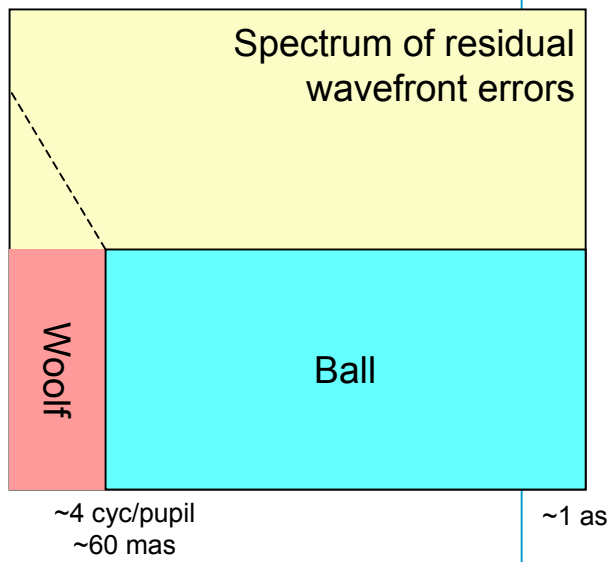

# Response to Nick Woolf (2 of 2)

- Dynamics model shows that in spatial frequency domain >4 cycles/pupil, PSD from damped reaction wheels operated away from resonance is below our spec.
  - We assume active optics (e.g. set/forget), not adaptive (e.g. fast servo) — remove or isolate vibration, rather than fixing it post facto
  - End-to-end results show that observed vibrations meet or nearly meet the stray light requirement at the planet pixel
  - No accelerometers or other feedback control of the wavefront in these spatial frequencies is necessary during an observation.
- Applicability of lab experience
  - SIM experience with nm-scale vibration is primarily for piston and tip/tilt
    - Applicable to TPF-interferometer
  - TPF coronagraph has different driving requirements
    - Has enormous starlight flux for controlling tip/tilt
    - Insensitive to piston, focus, astigmatism, spherical
    - Only higher-order aberrations matter
- TPF (both IR and visible) and all its successors must somehow solve this problem satisfactorily

# Conclusions

- Stray light control is the driving requirement
  - Stability over hours to days is needed
  - Thermal control will be a central issue
  - Low-vibration environment needed
- Serendipitous or targeted astrophysics observations possible
  - May be limited by bright-star stray light
  - Benefits from primary mirror actuators but not from the main DM
- Innovative design ideas
  - Kaiser and prolate-spheroid pupil shapes
    - Better attenuation with binary CFO masks
    - Possible control of amplitude errors with pupil edge actuation
  - "Filter wheel" selection of masks
    - Entrance pupil: ellipse or shaped pupil
    - CFO mask: Gaussians, X patterns in different sizes
    - Lyot stop: Ellipse/other shapes, different sizes

# Conclusions
# Comparison -- classical vs. shaped pupil

- Classical
  - Graded-attenuation masks
  - We expect to compensate some amplitude profile error with phase at DM — will sacrifice half the FOV
  - Allows wide "opening angle" for close-in observations
- Shaped pupil
  - Can use binary (on/off) masks in both pupil and CFO
  - For useful "opening angle" for close-in observations, need multi-pupils
    ⇒ added complexity in pupil mask
  - May be able to compensate some amplitude errors without sacrificing half the FOV
  - Way cool

# Conclusions
# Inner working distance

- Shaped pupil
  - Works down to ~4 lambda/D (50 mas at 500 nm, 40 mas at 400 nm)
  - Fairly hard inner limit there -- even bright planets may be undetectable inside this IWD
  - Color leakage is a significant threat which needs further study
  - Azimuth range is limited at innermost angles -- mitigated with multi-pupils
- Classical
  - Works down to ~60 mas for ~20% passband at 500 nm
  - Softer inner limit -- throughput and SNR fall, but bright inner planets could be detected through CFO
  - Effect of color leakage not understood yet -- could be a challenge also
- Both
  - Low spatial frequency WFE could limit achievable IWD
    - Thermal effects still not thoroughly understood
    - Vibration seems under control, but its effects would enter here also

# Further work

- Thermal-structural modeling
- Planet spectrometer design
- Ghost images
- Mostly-spherical optical design

# Backup charts

# Top-level stray starlight budget

- This shows an allocation of allowable planet pixel background contributions
- They are defined as fraction of the star brightness
- They are also represented with a "Q" contribution calculated for a canonical planet brightness = 1e-10 of the star brightness
- This budget example does not meet the goal of planet "Q" = 1
- This goal is still soft because of uncertainties in the impact of systematic variations in the backgrounds

| | Fraction of star per pixel | Q value | Model results* |
|---|---|---|---|
| Planet pixel background from star | 1.34E-10 | 1.34 | |
| Wavefront – phase | 1.03E-10 | 1.03 | |
| WFE – Thermal | 1.00E-11 | 0.1 | not yet |
| Beamwalk – Attitude control | 2.08E-11 | 0.21 | not yet |
| Beamwalk – Bench thermal | 2.00E-11 | 0.2 | not yet |
| Dynamic WFE | 2.00E-11 | 0.2 | close |
| Pointing jitter | 1.00E-11 | 0.1 | close |
| DM – Residual WFE | 1.00E-11 | 0.1 | close** |
| DM – Thermal | 1.23E-11 | 0.12 | close** |
| Wavefront – amplitude | 3.00E-11 | 0.3 | |
| DM correction BW-error | 2.00E-11 | 0.2 | yes** |
| Drift in correction | 1.00E-11 | 0.1 | not yet** |
| Dust/haze | 1.00E-12 | 0.01 | |

* Do our models show we can meet these budget allocations?

** experimental data needed to address this question properly

# DM stroke error budget

**STROKE ERROR BUDGET**
**tpfcrn65off.1**

| Contributor | PV Error (nm, Surface) | Comment | Input value | Source |
|---|---|---|---|---|
| Optical system: CSF | 24.5 | To correct PM mid-freq. HST PSD model | 7.0 nm RMS,CSF | 6.5 m tpfcrn error tree |
| DM MIRROR FIGURE ERROR | 7 | To correct DM mid-freq. HST PSD model | 2.0 nm RMS, low freq | |
| INFLUENCE FUNCTION | 3.2 | 5 % of total stroke | 0.05 | |
| HYSTERESIS | 1.28 | 2 % of total stroke | 0.02 | |
| TEMPERATURE LEVEL | 1.3 | 1% of total stroke/C | +/- 2.0 C | |
| INTRABLOCK GAIN | 3.2 | 5 % of total stroke | 0.05 | |
| BLOCK-TO-BLOCK GAIN | 3.2 | 5 % of total stroke | 0.05 | |
| EPOXY DRY-OUT | 2.4 | from 0.3 %RH | 3.20E-04 /% RH | |
| EPOXY RADIATION CREEP | 2.5 | 1E-04 of thickness | 25 um, EPOXY | |
| PMN RADIATION CREEP | 5 | WF/PC2 AFM DATA | 1.9 mm, PMN | |
| ALGORITHM CORRECTION | 5 | | | |
| MARGIN | 5 | | | |
| TOTAL STROKE: RSS | +/- 27.8 nm | | | |
| **TOTAL STROKE:SUM** | **+/- 63.6 nm** | **DESIGN VALUE=** | **+/-64 nm** | |
| | | **+/- 64 nm** | wvl= 633 nm | |

| | | Primary Mirror | |
|---|---|---|---|
| | Rss | 6.3 nm rms | |
| Low spatial frequency (Figure) [LSF] | 0 to 3 | 4.6 nm rms | |
| Critical spatial frequency (DM-controllable ripple) [CSF] | 3 to 130 | 1.4 nm rms | 4.8 nm rms |
| Mid spatial frequency (Ripple) [MSF] | 130 to $10^4$ | 4.0 nm rms | |
| Low spatial frequency (Figure) [LSF] | $> 10^4$ | 1.0 nm rms | |

# DM WFE budget

| | | | | | | | | |
|---|---|---|---|---|---|---|---|---|
| **TPF CORONAGRAPH RESIDUAL WAVEFRONT** | | | | | | | 256 wide | |
| | | 50 mm thick PM | | | 4.2 mm thick PM facesheet | | | |
| **Short term effects, Stability between DM updates** | | | | | | | | |
| **tpfcrn65off.1** | | **4 cycles/aperture** | **4** | | **85 cycles/aperture** | **85.3** | 256 | |
| **Contributor** | **Error Value of Contributor** | **Scale factor** | **Induced Wavefront Error (nm P-V, Wavefront)** | **Error Value of Contributor** | **Scale factor** | **Induced Wavefront Error (nm P-V, Wavefront)** | | |
| **ALIGNMENT INSTABILITY** | | | | | | | | |
| PUPIL SHEAR | 0.9 um dx @ DM | 0.01 nm/um dx@DM | 0.0057 nm P-V | 0.9 um dx @ DM | 0.13 nm/um dx@DM | 0.1206 nm P-V | | |
| LOS STABILITY | 0.7 um dx @ DM | 0.01 nm/um dx@DM | 0.0044 nm P-V | 0.7 um dx @ DM | 0.13 nm/um dx@DM | 0.0938 nm P-V | | |
| OTA WAVEFRONT STABILITY | 0.200 C | 0.75 nm/C | 0.1500 nm P-V | 0.50 C | 0.06 nm/C | 0.0315 nm P-V | 1.50E-08 | ULE |
| **DEFORMABLE MIRROR** | | | | | | | | |
| **GAIN CHANGES** | | | | | | | | |
| TEMPERATURE TEMPORAL GRADIENT | 0.020 C | 0.01*full stroke/C | 0.0256 nm P-V | 0.030 C | 0.01*full stroke/C | 0.0384 nm P-V | +/- 64.0 nm | |
| **THERMAL EXPANSION** | | | | | | | low freq | |
| TEMPERATURE TEMPORAL GRADIENT:PMN | 0.020 C | 1.00E-06 /C | 0.0760 nm P-V | 0.020 C | 1.00E-06 /C | 0.0760 nm P-V | 1.9 mm, PMN | |
| BACKPLATE TEMPERATURE GRADIENTS | 0.0020 C | 1.00E-06 /C | 0.0716 nm P-V | 0.0020 C | 1.00E-06 /C | 0.0716 nm P-V | 17.9 mm, PMN | |
| **CREEP** | | | | | | | | |
| MECHANICAL CHANGES BETWEEN RESET | 0.000300 *full stroke | | 0.0384 nm P-V | 0.000300 *full stroke | | 0.0384 nm P-V | JPL TEST(TBR) | |
| **DM DRIVER VOLTAGE** | | | | | | | | |
| SETTING PRECISION | 1.0 mv | 3.33 nm/V | 0.0067 nm P-V | 1.0 mv | 3.33 nm/V | 0.0067 nm P-V | | |
| TEMPORAL INSTABILITY | 1.0 mv | 3.33 nm/V | 0.0067 nm P-V | 1.0 mv | 3.33 nm/V | 0.0067 nm P-V | | |
| **PHASE RETRIEVAL ALGORITHM** | | | 0.0040 nm P-V | | | 0.0600 nm P-V | | |
| NOISE | | | | | | | | |
| CCD PIXEL-TO-PIXEL RESPONSE | | | | | | | | |
| | | | | | | | | |
| | | **RSS WAVEFRONT TOTAL** | **0.189 nm P-V** | | **RSS WAVEFRONT TOTAL** | **0.20 nm P-V** | | |
| | | **Specification** | **< 0.20 nm PV** | | **Specification** | **< 0.20 nm PV** | | |
| | | | | | | | | |
| **Long term effects, Drift correctable with update of DM actuators** | | | | | | | | |
| | | | | | | | | |
| | | **4 cycles/aperture** | **4** | | **85 cycles/aperture** | **85.3** | 256 | |
| **Contributor** | **Error Value of Contributor** | **Scale factor** | **Induced Wavefront Error (nm P-V,** | **Error Value of Contributor** | **Scale factor** | **Induced Wavefront Error (nm P-V,** | | |
| **DEFORMABLE MIRROR** | | | | | | | | |
| **GAIN CHANGES** | | | | | | | | |
| TEMPERATURE SPATIAL GRADIENT | 0.01 C | 0.01*full stroke/C | 0.0128 nm P-V | 0.01 C | 0.01*full stroke/C | 0.0128 nm P-V | +/- 64.0 nm | |
| **THERMAL EXPANSION** | | | | | | | low freq | |
| TEMPERATURE SPATIAL GRADIENT:PMN | 0.01 C | 1.00E-06 /C | 0.0380 nm P-V | 0.01 C | 1.00E-06 /C | 0.0380 nm P-V | 1.9 mm, PMN | |
| TEMPERATURE SPATIAL GRADIENT:EPOXY | 0.01 C | 5.00E-05 /C | 0.0250 nm P-V | 0.01 C | 5.00E-05 /C | 0.0250 nm P-V | 25 um, EPOXY | |
| SPATIAL T GRADIENT:FACESHEET THICKNESS | 0.01 C | 3.90E-06 /C | 0.0156 nm P-V | 0.01 C | 3.90E-06 /C | 0.0156 nm P-V | 200 um, Si | |
| **CREEP** | | | | | | | | |
| VARIATION IN EPOXY THICKNESS | 1E-06 of epoxy thickness | | 0.0500 nm P-V | 1E-06 of epoxy thickness | | 0.0500 nm P-V | 25 um, EPOXY | |
| CHARGE LEAKNESS | | | | | | | | |
| BACKPLATE | | | | | | | | |
| **HUMIDITY EFFECTS** | | | | | | | | |
| VARIATIONS: EPOXY DRYOUT SHRINKAGE | 0.003 % RH | 3.20E-04 /% RH | 0.0480 nm P-V | 0.003 % RH | 3.20E-04 /% RH | 0.0480 nm P-V | 25 um, EPOXY | |
| PMN DRYOUT | | | | | | | | |
| BACKPLATE DRYOUT | | | | | | | | |
| **RADIATION EFFECTS** | | | | | | | | 1.60E-19 coul./electron |
| PMN | 1.73E-09 volts | 3600 p/sec-cm^2 | 1E-08 nm P-V | 1.73E-09 volts | 3600 p/sec-cm^2 | 1E-08 nm P-V | 5 years | column height=1.9 mm |
| EPOXY | 1E-06 of epoxy thickness | | 0.0500 nm P-V | 1E-06 of epoxy thickness | | 0.0500 nm P-V | 25 um, EPOXY | column width=1.0 mm |
| BACKPLATE | | | | | | | | C=1.00E-07 farads |

**Charley Noecker:**

Make a point

# WFE budget from Beam shear

| CHIEF RAY (Beam Centerline) Motion vs. FOV jitter | | | | | | | | | |
|---|---|---|---|---|---|---|---|---|---|
| x = long dimension | | | | **arcsec tol** | **PSD offset** | **PSD slope** | **PM diam** | **max cycles** | **kmax_PM** |
| y= short dimension | | | | **0.05** | **6.60E-15** | **1.1** | **10** | **85.33333333** | **53.61651462** |
| | X-slope micron/ arcsec | Y-slope micron/ arcsec | X-diam (mm) | Y-diam (mm) | | kmax (1/m) | dx (micron) | RMS contrib (nm) | kmax*dx (waves) |
| SM | 62.52153 | 62.8097 | 1438.477 | 574.337318 | | 372.7310671 | 4.431139969 | 0.000618703 | 0.000262864 |
| FSM | 456.0985 | 620.2137 | 142.2379 | 75.415736 | | 3769.496292 | 38.49320942 | 0.043127051 | 0.023093384 |
| Fold1 | 774.897 | 550.6891 | 225.6233 | 64.766693 | | 2376.373366 | 47.53219358 | 0.035157802 | 0.017977225 |
| TM | 677.8215 | 678.5347 | 584.6324 | 234.146765 | | 917.0978308 | 47.95444024 | 0.015056138 | 0.006999461 |
| FieldMirror | -508.938 | -499.057 | 258.7316 | 103.887171 | | 2072.283457 | 35.6397091 | 0 | 0.011754481 |
| Collimator | -785.557 | -791.825 | 259.3632 | 103.887286 | | 2067.236779 | 55.76932855 | 0.036387923 | 0.01834872 |
| DM | -9.75496 | -19.3244 | 256 | 256 | | 2094.395102 | 1.082349912 | 0.000714547 | 0.000360783 |
| ReImageM | 636.594 | 624.2298 | 259.3632 | 103.887286 | | 2067.236779 | 44.57899818 | 0.029086546 | 0.014666979 |
| | | | | | **RMS contribution due to beam walk:** | | | 0.074119514 | |

# LOS control error budget

| tpfcrn65off.1, 4/14/01, p.61 | @ CCD Focus | @ CCD Focus | Wavefront | | FWHM= | 23.8 um |
|---|---|---|---|---|---|---|
| RSS LOS Error= | 1.450 um | 0.97 m arcsec | 0.022 waves RMS | | FWHM= | 15.9 m arcsec |
| | | | | | | |
| | Component LOS Budget | | 1 sigma | | D= | 6500 mm |
| | Disturbance | @ CCD Focus | @ CCD Focus | Edge displacement | F/#= | 47.6 |
| M1 TILT | 0.13 m arcsec | 0.829 um | 0.55 m arcsec | 4.00 nm | f= | 309400 mm |
| M2 TILT | 0.95 m arcsec | 0.444 um | 0.30 m arcsec | 30.00 nm | TM Dia.= | 250 mm |
| M3 TILT | 4.13 m arcsec | 0.700 um | 0.47 m arcsec | 5.00 nm | Wavelength= | 0.5000 um |
| M1 DECENTER | 0.020 um | 0.577 um | 0.38 m arcsec | 20.00 nm | | 206265 |
| M2 DECENTER | 0.020 um | 0.493 um | 0.33 m arcsec | 20.00 nm | | |
| M3 DECENTER | 0.050 um | 0.389 um | 0.26 m arcsec | 50.00 nm | | |
| | | | | | | |
| | | | | | | |

| LOS ALIGNMENT SENSITIVITY (Microns at TPF Coronagraph CCD focus) | ADE SENSITIVITY PER ARC SEC | BDE SENSITIVITY PER ARC SEC | CDE SENSITIVITY PER ARC SEC | XDE SENSITIVITY PER MICRON | YDE SENSITIVITY PER MICRON | ZDE SENSITIVITY PER MICRON |
|---|---|---|---|---|---|---|
| | | | | | | |
| M1 TILT | 4620 | 4620 | 0 | | | |
| M2 TILT | 330 | 330 | 0 | | | |
| M3 TILT | 120 | 120 | 0 | | | |
| M1 DECENTER | | | | 20.4 | 20.4 | 0 |
| M2 DECENTER | | | | 16.6 | 18.2 | 0 |
| M3 DECENTER | | | | 5.5 | 5.5 | 0 |

# Infrared spectrum of Earth

All molecules

$H_2O$

$O_2$

$O_3$

$CH_4$
2x enhanced

$CO_2$

$N_2O$
2x enhanced

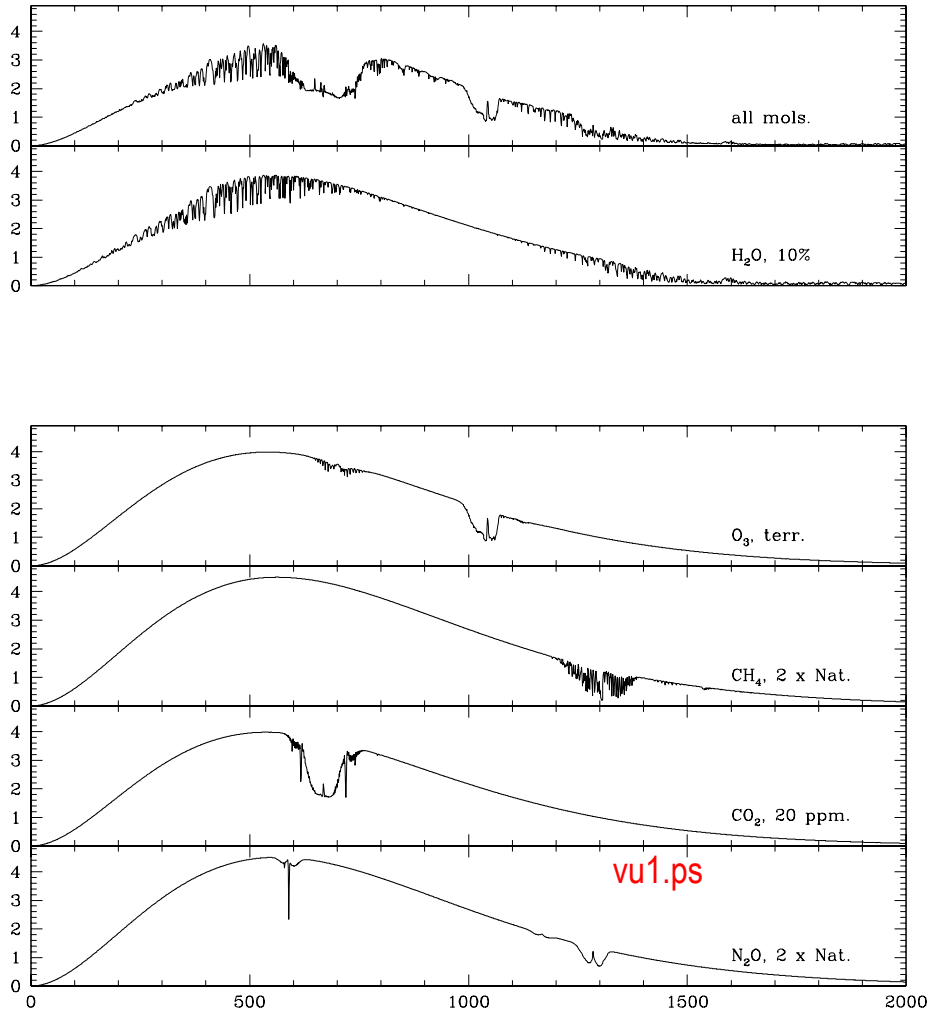

# Visible spectrum of Earth

All molecules

$H_2O$

$O_2$

$O_3$

$CH_4$
terrestrial & enhanced

$CO_2$
terrestrial & enhanced

$N_2O$

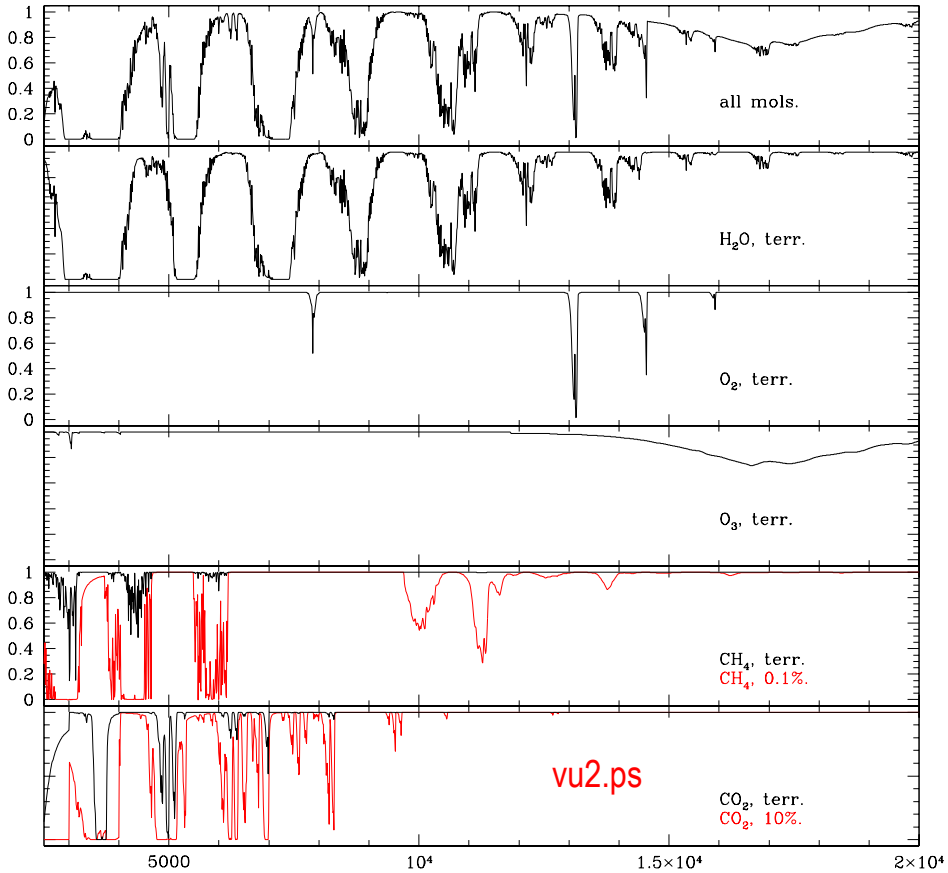

# Integration times for spectral lines

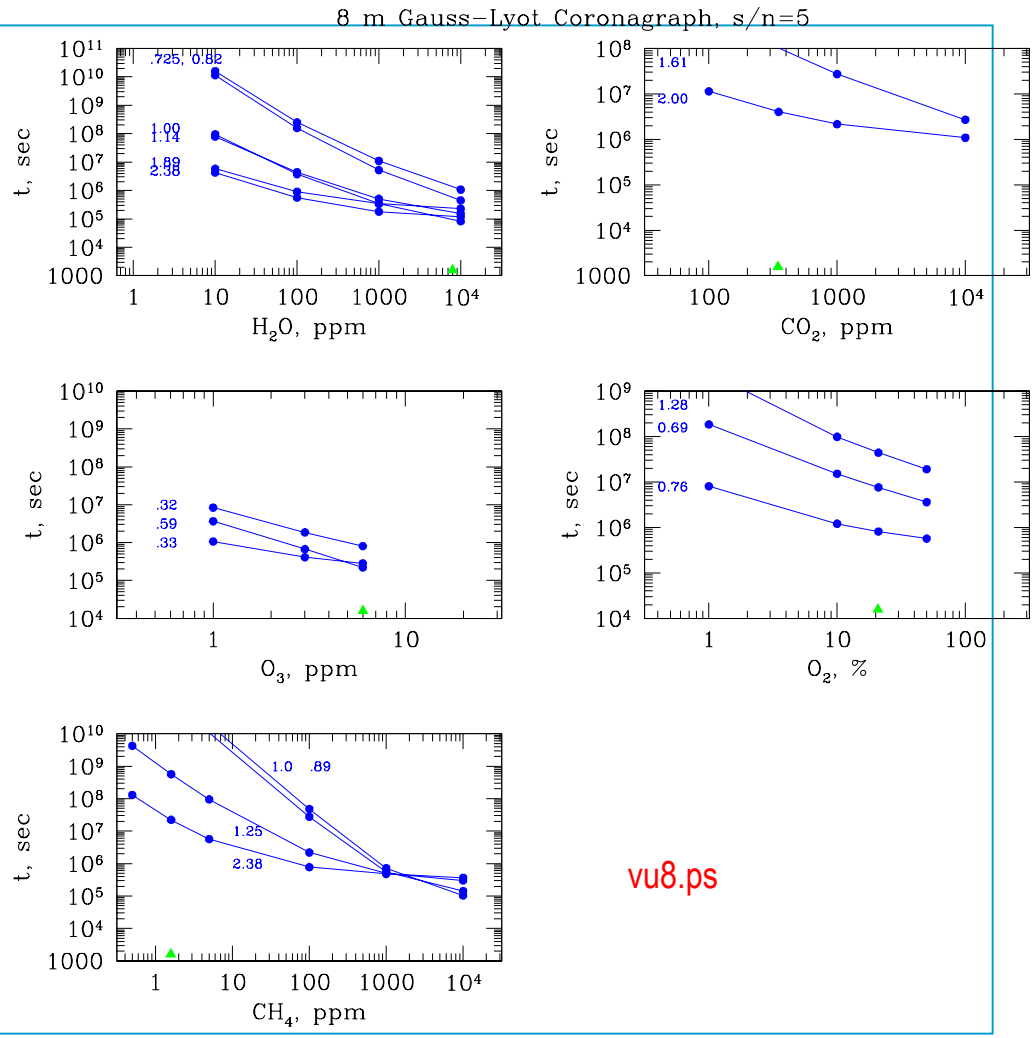


vu8.ps

# Ghost images

- Unintended reflections from optical surfaces might add stray light which obscures the planet signal
- The most likely example is a reflection from a glass surface
- The first transmitting window in the TPF coronagraph is the substrate that holds the coronagraphic field occulter (CFO) mask
  - The non-reflecting exit surface can form an etalon with the reflecting CFO mask itself
  - Mitigate with broadband AR coating, thicker window

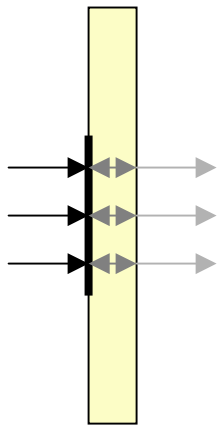

# Apodized square aperture

- Following charts show some work with apodized square apertures (graded attenuation masks at the entrance pupil)
- They illustrate the great improvement that is possible with a graded-attenuation mask vs. a binary square mask (hard-edged)
- The third chart shows dramatic degradation of the background stray light by the addition of a very small random intensity profile variation
  - This suggests that the manufacturing tolerances on the graded-attenuation profile may be quite stringent
  - This is a very preliminary result and should be studied more carefully

# Optimal Square Apodized Pupil

Same optimal function can be used in square apodized aperture

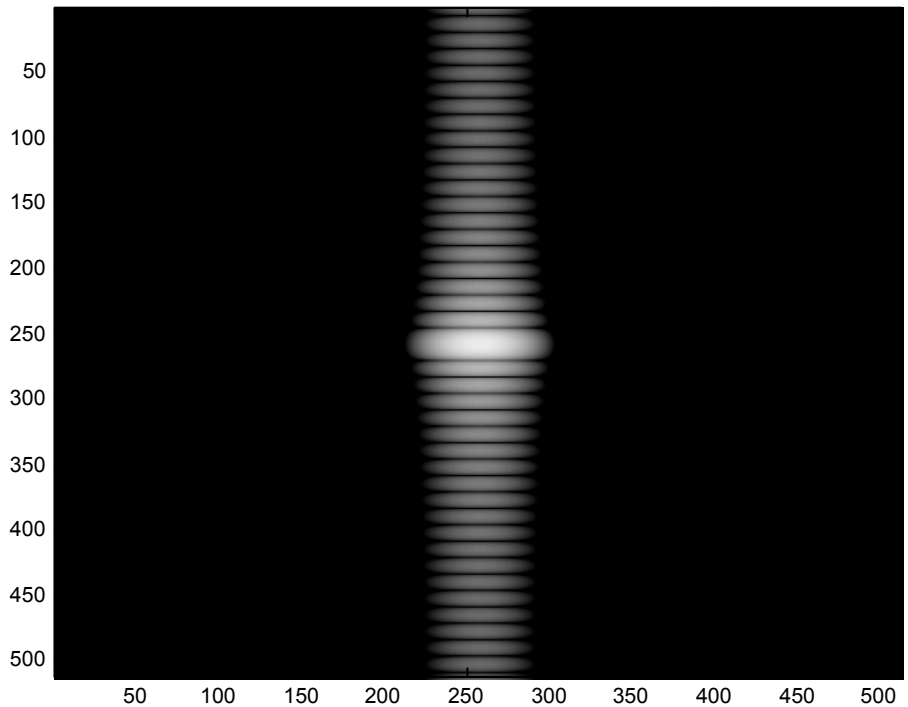


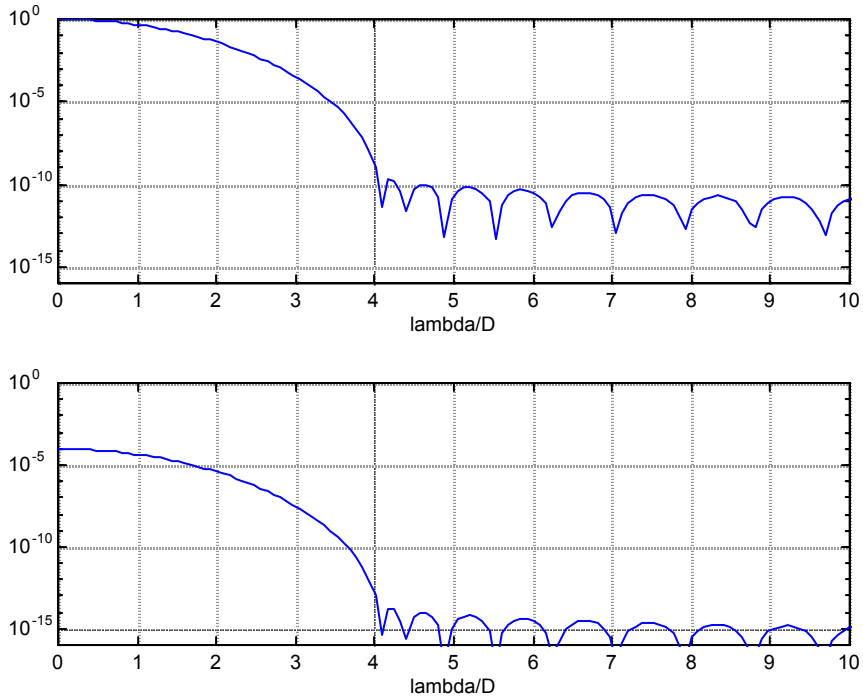


Asymmetric Prolate Spheroidal Apodization across x-dir only

Cross Sections of PSF at center (top figure) and off-axis (bottom)

# Optimal Apodized Pupil, cont.

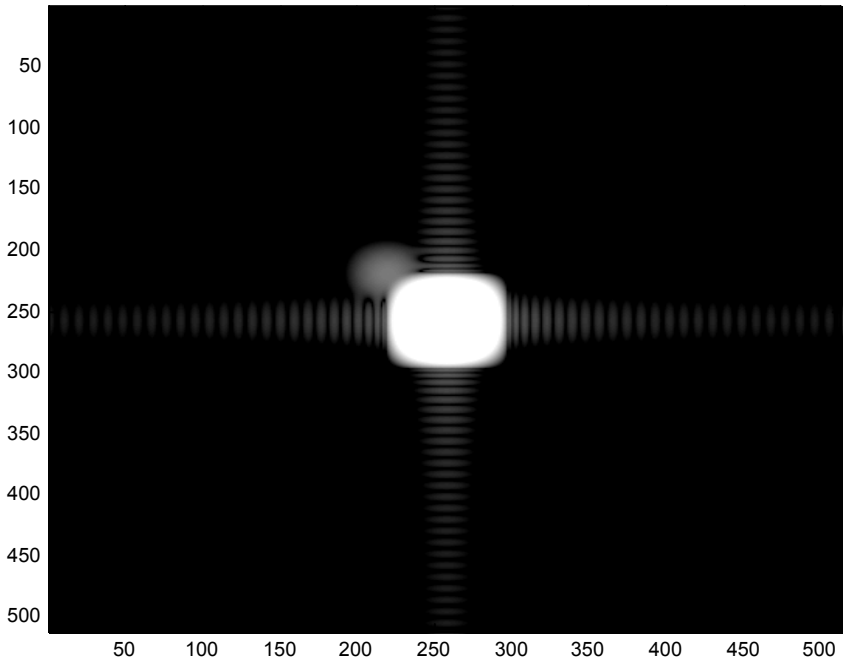


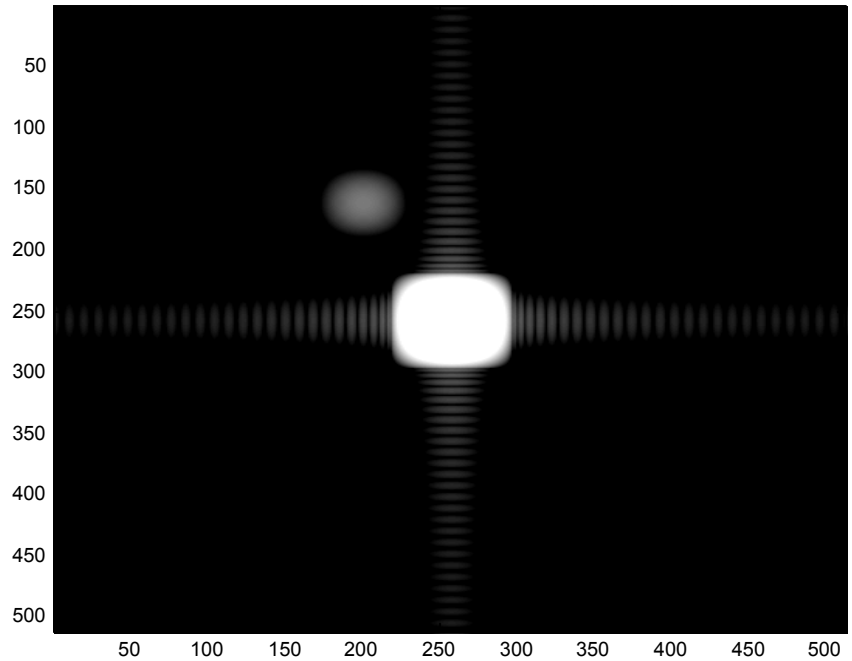


Optimal Symmetric Prolate Spheroidal Apodization (x and y) with planet at 4 λ/D (left) and 6 λ/D (right)

Note: apodization in this example reduced planet throughput by almost a factor of 10

# Apodized Pupil with Manufacturing Error

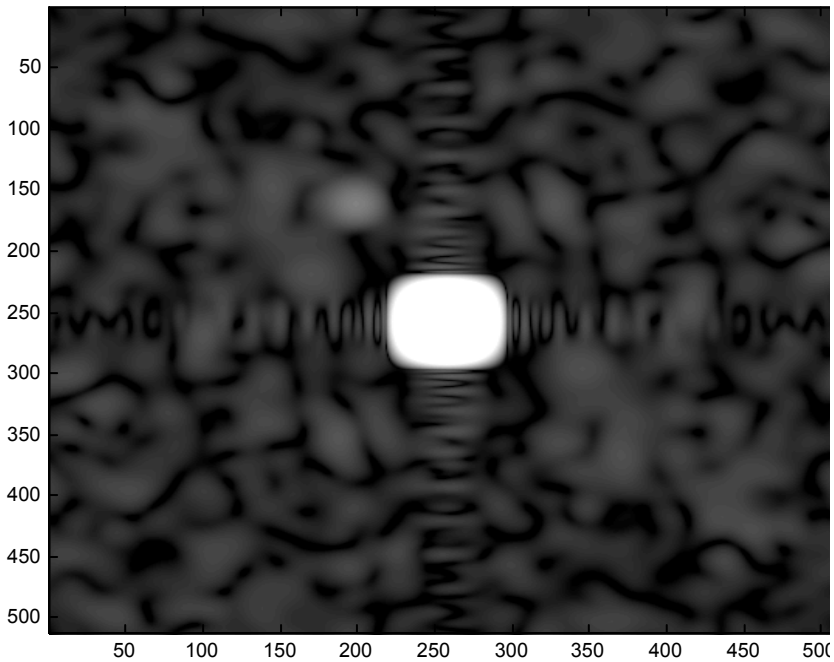


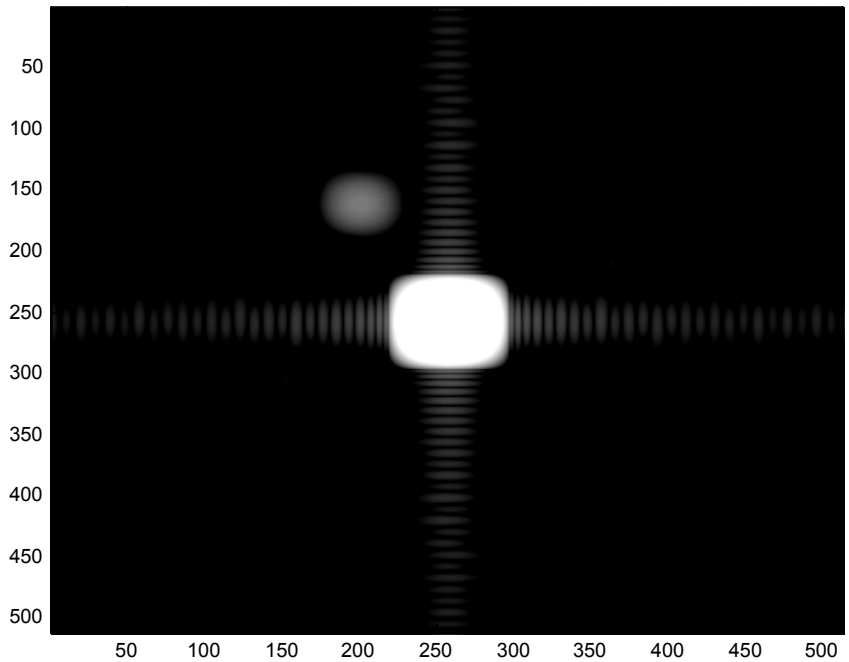


1σ = 1e-8

1σ = 1e-10

Planet at 6 λ/D

Return to presentation

# Detector Technology -- Introduction

- Efficient planet finding and characterization requires high quantum-efficiency detectors
  - A baseline TPF mission could fly with conventional CCD detectors, but other, more attractive alternatives are becoming available
- Here we consider only imaging focal plane arrays (FPAs) available in 2D formats with high quantum efficiency (QE) and low-noise performance in low background environments will be considered
  - Also must be immune to damage by bright light sources and most particle radiation, have very low read-noise (RN), and be insensitive to contamination by components outgassed from the spacecraft
  - Desirable features include the ability to detect individual photons, determine their arrival times, and measure their wavelengths or energies
- The following pages indicate that hybrid Si FPAs, or sub-electron-RN CCDs, may be the detectors of choice for TPF and precursor missions

# Detector Technology -- CCDs

- CCDs the most mature FPA technology, but not ideal, since current devices:
  - don't permit detection of individual photons
  - can't time-stamp photon arrivals on time-scales shorter than exposure time
  - don't provide any energy or wavelength information on their own
- Advantages of CCDs include:
  - technology readiness
  - large available formats, and convenient operating temperatures
- Disadvantages of CCDs, especially for small aperture precursor missions, include:
  - read noise and dark current
  - sensitivity to cosmic radiation
  - degradation of charge transfer efficiency (CTE) with prolonged exposure to energetic particle radiation.
- However, two breakthroughs in Si sensors that might detect single photon events at visible wavelengths are possible with sufficient funding for development of new read-out architectures to the FPA manufacturers:
  - CCDs with sub-electron read-noise
  - Hybridized Si sensors with direct non-destructive read-out circuits

# Detector Technology -- Sub-electron read noise CCDs

- Standard CCD outputs measure the voltage generated by the charge content of each pixel on the input gate of a FET
  - The charge is measured only once, and then dumped as the FET gate is prepared to read the next pixel.
- CCDs used for the detection of X-rays have been optimized to produce sub-electron read noise
  - Sub-electron read noise is achieved by enabling charge in each pixel to be measured multiple times on FET input gate capacitor before it is discarded
  - In principle, N non-destructive reads decreases read noise, RN, to new level, $RN_{eff} = RN / N^{1/2}$, but increases array read-out time by a factor of N
- Increased read-out time is not a problem for long exposures
  - If N can be increased to the point where $RN_{eff}$ is less than ~ 0.2 electrons per read (for RN = 2 $e^-$/read, N=128 non-destructive reads will ideally reduce the effective RN to RN_{eff} = 0.18 e/read). the detection of single photon events becomes possible with negligible chance of a false detection
    - In this circumstance, a CCD can be read continuously without any read-noise penalty, and the arrival time of each photon can be time-stamped to within the total time required to read the entire array.

# Hybridized Si Sensors

- Hybridized Si sensors with direct non-destructive read-out circuits (multiplexers -- MUXes) may also provide single photon detection capability, photon arrival-time stamping, and efficient particle event rejection
  - With effectively zero read-noise, photon-counting solid-state hybrid Si sensors could be mated to an integral field unit (IFU) fed spectrograph to determine photon energy
  - Hence, the next generation of ultra-low RN CCD or hybrid Si sensors may be ideal for TPF and precursor applications
- Hybrids can be bonded to materials tailored to sense wide range of wavelengths
  - Si faceplates with extended response in UV by mechanical thinning & fluorescent dyes
  - MUX bonded (`hybridized') to separate light-sensing layer of Si or other materials
  - Direct and/or non-destructive read-out capability for ultra-low noise operation
    - Multiple non-destructive reads yield readout noise << 1 e- per effective read
  - Capacitive coupling of the charge collected by the photo-sensitive layer permits multiple non-destructive reads (e.g Fowler sampling or `up-the-ramp' reading) and active discrimination of cosmic ray events for data recovery from affected pixels
- Multiple-quantum-well devices can be grown using MBE (molecular beam epitaxy) and tailored to any UV to near-IR wavelength region
  - Use lattices of Si, AlGaAs, InP, and other systems now in telecommunications use
- Extended near-IR and visible response can be obtained by hybridizing Si-MUXes to InSb faceplates, with excellent response to below 0.4 microns

# Detector Technology -- Spectral Methods

- Both detection and characterization of extra-Solar planets will be aided by measuring the photon energy or wavelength
  - Since, residual diffraction and error patterns are wavelength dependent, spectral techniques can be used to discriminate objects in the field from unwanted scattered light components. Furthermore, wavelength scaling can be used to help reconstruct the wave-front errors and to control phase errors with deformable mirrors
- Since the field image is two dimensional, spectral characterization of randomly placed objects requires implementation of an integral field spectrograph (IFS)
  - Though it is possible to obtain spectral information by acquiring multiple images through different filters or by scanning a slit across the field, these approaches are inefficient compared to integral field approaches and will not be considered further
- If a single candidate planet is identified in a field, its light can be placed on the slit of a conventional spectrograph & efficiently dispersed for characterization
  - However, a planetary system with N objects requires N separate spectral observations
- Fourier Transform Spectrometers (FTS) permit the detection of all of the power in an image all the time
  - However, to obtain a spectrum with a resolution R at any or all field points requires 2R settings of the delay line. Thus, like slit-scanning, FTSs are inefficient at extracting spectral information on multiple or extended sources

# Detector Technology -- Dense-Pack Integral Field Units (IFUs)

- Arrays of microlenses in the focal plane can be used to re-image the pupil so that the multiple pupil images, one per image element, occupy a very small portion of the pupil plane
  - This pupil plane can be masked and serve as input aperture to an imaging spectrograph whose dispersive element is arranged so that the spectrum of each pupil image lands in the dark space between the 0-th order pupil images
    - This type of IFU has been implemented in the TIGRE, OASIS, and SAURON spectrographs (e.g. Bacon et al. 1995).
- Dense-pack microlens-fed IFUs sample the entire image in the focal plane with any desired spatial resolution, generate full space-space-wavelength 3-D data cubes
  - Unlike conventional slit spectrographs, they are immune to small pointing errors
  - When mated to a photon-counting FPAs, they help generate `ideal' instruments for planet detection and characterization
    - For example, a sub-electron read-noise CCD or photon-counting hybrid FPA working at the image plane of an IFU can determine photon arrival time, spatial location, and energy

# Detector Technology -- Other Types of Photon-Counting Arrays

Several other categories of photon-counting devices exist, bu these have significant drawbacks with respect to the Si technologies discussed previously

- Multi-Channel Plates (MCPs:)
  - Electron avalanche amplifier devices which thus can be very efficient photon-counters
  - Available in megapixel formats
  - Two disadvantages
    - Require high-voltage operation
    - Can be permanently damaged by overlight conditions, typically by fluxes larger than 10^5 photons / second
      - In planet finding, the parent stars are likely to produce such large fluxes if they miss the coronagraphic mask.
- Hybridized Avalanche Photo-Diode Arrays (APDs):
  - Single pixel-devices in common use in optical fiber communications
  - Possible to build solid-state low-voltage avalanche photo-diode arrays
    - However, large FPAs based on this technology are not presently available

# Detector Technology -- Energy-Resolving Arrays

- Superconducting Tunnel Junctions (STJs):
  - Arrays of Josephson junctions operating at temperatures of order 1 K or lower
  - Single photon events can be detected and the photon energy measured to about 1% precision in current devices
  - Thus, STJs naturally provide simultaneous determinations of photon arrival time, energy, and position in the focal plane
  - Drawbacks for TPF and related applications
    - Require cryogenic operation operation at T < 1 K
    - Large input window formats and high bandwidths might create severe practical problems for operating these devices
    - Large arrays have not been demonstrated
- Micro-bolometers
  - The workhorse of cosmic microwave background studies
  - Energy sensitive devices operated at temperatures below 300 mK
  - Have been fabricated with formats of up to several hundred elements
    - Orders of magnitude gains in FPA size are likely during the next decade
  - Best available sensors for broad-band imaging at sub-mm and mm wavelengths
  - Adaptation to visual wavelength imaging will require shrinking current bolometer designs by orders of magnitude
  - As with STJs, cryogenic requirements of large format arrays may be extreme

# Isolator design tool 1.5-Hz input/output

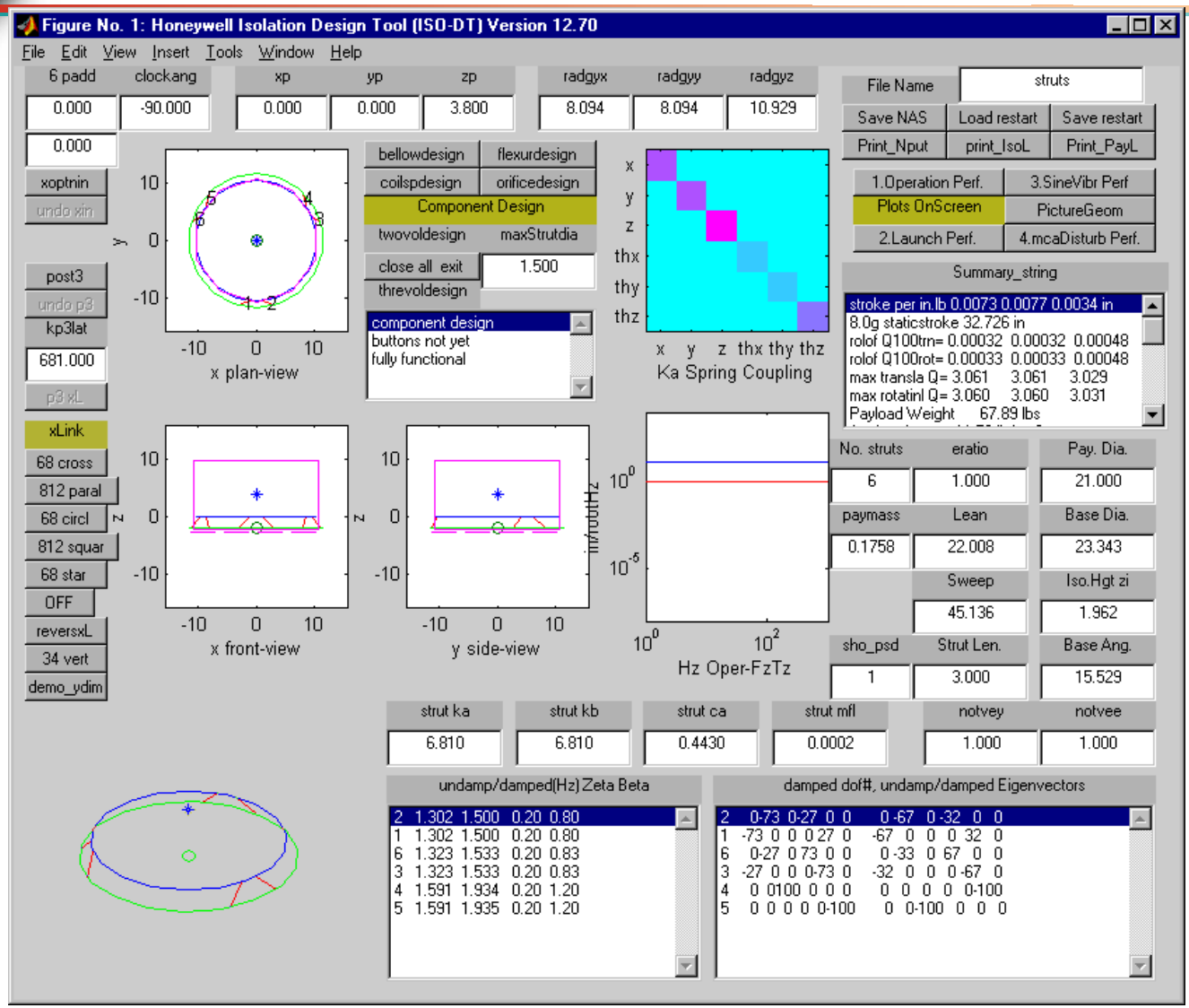

# Isolator design tool ideal geometry

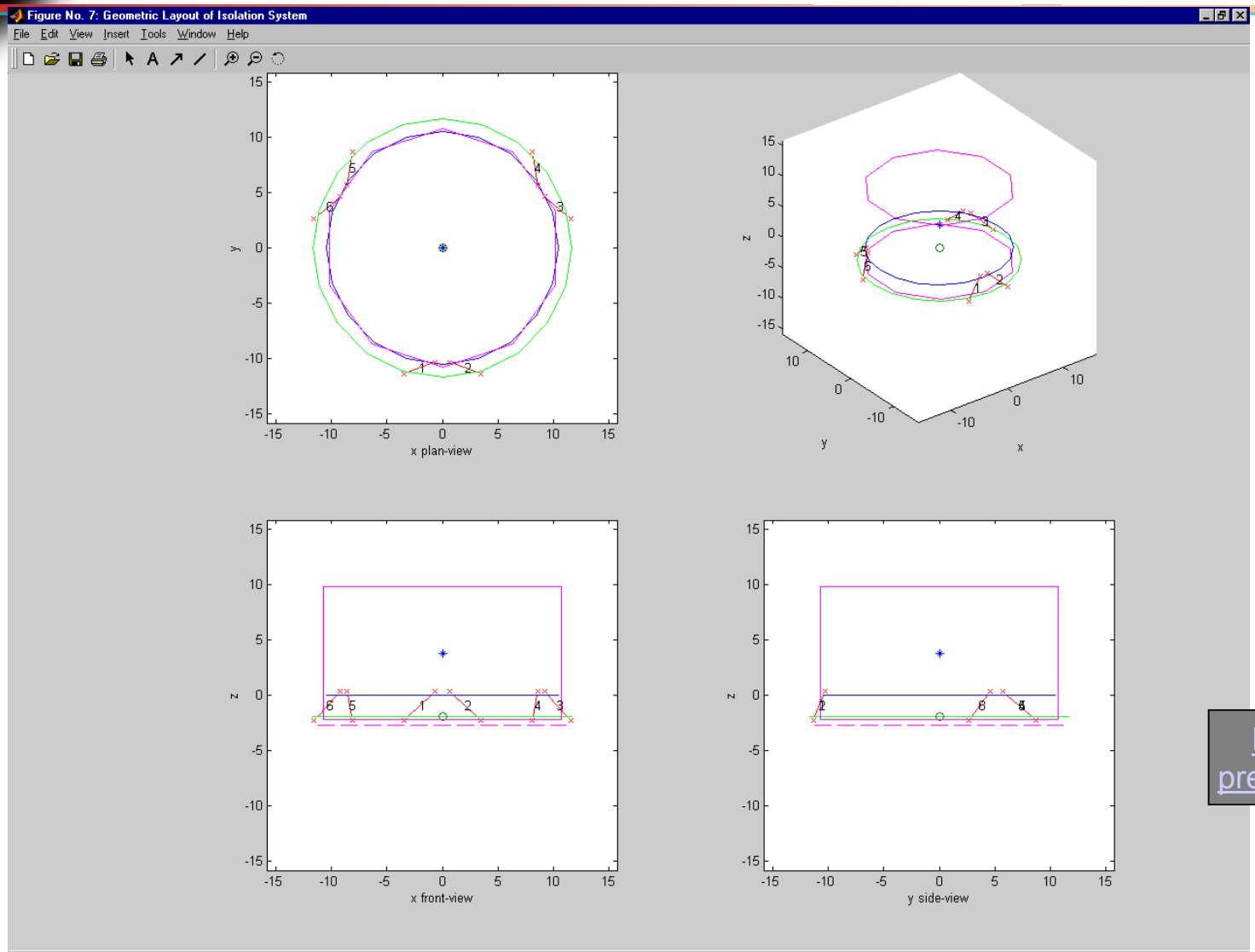


Back to presentation